Effect of oxygen availability on the corrosion rate of reinforced concrete in marine exposure zones: inference from site and lab studies

Amy Moore

Supervised by:

Professor Hans Beushausen

Co-supervised by:

Dr Mike Otieno

Submitted to the University of Cape Town in partial fulfilment of the requirements for the degree of Master of Science in Engineering

Plagiarism Declaration

i) I know that plagiarism is wrong. Plagiarism is to use another's work and to pretend that it is one's own.

ii) I have used the Harvard Convention for citation and referencing. Each significant contribution to and quotation in this report form the work or works of other people has been attributed and has been cited and referenced.

iii) This report is my own work

iv) I have not allowed and will not allow anyone to copy my work with the intension of passing it as his or her own work.

MRXAMY002

Moore, Amy

Signed by candidate

Abstract

Corrosion of steel in reinforced concrete structures is a large problem facing engineers today. The marine environment is considered to be the most severe owing to the high levels of chlorides available, and so structures located here are particularly vulnerable to chloride attack and chloride-induced corrosion of steel.

In order to intervene and address the concern of premature deterioration in the marine environment, design guidelines and frameworks have been developed and implemented. For example, the Eurocode (EN 206, 2013) provides three class designations in order to predict the severity of potential steel corrosion. The three exposure zones, namely i) structures exposed to airborne salts but not in direct contact with sea water, ii) submerged structures, and iii) structures in the tidal, splash and spray zones are given here in order of increasing assumed probability of corrosion.

However, it has been found through condition assessments of structures along the Atlantic Ocean and Indian Ocean coasts of Southern Africa that structures in the tidal zone generally show no signs of corrosion damage despite having high levels of chlorides at the depth of reinforcement. Often, on a structure where both zones have the same cover to reinforcing, the splash and spray zone will show significant damage while the tidal zone shows no signs of reinforcement corrosion. These findings challenge the existing idea that the tidal zone can be characterised as the most severe exposure zone.

In order to further understand the mechanisms of reinforcement corrosion within different marine environmental conditions, a total of 36 corrosion cells were manufactured with dimensions of 120 × 122 × 380 mm and placed in simulated marine environmental conditions. These three environmental conditions included submerged, cyclic wetting and drying, and periodic splashing. In order to simulate the submerged environment, the cover surface of the specimens were permanently saturated with a 5% NaCl solution while for the splash zone concrete specimens were sprayed with 5% NaCl solution every second day. The tidal zone attempted to simulate natural tidal conditions by exposing the corrosion cells to 12 hour cycles consisting of 6 hours wetting and 6 hours drying

All 36 corrosion cells were connected to a data logger where the voltage was measured weekly across a resistor of 100Ω. Ohm's law was then used to determine the current flowing through the circuit. The concrete cover depth was varied in the corrosion cells (10, 20 and 30 mm) as well as the w/b ratio (0,5 and 0,8). The corrosion current resulting from these corrosion cells were used to infer relationships between all 3 parameters (cover depth, w/b ratio, and exposure conditions) and their influence on the corrosion current.

Three companion moisture specimens were cast per mix in order to establish moisture profiles in the different exposure zones. From these specimens, the relative humidity of the concrete at different cover depths and w/b ratio's could be determined for corrosion cells located in different

exposure conditions. Companion cubes were also cast with the corrosion cells in order to determine the durability index values.

The results of the experiments indicate that the exposure condition has a very large impact on the availability of oxygen, and hence the corrosion rate. High relative humidity (or moisture content) in concrete stifles the supply of oxygen to the steel, and hence prevents active corrosion. For concrete submerged and partially or completely saturated with water, oxygen accessibility can become limited at the steel surface. The results obtained conform to the widely accepted principle that submerged concrete is less vulnerable to corrosion as a result of insufficient oxygen supply at the reinforcing steel.

For concrete exposed to a 6 hour cycle of wetting and drying, the corrosion rate was significantly lower at higher cover depths due to the short cycle durations, the pores surrounding the steel were still partially or fully saturated with water. As a result, oxygen diffused slower through the cover layer. Consequently, where the concrete in the tidal zone has drying times of about 6 hours and a cover depth exceeding 30 mm, the steel will be deprived of oxygen, and corrosion will be stifled. This means that the concrete in the tidal zone would theoretically perform as if it were permanently submerged (provided sufficient cover depth exists).

Specimens exposed to a splash environment performed as expected. A low moisture content showed that oxygen is able to diffuse through the pore system and facilitate corrosion in the specimens. This is owing to the pores around the steel not being saturated with moisture, and oxygen being readily available to participate in the cathodic reaction. In the case of these specimens, the electrical resistivity of the specimens was found to be the main limiting factor in controlling the corrosion rate (and not cathodic control as with tidal and submerged specimens).

As a result, it is recommended that the current SANS exposure classification be broadened to include concrete exposed to cyclic wetting and drying (i.e. tidal zone exposure) a separate category, and not be classified as having the same severity as the splash zone. The application of these research findings is in infrastructure that is primarily exposed to only tidal and submerged marine conditions.

Acknowledgements

I would like to express my sincere gratitude to my supervisor Professor Hans Beushausen for his guidance and technical support during my time at UCT. It was a great privilege to study under your supervision. I also wish to thank my co-supervisor Dr Mike Otieno for his insightful comments and support.

Finally, I would like to thank the two most important people on the planet, my mom and dad, whose hugs and endless support will forever be appreciated.

Rust's a must

Mighty ships upon the ocean
Suffer from severe corrosion,
Even those that stay at dockside
Are rapidly becoming oxide
Alas that piling in the sea
Is mostly Fe_2O_3,
And where the ocean meets the shore
You'll find there's Fe_3O_4,
'Cause when the wind is salt and gusty
Things are getting awful rusty.

We can measure we can test it,
We can halt it or arrest it,
We can gather it and weigh it,
We can coat it, we can spray it,
We can examine and dissect it,
We cathodically protect it,
We can pick it up and drop it,
But heavens knows, we'll never stop it.

So here's to rust, no doubt about it,
Most of us would starve without it.

T.R.B Watson, June 1974

Table of Contents

Plagiarism Declaration i
Abstract i
Acknowledgements iii
Table of Contents iv
Abbreviations and Notations viii
Mix labels viii
1 Introduction 1-1
1.1 Background 1-1
1.2 Subject of research 1-2
1.3 Research problem statement 1-4
1.4 Research aims and objectives 1-4
1.5 Scope and limitations of study 1-5
1.6 Significance of the study 1-5
1.7 Conceptual framework 1-6
1.8 Research layout 1-7
2 Literature Review 2-1
2.1 Fundamentals of steel corrosion 2-1
2.1.1 Corrosion as an electrochemical process 2-1
2.1.2 Corrosion products 2-1
2.1.3 Expression of corrosion rate 2-2
2.2 Service life of reinforced concrete structures 2-3
2.2.1 Initiation of corrosion 2-3
2.2.2 Propagation of corrosion 2-6
2.3 Review of selected factors affecting the corrosion rate 2-10
2.3.1 Exposure classes 2-10
2.3.2 Cover depth 2-13
2.3.3 Concrete quality 2-15
2.3.4 Temperature 2-17
2.3.5 Chloride ion concentration 2-19

2.3.6 Concrete resistivity 2-20
2.3.7 Oxygen availability 2-21
2.3.8 Marine fouling 2-24
2.4 Transport mechanisms for corrosion inducing species 2-25
2.4.1 Moisture transfer 2-25
2.4.2 Chloride ingress 2-31
2.5 Review of exposure classes in international standards 2-35
2.5.1 European Standard EN 206-1: 2013 2-35
2.5.2 Australian Standard AS 3600: 2009 2-36
2.5.3 Canadian Standard CSA A23.1: 2009 2-36
2.5.4 North American Standard ACI 318: 2014 2-38
2.5.5 South African Standard SANS 10100-2: 2009 2-39
2.5.6 Criticisms of the current approach 2-41
2.6 Techniques for accelerating corrosion initiation and propagation 2-41
2.6.1 Impressed current 2-42
2.6.2 Admixing chlorides 2-42
2.6.3 Wetting and drying 2-43
2.6.4 Elevated temperature 2-43
2.7 Techniques for corrosion assessment in concrete 2-44
2.7.1 Polarization resistance method 2-44
2.7.2 Macrocell corrosion method 2-45
2.7.3 Corrosion rate indicators 2-46
2.8 Closure 2-49
3 Field structures in Southern African harbours 3-1
3.1.1 Jetty, Walvis Bay Namibia 3-2
3.1.2 Repair jetty, Walvis Bay Namibia 3-3
3.1.3 Caisson, Saldanha Bay 3-4
3.1.4 Small Craft Harbour, Saldanha Bay 3-6
3.1.5 Tidal pool, Strandfontein 3-7
3.1.6 Launch ramp, Hangklip 3-7
3.1.7 Cover depth versus level of deterioration 3-9

3.2 Closure 3-10

4 Research methodology 4-1

4.1 Introduction 4-1

4.2 Variables 4-1

4.2.1 Concrete cover depth 4-1

4.2.2 Water/binder ratio 4-1

4.2.3 Exposure conditions 4-2

4.3 Specimen details 4-2

4.3.1 Mix design 4-2

4.3.2 Material selection 4-2

4.3.3 Casting 4-3

4.3.4 Curing 4-3

4.3.5 Manufacture of corrosion macrocell 4-4

4.3.6 Manufacture of moisture specimens 4-7

4.4 Exposure zone set-up 4-8

4.4.1 Submerged Zone 4-8

4.4.2 Splash and Spray Zone 4-9

4.4.3 Tidal Zone 4-9

4.4.4 Chloride Solution 4-10

4.5 Monitoring of specimens 4-10

4.5.1 Cover measurements 4-10

4.5.2 Corrosion performance 4-10

4.5.3 Moisture profile 4-11

4.5.4 Durability tests 4-12

4.5.5 Compressive strength 4-12

4.6 Timeline of experimental programme 4-12

5 Results and discussion of experimental testing 5-1

5.1 Time variant corrosion current ($Icorr$) 5-1

5.1.1 3-point moving average 5-1

5.1.2 Observations about time variant corrosion current 5-3

5.2 Total Integrated Current 5-6

5.2.1 Comparison of $TICcorr$ in different exposure conditions 5-7
5.2.2 Comparison of $TICcorr$ for specified cover depths 5-8
5.2.3 Comparison of $TICcorr$ for specified w/b ratios 5-9
5.3 Effect of moisture content on $TICcorr$ corrosion rate 5-10
5.3.1 RH results from moisture specimens 5-10
5.3.2 Submerged zone 5-11
5.3.3 Tidal zone 5-13
5.3.4 Splash zone 5-15
6 Conclusions and recommendations 6-1
6.1 Short summary of research aims and methodology 6-1
6.2 Rebar corrosion damage in structures exposed to real marine conditions 6-1
6.3 The influence of cover depth on reinforcement corrosion for site and experimental data 6-2
6.4 The influence of quality on reinforcement corrosion for site and experimental data 6-3
6.5 The influence of exposure environment on rebar corrosion 6-3
6.6 Critique of design standards 6-4
6.7 Practical implications 6-5
6.8 Recommendations 6-6
6.8.1 Amendment of corrosion cell design 6-6
6.8.2 Amendment of accelerated corrosion technique 6-6
6.8.3 Implications of modern binder types 6-6
6.8.4 Correlation to structures in natural conditions 6-6

Abbreviations and Notations

RC	Reinforced concrete
w/b	water binder ratio
OPC	Ordinary Portland cement
RH	Relative Humidity
SCM	Supplementary Cementitious Materials
ITZ	Interfacial transition zone
C & CI	Cement and Concrete Institute
LED	Light emitting diode
TIC	Total integrated current
OPI	Oxygen permeability index
WSI	Water sorptivity index
CCI	Chloride conductivity index
ANOVA	Analysis of variance
S&S	Splash and spray

Mix labels

C10 – 50	Specimens with cover 10 mm and w/b 0,5
C10 – 80	Specimens with cover 10 mm and w/b 0,8
C30 – 50	Specimens with cover 30 mm and w/b 0,5
C30 – 80	Specimens with cover 30 mm and w/b 0,8
C20 – 50	Specimens with cover 20 mm and w/b 0,5
C20 – 80	Specimens with cover 20 mm and w/b 0,8

1 Introduction

1.1 Background

Concrete, and more particularly reinforced concrete (RC), is a popular choice of material for structures built in the marine environment. Concrete's affordability, resistance to abrasion caused by wave action, and ability to withstand impacts from ships are some of the reasons concrete is suitable for coastal applications (Alexander, 2016). The growth of ports and harbours around the world is crucial for the development of the economy through the expansion of the tourism industry and the international trade industry to name but a few. This is of particular relevance to developing countries such as South Africa.

While there are many advantages to using reinforced concrete as a construction material, there remains the pervasive issue of its durability. Corrosion of steel in reinforced concrete structures is a large problem facing engineers today. The marine environment is considered to be the most severe owing to the high levels of chlorides available, and so structures located here are particularly vulnerable to chloride attack and chloride-induced corrosion of steel. Chloride-induced reinforcement corrosion leads to reduced steel cross-sections, cracking, delamination and spalling, and may over time diminish the integrity of the structure. In South Africa, many cases exist where a combination of low cover and poor quality of the covercrete (especially in the aggressive marine environment) has led to rapid deterioration.

The economic consequences of corrosion are high, reflected by the millions of rand spent every year on repairing, rehabilitating or replacing damaged structures (Budget, 2018). In the case where replacing a structure is required, there is also a cost to the environment, as old concrete is discarded and energy and materials are consumed to produce new concrete. Therefore in order to help conserve energy and resources, and reduce pollution that comes from waste, it is crucial that reinforced concrete structures perform effectively for the duration of their service life.

In order to intervene and address the concern of premature deterioration in the marine environment, design guidelines and frameworks have been developed and implemented. For example, the Eurocode (EN 206, 2013) provides three class designations in order to predict the severity of potential steel corrosion (Table 1- 1). The three exposure zones, namely i) structures exposed to airborne salts but not in direct contact with sea water, ii) submerged structures, and iii) structures in the tidal, splash and spray zones are given here in order of increasing assumed probability of corrosion. These classifications take into account, for the most part, the environmental factors in the exposure zone that will affect the rate of deterioration due to corrosion (Richardson, 2002).

However, it has been found through condition assessments of structures along the Atlantic Ocean and Indian Ocean coasts of Southern Africa that structures in the tidal zone generally show no signs of corrosion damage despite having high levels of chlorides. Often, on a structure where both zones

have the same cover to reinforcing, the splash and spray zone will show significant damage while the tidal zone shows no signs of reinforcement corrosion. These findings challenge the existing idea that the tidal zone is the most severe. This requires further investigation in order to improve engineers' understanding of the mechanisms of corrosion associated with various environments. Moreover, investigating this phenomenon will verify if the tidal zones severity ranking is excessive and unnecessary. The results of this research could therefore be used to develop more and informed guidelines for design and condition assessment of structures in the marine tidal exposure.

Table 1- 1: Marine exposure classes according to EN 206 (2013)

Degradation phenomenon	Class designation	Description of environment
Corrosion induced by chlorides from seawater	XS1	Exposure to airborne salt
	XS2	Permanently submerged
	XS3	Tidal, splash and spray zones

Previous research by Golden (2015), showed for different binder types and w/b ratios, that the corrosion rate decreased with a decrease in the drying time of concrete exposed to cyclic wetting and drying. The effect of drying time was more prominent in PC specimens and specimens with a high w/b ratio. In this research, it was inferred that the reason for this was a possible limited supply of oxygen at the level of the steel to facilitate the cathodic reaction. While this was useful in showing that the drying time does affect the corrosion rate, a direct verification of the role oxygen plays in the tidal zone is required. Consequently, this research sets out to indirectly measure the supply of oxygen at the steel level by eliminating all other corrosion limiting factors and thus advance the understanding of the link oxygen has to moisture profiles and corrosion rates.

There is ample literature on the influence of oxygen on the corrosion rate in the submerged zone and air dry conditions (Hussain, 2011) (Raupach, 1996), while little research has been conducted in the area of concrete exposed to short cycles of wetting and drying. In addition, the drying duration used in previous experiments did not reflect adequately the approximate 6 hour natural tidal cycles. It would be useful to see the effects of oxygen diffusivity on the corrosion rate under these conditions, as this could be better understood in the context of real life structures.

1.2 Subject of research

Corrosion of steel is often the primary mode of degradation in reinforced concrete structures. Exposure to aggressive environments can accelerate corrosion and lead to the structures premature deterioration. The electrochemical reaction (which consists of anodic and cathodic reactions) is initiated through the movement of harmful substances through the concrete cover to the steel level, and further propagated through the availability of moisture and oxygen (Figure 1 - 1).

Oxidation reaction $$Fe \rightarrow Fe^{2+} + 2e^{-}$$ (1- 1)

Reduction reaction $$H_2O + \frac{1}{2}O_2 + 2e^{-} \rightarrow 2OH^{-}$$ (1- 2)

Electrons are released at the anode through the dissolution of iron (Equation 1-1) and consumed at the cathode in the presence of moisture and oxygen (Equation 1-2). These reactions are known as oxidation and reduction reactions respectively, and together form the basis of the corrosion process.

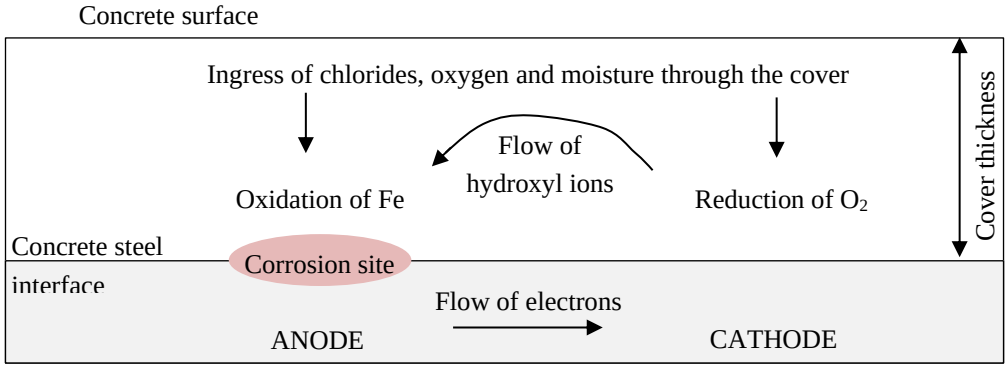

Figure 1 - 1: Corrosion mechanisms of steel (after Broomfield, 2006)

The high alkalinity of concrete (pH 12 to 13) leads to the formation of a passive layer around the steel which hinders corrosion (Broomfield, 2006). However, this self-forming layer can be destroyed by the ingress of chlorides into the concrete once the critical chloride threshold at the level of the steel is reached. Once the steel has been de-passivated by a significant quantity of chlorides, the anodic part of the corrosion process which involves the dissolution of iron proceeds.

Once the passive layer has been disrupted, and corrosion has been initiated, further supply of specific elements is required to propagate corrosion. One of these elements, oxygen, is reduced at the cathode to form hydroxyl ions (OH^{-}) that are used to form corrosion products. When the oxygen supply to concrete is limited, the cathodic reaction is retarded and hence high corrosion rates are prevented from occurring. The other element which facilitates corrosion is moisture, which participates in the corrosion reaction, as well as completes the electrochemical circuit by allowing hydroxyl ions (OH^{-}) to flow from the cathode to the anode.

From this description, it can be seen that after the initiation of corrosion the quantities of oxygen and moisture in the concrete are the most crucial components governing the rate at which the reaction proceeds (along with resistivity of the concrete).

When concrete is submerged in water, the high moisture content reduces the resistance of the pathway between the cathode and anode, while simultaneously stifling the supply of oxygen to the cathode. This results in a suppressed corrosion rate and is the reason the submerged zone is classified as less severe.

In contrast, very ‘dry’ concrete with low moisture content has sufficient levels of oxygen available for corrosion to proceed, but the high resistance of the electrolyte prevent ions from completing the corrosion circuit. This again, results in a suppressed corrosion rate.

The tidal zone along with the splash and spray zone are considered to be the most severely affected by chloride-induced steel corrosion. This is owing to the high levels of chlorides expected to be found in the concrete and assumed optimum values of moisture and oxygen. However, as stated in Section 1.1, condition assessments of RC in the tidal zone of existing structures have shown no corrosion – an unexpected observation. As the distribution of chlorides in the concrete is usually found to be high, and there is clearly sufficient moisture from the direct contact with seawater, it seems plausible that limited oxygen availability is governing the rate of corrosion.

As concrete in the tidal zone experiences relatively short cycles of wetting and drying, it is likely that the concrete is not drying out to the level of the embedded steel before the next high tide (and thus limiting the oxygen availability). This could potentially lead to the corrosion rate being cathodically controlled and thus explain the lower than expected corrosion damage found in the tidal zone. The idea that restricted oxygen levels could potentially be influencing steel corrosion in the tidal zone forms the premise of this research.

1.3 Research problem statement

The mechanisms for reinforcement corrosion of concrete in different marine exposure classes is not well understood (particularly the role oxygen availability plays). The exposure classes of the marine environment include concrete permanently submerged, concrete exposed to cyclic wetting and drying, and concrete experiencing splashing of seawater.

1.4 Research aims and objectives

- Provide information on the influence of exposure conditions (submerged, tidal, and splash and spray) on the corrosion rate of concrete in the marine environment
- Confirm whether oxygen availability at the level of the reinforcing is valid reason for any observed influence of the exposure zone.
- Develop relationship between cover depth and quality of the cover on the durability of structure within each exposure zone (submerged, tidal, and splash and spray).
- Advance knowledge of underlying mechanisms of corrosion in the marine environment
- Refine current durability guidelines (SANS) for reinforced concrete structures in the marine environment

1.5 Scope and limitations of study

The scope of the work includes experimental testing in a laboratory, on concrete made from CEM I (Ordinary Portland Cement). The experimental programme ran for 23 weeks, and includes the collection of corrosion rates and relative humidity values. Only uncracked specimens were investigated. Six field structures were assessed for corrosion in order to validate the research problem.

As corrosion is a long term process, and there are time constraints for this research, techniques must be used to accelerate the corrosion process. This could potentially be a limitation to the study as the corrosion mechanism of accelerated techniques have been shown to not be identical to those exposed to a natural marine environment (El Maaddawy & Soudki, 2003).

Testing of in-situ structures to infer these relationships would be beneficial to this study. However, limited resources and access restrictions to structures along the coast of Southern Africa (especially when using invasive testing methods) proves to be difficult under the time constraints of this research. Nonetheless, information on the condition of marine structures that have been established and are available, will be used to support the claims made in the laboratory based research. This information can also be used to verify the assertion that RC in the tidal zone has no traces of corrosion, despite the high levels of chlorides.

1.6 Significance of the study

The importance and implications of undergoing this study for researchers, engineers and policy makers is outlined below:

A proper understanding of the deterioration mechanisms is crucial for designers, in order to be able to predict the performance of a structure in a given environment. This is particularly true for harsh environments, where the consequences of inadequate design are high. The outcome of this research contributes to the knowledge gap identified in Section 1.3, and allows designers to predict, with better accuracy, the performance of structures in different chloride environments.

The findings of this study can also contribute towards achieving optimum repair strategies. One of the most crucial steps in achieving satisfactory repair of structures is to correctly define the deterioration problem. Once the cause of the deterioration has been identified and understood, the most appropriate repair strategy can be specified. This leads to more sustainable and economical repair decisions.

Research on topics of corrosion mechanisms for different exposure classes also have influence on a policy level. Exposure classifications given in local and international standards can be refined and changed to more adequately reflect real performance of marine structures. is arguably the most significant implication of research in this field.

The application of this is in infrastructure that is primarily exposed to only tidal and submerged marine conditions. A common example is concrete pipes where many pipelines have been in service for more 50 years despite sometimes having cover to reinforcement of as little as 20mm. These research findings are therefore directly applicable and of interest for concrete pipelines.

1.7 Conceptual framework

A schematic was developed to serve as a tool and organise the concepts associated with the research topic. Figure 1 - 2 contextualises the research and presents the variables.

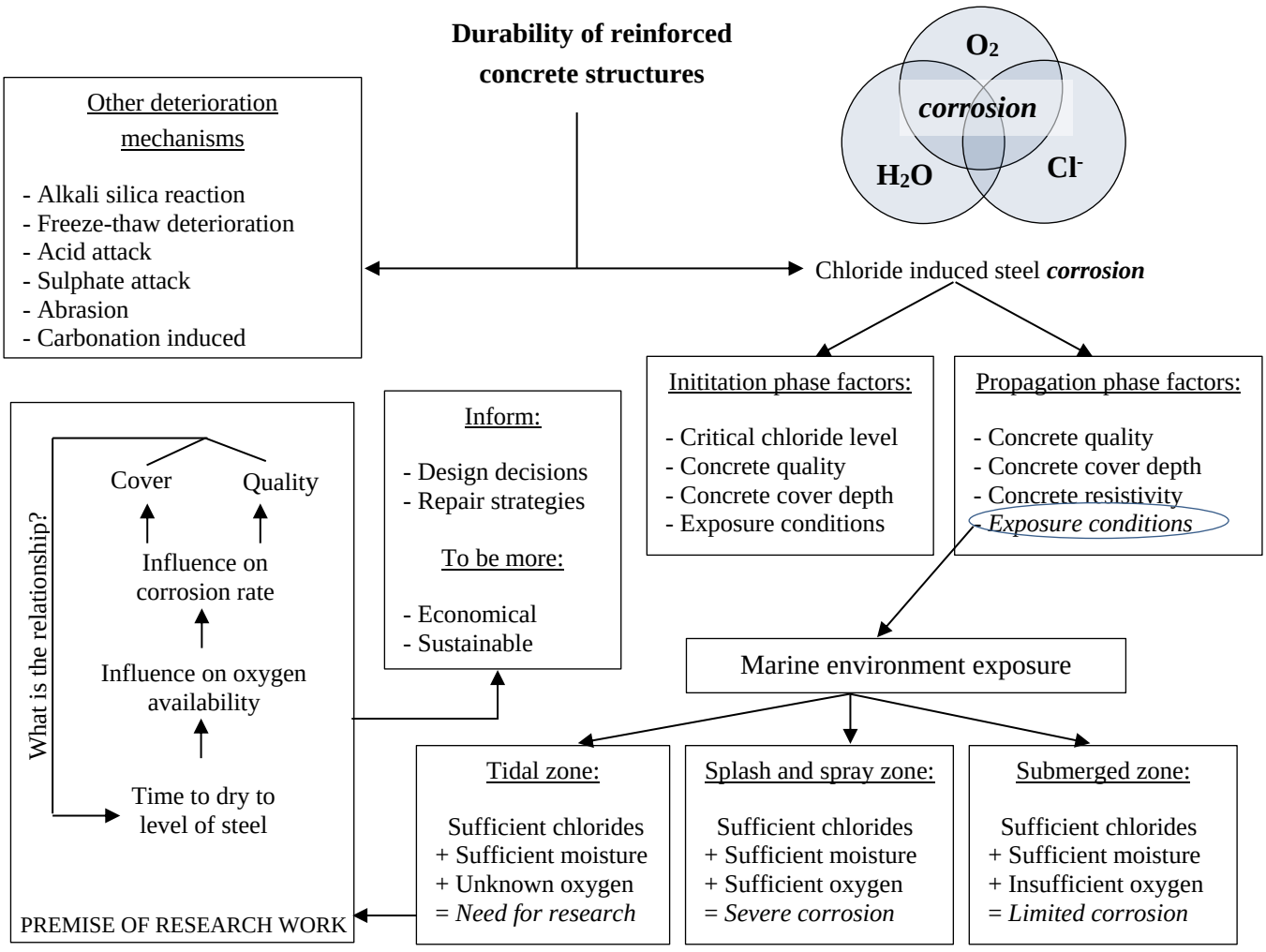

Figure 1 - 2: Conceptual framework for research work

1.8 Research layout

Chapter 1 gives an **introduction** to the research topic by providing a brief background, the scope and limitations to the study, and the aims and objectives to be achieved.

Chapter 2 presents a review on **literature** where similar research was undertaken. This chapter also includes the fundamental concepts of corrosion and reinforced concrete.

Chapter 3 illuminates the problem further by presenting corrosion observations of **field structures** along the coast of Southern Africa.

Chapter 4 provides a detailed outline of the **methodology** that was followed for this research. This includes the testing techniques that were implemented and the configuration details of all specimens cast.

Chapter 5 presents the key experimental **results**. This section also sets out to **discuss** any trends that can be inferred from the data and the significance of any results.

Chapter 6 **concludes** the research by summarising and reviewing the ideas presented in the preceding chapter. Suggestions and **recommendations** are given for future research that might be undertaken as a result of this project.

A list of appendices is published at the end of the report which supplements the information presented in the main chapters of the report.

2 Literature Review

This chapter addresses the fundamentals of steel corrosion in concrete, with emphasis given to chloride induced corrosion. The initiation and propagation phases of corrosion are then discussed together with a select review of factors that influence the rate of propagation in RC structures. Additionally, the transport mechanisms associated with the movement of relevant substances are presented. The chapter concludes by evaluating the feasibility of techniques for measuring both the corrosion rate in concrete and accelerating steel corrosion in laboratory based experiments.

2.1 Fundamentals of steel corrosion

This study attempts to further understand the mechanism of corrosion failure within different marine exposure conditions. It is therefore important to appreciate that some fundamental aspects of corrosion should be understood to develop an effective experimental programme and interpret results. Accordingly, this section discusses corrosion as an electrochemical process, the corrosion products that can occur under different conditions, and different ways to express the corrosion rate.

2.1.1 Corrosion as an electrochemical process

Steel used for the reinforcement of concrete structures is made from the element iron, which in its natural form is found as iron ore. Energy is used in the production process to turn iron into steel, which over time has the tendency to want to revert back to its original state (Angst, 2011). The process of unstable steel turning back into more stable forms, such as iron oxides, is the well-known process of rusting, which is the primary mechanism affecting most reinforced concrete structures.

These two half-cell reactions presented in Section 1.2 occur simultaneously and at the same rate, as the amount of electrons released must be equal to that consumed. The overall reaction can be expressed by Equation 2-1(2- 1). The corrosion product shown here is usually oxidised further to produce other corrosion products.

Net reaction
$$Fe + H_2O + \frac{1}{2}O_2 \rightarrow Fe(OH)_2 \quad (2\text{- }1)$$

2.1.2 Corrosion products

The expansive nature of the corrosion products can result in an increase in its volumetric change by up to 600% (Mehta, 1991). As the corrosion products begin to form, there is insufficient space within the concrete pores to accommodate the iron oxides. Consequently, expansive forces are induced which owing to concrete's poor tensile capacity causes cracking of the concrete cover. Depending on which type of corrosion product is formed, the volumetric increase can vary and therefore have different influences on potential cracking. Figure 2 - 1 shows the relative volume of iron (Fe) when compared with its forms of iron oxides.

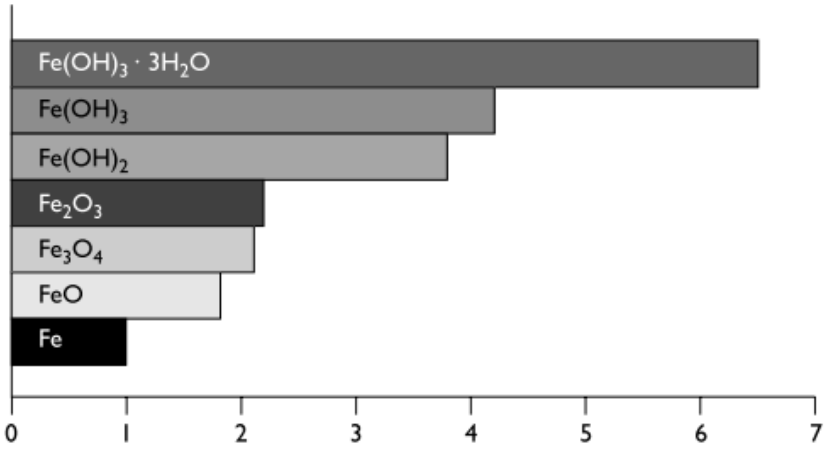

Figure 2 - 1: Relative volume of iron and its oxides (Broomfield, 2006)

2.1.3 Expression of corrosion rate

Quantifying the electrochemical reactions associated with the corrosion process is vital for calculating the residual service life of structures vulnerable to chloride induced corrosion. In reinforced concrete, the speed at which electrons move from the site of the anode to that of the cathode is indicative of the speed of the deterioration of the metal. Accordingly the corrosion rate, which can be evaluated through electrochemical techniques, is often expressed in terms of current (measured in µA) or corrosion current density (measured in µA/cm^2). Different corrosion current densities have been associated with different corrosion rate criteria as shown by Alonso et al. (1998) and (Broomfield et al., 1994). For example, Alonso et al. (1998) states that corrosion current densities exceeding 0.1 to 0.2 µA/cm^2 correspond with significant corrosion rates, while according to Broomfield et al. (1994) high corrosion rates are linked to corrosion currents of above 1 µA/cm^2. Furthermore, Heckroodt (2002) gives a guide for interpreting the corrosion current in terms of corrosion severity, which also shows different results to that of other researchers (Table 2 - 1). These varying interpretations can possibly be attributed to the use of different devices and different electrochemical techniques. This table was considered the most relevant as it was most recent and also took into account the results of other studies.

Table 2 - 1: Qualitative guide for assessing the severity of the corrosion of structures on site (Heckroodt, 2002)

Corrosion rate (µA/cm^2)	Qualitative assessment of corrosion rate
>10	High
1.0 – 10	Moderate
0.2 – 1.0	Low
< 0.2	Passive

Although corrosion rate is often expressed as the current or corrosion current density, these expressions can be converted using Faraday's law (Equation 2 - 2) into penetration rates, such as cross-section reduction over time (measured in mm/year) or the weight loss per unit area over time (g/m^2/day). (Stansbury & Buchanan, 2000). Using this approach, the corrosion rate can be presented in a number of interchangeable formats, such that 1 $\mu A/cm^2 \approx 12$ µm/year $\approx 0{,}25$ g/m^2 day (Hunkeler, 2005).

Faraday's law
$$M = \frac{ItA_w}{nF} \qquad (2\text{- }2)$$

Where M = mass of dissolved steel (g); I = current (A); t = time (sec); A_w = atomic weight of steel (g/mol); n = valency of steel (unitless) and F = Faraday's constant (96 500 A·sec).

2.2 Service life of reinforced concrete structures

The service life of corrosion-affected RC structures is commonly divided into two distinct phases (Figure 2 - 2). The first phase is termed the initiation phase, and refers to the period of time that leads to loss of passivity of the steel embedded in concrete, as a result of either carbonation or chloride penetration. The second phase is the propagation phase, which begins at the onset of depassivation, and includes the active corrosion of embedded steel until the consequences of corrosion in the structure become unacceptable. Both of these phases are critical when assessing reinforcement corrosion of steel in the marine environment (Bertolini et al., 2013), and will therefore be discussed in greater detail in the sections below.

2.2.1 Initiation of corrosion

Before the corrosion process described in Section 2.1.1 can occur, the passive layer surrounding the steel has to be disturbed. This passive layer, which is made up of protective oxides is formed as a result of the hydration of cement. Hydration products, such as calcium hydroxide cause the concrete to have a pH between 12 and 13 (a very alkaline environment), which establishes a gamma ferric oxide layer ($\gamma - Fe_2O_3$). As a result the dissolution of the iron Fe^{2+} into the electrolyte (or the oxidation reaction) is prevented, and thus the progression of corrosion is inhibited. (Ballim, Alexander & Beushausen, 2009)

Carbonation and chloride ion diffusion are the two most common mechanisms that cause the de-stablisation of the protective layer. Substantial levels of chlorides are present in seawater, and hence chloride induced attack is particularly relevant for structures exposed to the marine environment. Accordingly only chloride induced corrosion will be discussed further.

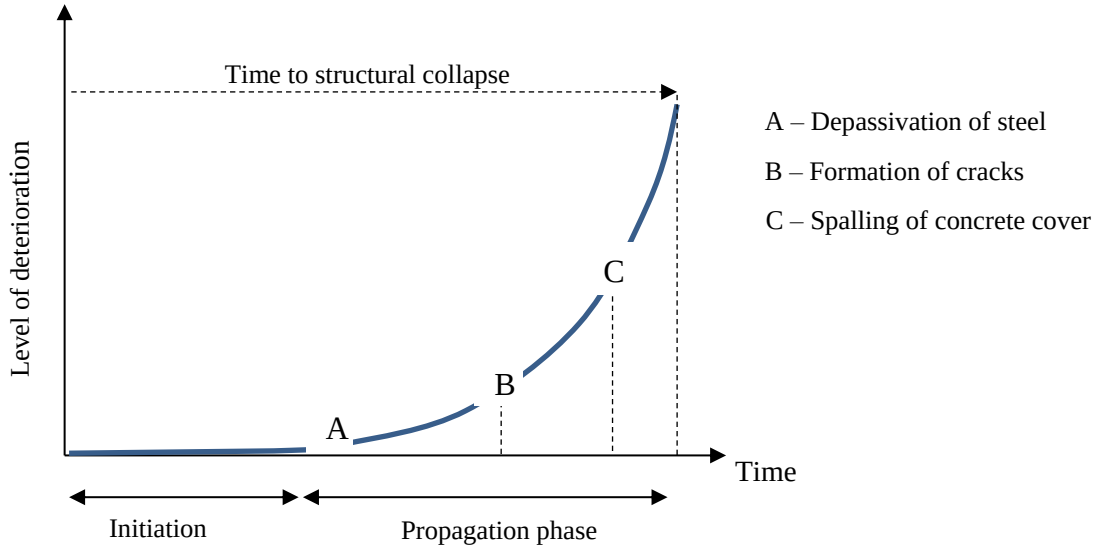

Figure 2 - 2: Service life of corrosion affected RC structures (After Tuutti's 1982 model)

2.2.1.1 Chloride induced corrosion

Chloride ions, which can be introduced into concrete either in the mixing stage or after exposure to chloride rich environments, act as a catalyst for corrosion. The chloride ions aren't consumed in the process of corrosion but rather break down the passive layer and cause corrosion to happen faster (Broomfield, 2006).

When chlorides originate from the environment, the duration of the initiation phase will depend on the rate of penetration of the chlorides from the concrete surface to the embedded steel (Mangat & Molloy, 1992). Several parameters, including those related to the concrete itself (cover depth, quality of the cover), and environmental factors (temperature, moisture conditions) influence the time it takes for the chloride ions to reach the steel (Yong Ann & Song, 2007). However, it is not enough for chlorides to just reach the reinforcing steel, but rather a critical quantity of chlorides is required in order for corrosion to be initiated. This critical quantity is commonly termed the chloride threshold value and is a crucial parameter in service life prediction models (Otieno, 2008).

2.2.1.2 Bound chlorides

Not all chlorides are free to move through the concrete and hence be involved in initiating corrosion. Some chloride ions that enter the concrete pore solution are bound by hydration products leaving only some ions to be mobile and move through the concrete cover. Through this phenomenon the corrosion initiation can be delayed or prevented entirely in the following two ways:

- Glass & Beunfeld (1997) showed that bound chlorides are less effective in promoting depassivation of steel, while only free chlorides dissolved in the pore solution are considered to initiate corrosion. Therefore, any chlorides that are bound in the concrete are effectively

eliminated as a contributor towards attaining a critical chloride concentration (Nilsson et al., 1996).

- Furthermore, chloride binding extracts chloride ions from the pore solution resulting in a reduction in the overall pore solution's concentration. This leads to changes in the chloride concentration gradient in concrete which is the driving force for ionic diffusion. By slowing down the movement of chloride ions through the concrete, the time to the initiation of the steel is extended. (Nilsson et al., 1996) (Glass, Hassanein & Beunfeld, 1997).

2.2.1.3 Chloride threshold values

Concrete's chloride threshold value is understood to be the content of chloride necessary at the level of steel to sustain breakdown of the passive film and is usually expressed as the percentage of total chloride content relative to the weight of cement (Yong Ann & Song, 2007).

A considerable amount of research has been done to establish the chloride threshold value without a consensus being reached. The large variation on published threshold values could be as a result of differences in testing, sample preparation or exposure conditions. Some chloride threshold values vary by over an order of two magnitudes and range from 0,02 (Trejo & Pillai, 2003) to 3,0 (Lambert, Page & Vassie, 1991) percent chlorides by weight of cement. Despite this, conservative chloride threshold values such as 0,2 or 0,4 percent per weight of cement has been used to predict the service life of reinforced concrete (Yong Ann & Song, 2007). Figure 2 - 3 shows a typical chloride profile distribution in concrete, with higher concentrations of chlorides evident at the concretes surface and less concrete deeper in the concrete. A conservative chloride threshold of 0,4 % by weight of cement as determined by Pullar-Strecker (2002) is also indicated on the figure.

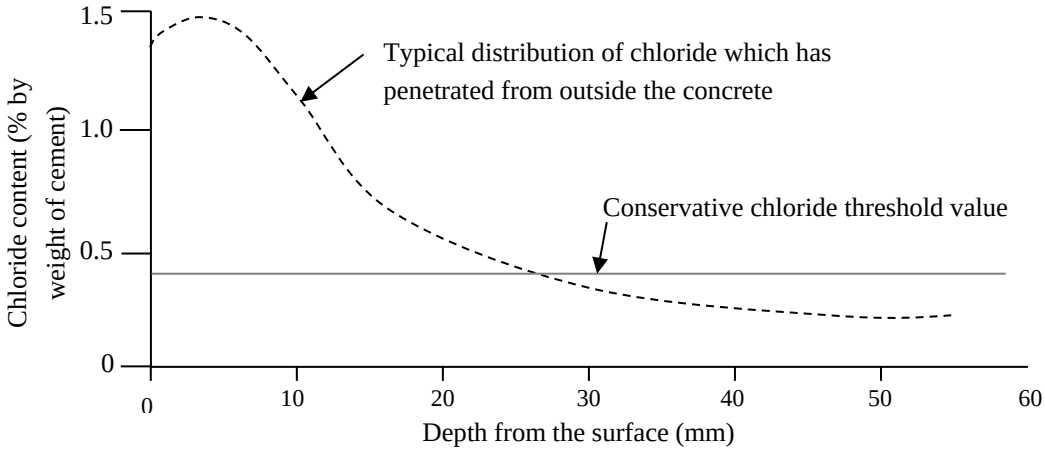

Figure 2 - 3: Typical chloride profile of concrete in the marine environment (Pullar-Strecker, 2002)

2.2.2 Propagation of corrosion

The propagation phase of corrosion commences once corrosion has been initiated and can be associated with minor or major corrosion damage to the embedded steel. As rust products start to accumulate on the surface of the reinforcing steel, the resulting volume expansion generates internal stresses leading to cracking of the concrete cover. The corrosion rate is initially slow and highly dependent on the oxygen and moisture availability (Hunkeler, 2005). However, as a by-product of the corrosion reaction, water is produced and develops a self-sustaining chemical reaction. With sufficient supply of water and oxygen, the rate of corrosion will accelerate, ultimately leading to widespread cracking and spalling of the concrete cover.

2.2.2.1 Conditions for corrosion of steel

There are four conditions that need to be fulfilled in order for corrosion of steel in concrete to occur (Table 2 - 2). The first condition is that the anodic reaction i.e. the dissolution of Fe^{2+} ions must be allowed to proceed. This only occurs at the end of the initiation period once sufficient chlorides have penetrated to the level of the steel. The second and third condition are fulfilled during the propagation phase and involve the availability of oxygen and moisture respectively. Without sufficient oxygen available at the level of the reinforcing, the cathodic reaction cannot proceed, while without sufficient moisture the conductivity between the site of the anode and cathode would be poor. The fourth condition is that there must be a metallic connection between the cathode and the anode, so that electrons resulting from the dissolution of the steel can flow from the anode to the cathode. This requirement is almost always met in reinforced concrete structures.

Table 2 - 2: Conditions for corrosion of steel in concrete (after Hunkeler, 2005)

Condition for corrosion of steel	Condition fulfilled, if:
Anodic reaction possible	The passive layer of the steel breaks down and depassivation of the steel occurs. This is caused when the ingress of chloride into the concrete reaches a critical level
Cathodic reaction possible	Oxygen as the driving force of the corrosion process is available at the interface of the steel in a reasonable amount
Flux of ions between anodic and cathodic site	The environment between the site of the anodic reaction and the site of the cathodic reaction permits good conduction (owing to moisture and high levels of chlorides)
Flux of electrons	There is a metallic connection between the anodic and cathodic sites. Condition fulfilled for most reinforced concrete structures

2.2.2.2 Limiting factors in corrosion propagation

Taking due cognisance of the four conditions in Table 2 - 2, it is clear that eliminating or mitigating any one of these factors will prevent significant corrosion from occurring. If one considers these four components to be connected in a circuit, it is evident that the flow of electrons (i.e. current) through each component must be the same and are limited only by that of the component with the smallest current (Bertolini et al., 2013).

$$I_{overall\ corrosion} = I_{anode} = I_{cathode} = I_{steel} = I_{electrolyte} \quad (2\text{- }3)$$

Where $I_{overall\ corrosion}$ = the overall corrosion current; I_{anode} = current of the anode; $I_{cathode}$ = current of the cathode; I_{steel} = current of the steel; and $I_{electrolyte}$ = current of the electrolyte.

Raupach (1996) makes use of a similar concept to model corrosion of steel as an electric circuit that considers the combined resistance of the four components. It can be seen from Figure 2 - 4 that the component with the highest resistance will govern the rate at which corrosion proceeds.

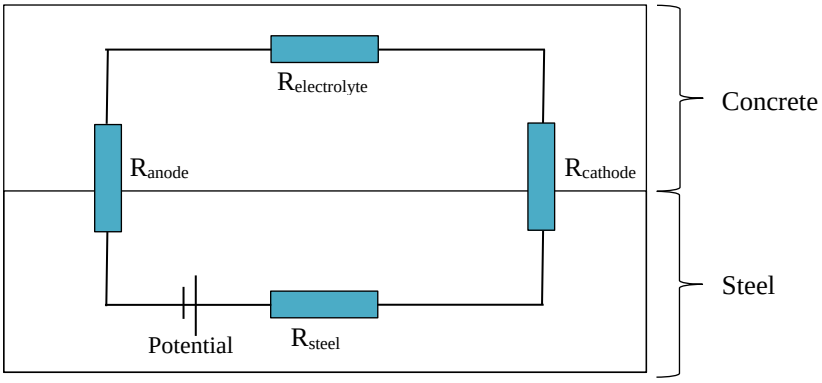

Figure 2 - 4: Simplified model showing equivalent electric circuit (After Raupach, 1996)

The resistance of the metal is generally insignificant in reinforced concrete structures ($R_{steel} \approx 0$). Nonetheless, the three remaining components can individually thwart the corrosion rate as follows (Stansbury & Buchanan, 2000).

(i) Anodic control: During anodic control, the dissolution of steel into ions and electrons is inhibited by the presence of a passive layer. Anodic control usually occurs during the initiation phase of a structures service life ($R_{anode} \approx \infty$).

(ii) Cathodic control: Under cathodic control, the lack of available oxygen is limiting the rate of the cathodic reaction. This happens in the propagation phase and is usually as a result of a poor oxygen diffusion coefficient ($R_{cathode} \approx \infty$).

(iii) Electrolytic control: Also referred to as Ohmic control, this occurs when the resistance of the concrete connecting the anode and the cathode is very high. As a consequence there is opposition to the flow of ions within the concrete and the overall corrosion current is significantly reduced ($R_{electrolyte} \approx \infty$).

2.2.2.3 Microcell and macrocell corrosion

Corrosion can occur in the form of microcells or macrocells (Broomfield, 2006). Macrocell corrosion involves the separation of the small anodic region from the large cathodic region. This type of corrosion is commonly associated with local corrosion of steel and is characterised by pitting corrosion (Poursaee, 2016). Furthermore, macrocell corrosion is frequently found in structures near the coast, where a high concentration but uneven distribution of chloride ions is found. The high moisture content of concrete generally associated with high chloride levels, results in low electrical resistivity of the concrete. This leads to ease of movement of ions and allows further separation of the cathode and anode from each other (Miyazato & Otsuki, 2010).

In microcell corrosion, the anodic and cathodic sites are adjacent to each other (Otieno 2008) and normally occurs in concrete with carbonation induced corrosion. When the resistivity of concrete is high, for example the case of concrete with a very low moisture content, there also frequently microcell corrosion. This is because the concrete's high resistance to the flow of ions impedes the movement of hydroxyl ions. Corrosion in microcells are characterised by uniform loss of the steel cross-section over a large area of the reinforcing. A schematic diagram of the microcell and macrocell is show in Figure 2 - 5.

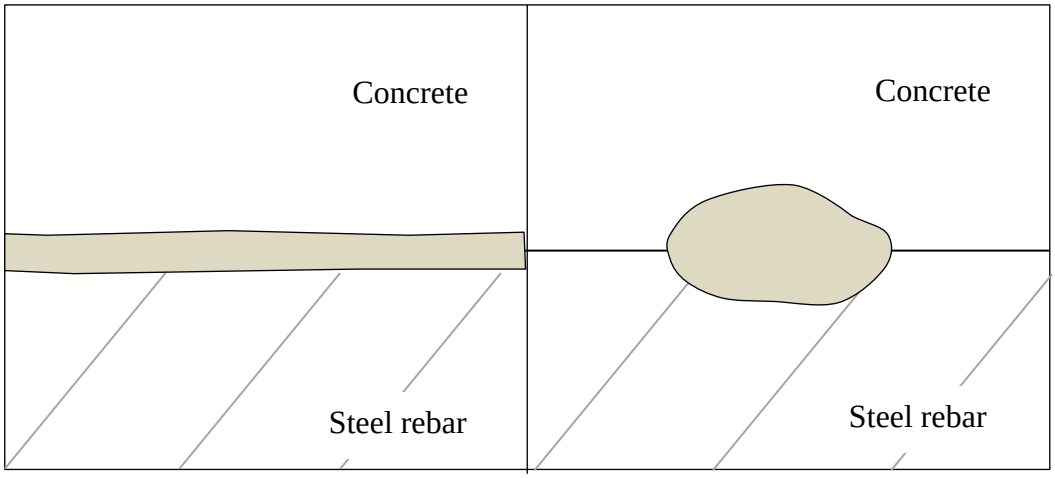

Figure 2 - 5: Schematic diagram showing (a) microcell and (b) macrocell corrosion (After Zhang, Castel & Francois, 2009)

It should be emphasized that there is often both microcell and macrocell corrosion occurring in a structure simultaneously. While macrocell corrosion is easily measured, microcell corrosion is not and is often neglected. A study by Hansson, Poursaee & Laurent (2006) showed that in Ordinary Portland Cement (OPC) concretes, the microcell corrosion value was almost double that of the macrocell corrosion value. Furthermore, concrete made using fly ash and slag was shown to have negligible macrocell corrosion inferences compared to that of the microcell corrosion because of the concretes high resistance. These results show the need to be cautious when interpreting macrocell results to indicate the corrosion rate, particularly for concrete containing extenders.

2.2.2.4 Prediction of corrosion propagation

In the past, most service life models such as Mackechnie's (1996), Duracrete (1998), and ClinConc (Tang, 2008) considered the time to corrosion initiation to define the end of the service life of a corrosion-affected structure. However, it has been established that even at the end of the initiation phase, the structure still has sufficient residual structural capacity to maintain serviceability for years. For example, the study of the corrosion process of a 17 year old reinforced concrete structure showed that the load bearing capacity was still adequate during a significant portion of the propagation period, and that this time should be included as part of the limit state (Vidal, Castel & François, 2007). Service life models should be redefined to incorporate accurate predictions of the propagation period so that remedial action is taken when it is necessary. This leads to cost effective and more informed maintenance strategies, while still also taking into consideration sustainability concerns. Accurate predictions of the propagation phase are still being developed, as the duration of this phase is complicated and depends on the corrosion rate, which in turn is influenced by many other factors (Discussed in Section 2.3). This concept is relevant to this study, whose understanding of the influence of exposure environments on the corrosion rate can be used as a further step in accurately modelling the time of the propagation period.

2.2.2.5 Limit state indicators

It is crucial to divide the propagation phase into sub-phases so that an appropriate indicator can be used to define the limit state of a structure. Some possible corrosion damage indicators that can be considered are given by Otieno, Beushausen & Alexander (2010) and include the following (i) loss of steel cross-sectional are, (ii) loss of steel-concrete interface bond, (iii) appearance of corrosion-induced cracks, (iv) loss of members ultimate load capacity, or (v) loss of flexural stiffness.

Different corrosion indicators are more relevant for certain types of corrosion. In carbonated concrete, there tends to be more widespread and uniform corrosion, often resulting in early cracking of concrete with a comparatively small reduction in the steel cross-sectional area. While in contrast, chloride contaminated concrete frequently results in pitting corrosion and a rapid loss of the steels cross-sectional area (Hunkeler, 2005). Accordingly, for structures more vulnerable to carbonation induced corrosion the appearance of cracks is a suitable limit state indicator, whereas the loss of the steel cross-sectional area is a suitable indicator for structures exposed to chlorides.

According to Nimmo & Hinds (2003) uniform corrosion accounts for around 30% of structural failures while localised corrosion accounts for approximately 70%. This is attributed to the fact that localised corrosion often shows no visible signs of damage, and results in ductility problems (Cairns et al., 2005). In spite of this many sources (Chen, Baji & Li, 2018) (Ahmad, 2003) (Cabrera, 1996) state that cracking of the concrete cover is the most useful indicator for assessment of structural integrity.

2.3 Review of selected factors affecting the corrosion rate

Once corrosion has been initiated as a result of sufficient chloride presence in the concrete, the propagation of corrosion depends on factors that influence the adequate supply of corrosion-sustaining agents (such as oxygen and water). These factors include, but are not limited to, variations in cover depth and cover quality, resistivity of concrete, temperature of environment other environmental considerations. These factors all influence the oxygen and moisture supply to the reinforcing steel in concrete and are strongly interrelated.

2.3.1 Exposure classes

The marine environment is typically divided into four main exposure zones, as shown in Figure 2 - 6. The exposure environment has a large influence on the rate at which corrosion propagates and affects the transport mechanisms of corrosion promoting agents such as oxygen, moisture and chlorides. The subsequent sections will briefly discuss the effect of the submerged, tidal and splash zones which are relevant to this study.

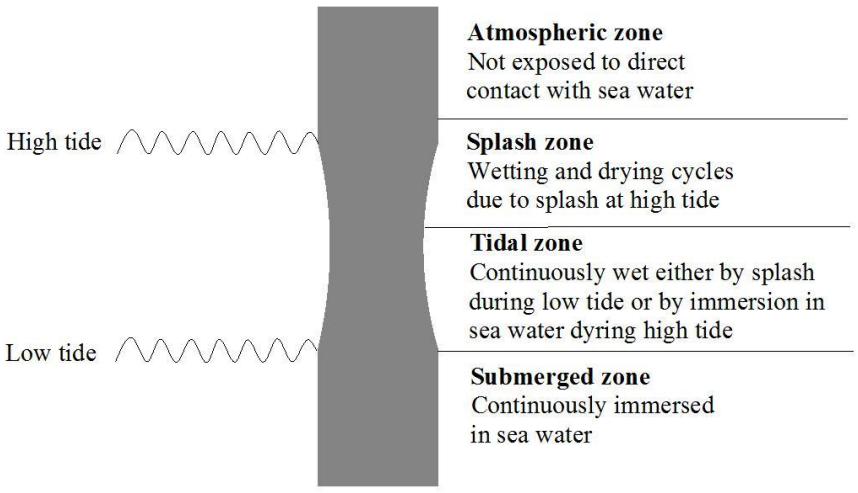

Figure 2 - 6: Marine exposure zones for concrete structures (after Mehta, 1991)

2.3.1.1 Splash zone

The splash zone (sometimes termed splash/spray zone) is located above the high tide level where wave action causes moisture to splash onto the concrete surface, as shown in Figure 2 - 6. Both the chloride penetration and the subsequent corrosion of steel are relatively rapid within this region (Polder & de Rooij, 2005). The penetration of chlorides in the splash zone is exacerbated by partial drying of the cover concrete which leads to capillary absorption of sea water. This leads to greater chloride concentrations than expected in the submerged zone. Furthermore, the unsaturated condition of the cover concrete creates a condition where sufficient dissolved oxygen is available to initiate and sustain corrosion of steel. Adequate moisture is also available to the concrete as a result of the exposed splashing which allows for easy flow of ions within the concrete, while not limiting the influx of oxygen. The availability of both chlorides, moisture and dissolved oxygen leads to a fairly rapid corrosion rate of structures in the splash zone. A more complex review of the transport mechanisms of moisture and chloride ions in concrete in the splash zone is given in Section 2.4.

2.3.1.2 Submerged zone

The submerged zone can be classified as concrete permanently submerged and saturated to the level of the steel, and is generally considered to have the least severe corrosion potential. When permanently submerged, the pore structure within the concrete cover is saturated and the chloride ions move to the level of the steel through diffusion. These conditions provide sufficient chlorides to depassivate the embedded steel (Polder & de Rooij, 2005). However, for concrete that is fully submerged, less chloride enters the concrete than the tidal zone as the dominant transport mechanism is diffusion (which is slower than capillary suction in the case of the tidal zone). This is largely the reasoning for why the submerged zone is classified as less severe than the tidal zone. Further details on the transport mechanisms of chloride and moisture in the submerged zone are given in Section 2.4.

In addition, availability of oxygen required for steel to corrode is also considered. Oxygen has a substantially lower diffusion coefficient in saturated concrete than it does in air. The diffusion of oxygen through air can be up to 4 orders of magnitude higher than the diffusion of oxygen through water. Because concrete in the submerged zone is saturated, the oxygen will have a low rate of diffusing into the concrete. Gjorv (1972) also stated that the concentration of oxygen in air is 210ml/litre, whereas the maximum concentration of dissolved oxygen in seawater is only 5-10 ml/litre. This shows how concrete that has fully saturated pores in the submerged zone has lower oxygen concentration, which minimises it’s availability for the electrochemical corrosion process at the cathode.

It is evident from the mechanisms given above, that although there may be considerable levels of chlorides at the level of the steel, the availability of oxygen is a limiting factor for steel corrosion in the submerged zone.

2.3.1.3 Tidal zone

The tidal zone is the region between the high and low tides. High and low tides occur on average twice a day, separated by approximately 12 hours and 25 minutes (Mehta, 1991). However, this value varies from season to season and from region to region. As a result, marine structures experience cycles of wetting and drying each day, which may also have an associated heating and cooling effect. The cyclic effect of wetting and drying has been found to accelerate durability-related problems, as it can lead to the accumulation of species such as chlorides in the concrete.

When concrete is partially dry, and exposed to salt water, the salt water will penetrate the concrete through capillary suction. The concrete will continue to absorb the salt water until saturation or until there is no more salt water available (as in the case of low tide). A chloride concentration gradient will then develop in the concrete. If the external environment is dry, moisture evaporates from the pores of the concrete, leaving behind crystal salt precipitate. When the concrete is wetted again (during high tide), salt crystals precipitates get reabsorbed, and more chloride ions are carried further into the concrete. As the concrete undergoes more cycles of wetting and drying, the chlorides penetrate deeper into the concrete. The chloride concentration at the level of reinforcing also increases with each cycle (Figure 2 - 7). In this way, corrosion initiation is facilitated when the critical chloride concentration is reached at the level of reinforcing. Details of the transport mechanisms of chlorides in the tidal zone are given in Section 2.4.

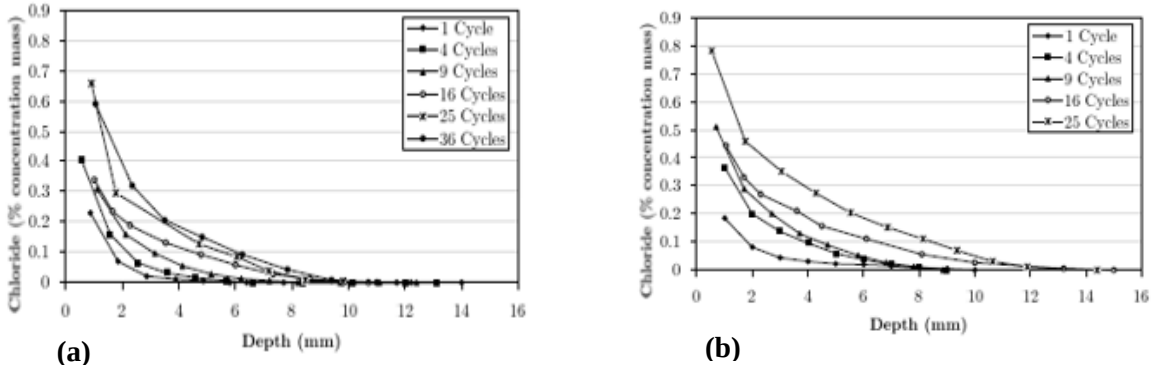

Figure 2 - 7: Chloride profiles for concrete exposed to (a) 6 hours wetting and 18 hours drying and (b) 6 hours wetting and 66 hours drying (Hong, 1998)

However, chlorides are not the only requirement to facilitate the process of corrosion. Oxygen availability at the level of the steel also needs to be taken into consideration especially for the propagation phase. As concrete dries out, and the pores become less saturated, the diffusivity of oxygen into the concrete is increased and hence it can sustain the corrosion process. This increase in availability of oxygen would therefore result in higher levels of corrosion in concrete in the tidal zone. This is the premise of the statement that RC structures subject to wetting and drying exposure are more prone to deterioration due to steel corrosion than those permanently submerged.

Nonetheless, recent research by Hong (1998) and then Golden (2015) has suggested that the duration of wetting and more importantly drying times of concrete has a significant effect on the corrosion rate of steel within the concrete. The research shows that for shorter drying times, the rate of corrosion is significantly reduced, especially for concretes with low quality and high cover depths. This effect is seen to a lesser extent in high quality concretes (which is probably owing to the denser pore structure which effectively slows the transport of moisture and oxygen even at longer drying times) (Scott, 2004). A possible explanation for this is that for short drying times, the concrete cover does not have sufficient time to dry to the level of the steel. The pores surrounding the steel are therefore still partially or fully saturated with water. Consequently, where the concrete in the tidal zone experiences short drying periods, the steel will be oxygen deprived, and corrosion will be stifled. This means that the concrete in the tidal zone would theoretically perform as if it were permanently submerged (provided sufficient cover depth and cover quality).

2.3.2 Cover depth

Cover depth affects the ease of transport of ions, oxygen and moisture into the concrete cover layer, and is therefore important in governing the corrosion rate of steel in concrete. SANS 10100-2 recommends that a minimum cover depth of 65 mm be used for concrete with surfaces in contact with seawater, which is in accordance with the recommended cover of between 50 and 70 mm given by Alexander & Mackechnie (2003). While increasing the concrete cover is crucial for mitigating corrosion, concrete cover that exceeds 75 mm has been found to result in cracking, which is detrimental to corrosion (Otieno, 2014).

Alexander & Mackechnie (2003) state that the cover depth is more significant in reducing the corrosion rate than the quality of the concrete cover. For example, even if the quality of the concrete cover is excellent, insufficient cover depth can be harmful. This is contrary to findings by Otieno (2017), who showed that in cracked concrete, the concrete quality has a dominating role over the cover depth on corrosion rate. The effect of the cover depth and cover quality on the availability of oxygen and moisture content is discussed in further detail below.

2.3.2.1 Influence on oxygen availability

Reducing the concrete cover thickness lessens the path that oxygen is required to travel from a structure's surface to the embedded steel (Hawkins & McKenzie, 1996). The faster that oxygen can travel to reinforcing in concrete, the more oxygen is available for the cathodic reaction to proceed. Bentur, Diamond & Berke (1997) showed the effect of increasing the cover depth from 20 to 50 mm on oxygen availability. The study proposed that at a RH of 60%, the oxygen diffusion flow rate decreases from 1,1 to 0,1 g/cm^2/year as a result of the increase of the cover depth by 30 mm.

The effect of the cover depth on the availability of oxygen availability is also shown in Figure 2 - 8. It can be depicted from the graph that given the corrosion rate is cathodically controlled, higher

cover depths result in a reduction in the availability of oxygen (Scott & Alexander, 2007). The graph also proposes that if there is sufficient oxygen available to allow for high corrosion rates (possibly at a cover of less than 10 mm), the resistivity of OPC will become the controlling factor in the corrosion rate.

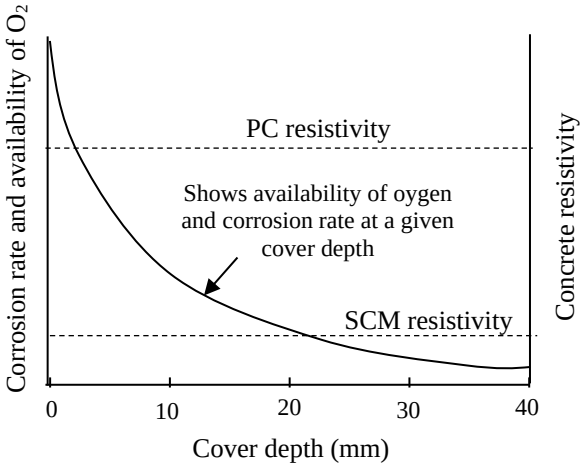

Figure 2 - 8: Schematic of relationship between corrosion rate, O_2 availability and resistivity (After Scott & Alexander, 2007)

2.3.2.2 Influence on moisture content

It can be seen from Figure 2 - 9.a that the severity of the moisture loss in concrete is dependent on the exposure conditions. Concrete directly exposed to sunlight and wind will dry out faster than concrete sheltered from the elements. Seasonal changes that influence the temperature and climate also heavily influences the rate at which concrete dries. However, Hunkeler (2005) showed that short term environmental factors cannot influence the internal water content of concrete beyond a depth of 60 mm, while the water content can be influenced by as much as 30% within the first 10 mm of concrete cover. Figure 2 - 9.b shows that sufficient cover depth could prevent drying to the level of the reinforcing thus inhibiting corrosion propagation by limiting the movement of oxygen. This graph further reinforces the concept that longer drying times lowers the moisture content at any cover depth.

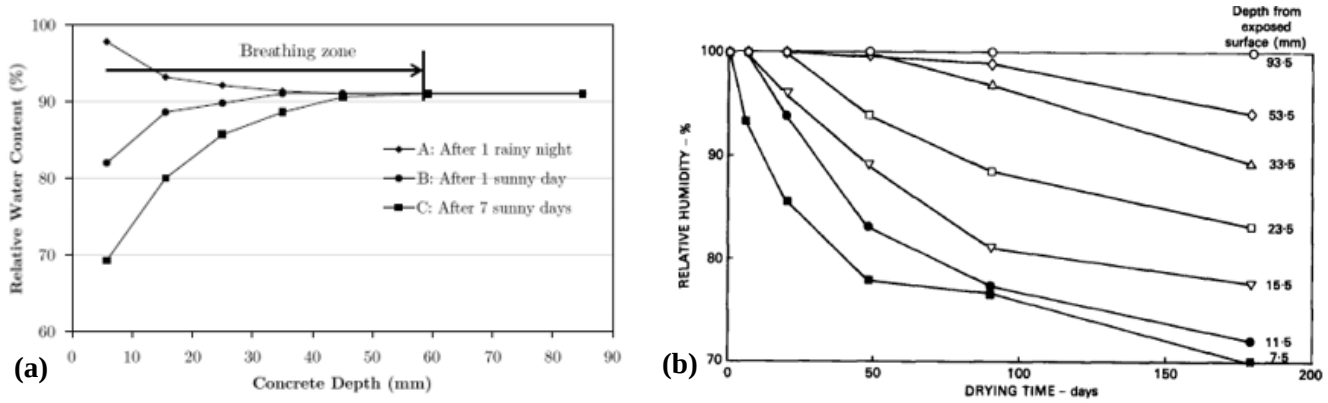

Figure 2 - 9: (a) Water content in cover concrete (Hunkeler, 2005) and (b) reductions of relative humidity at different cover depths (Parrott, 1988)

2.3.3 Concrete quality

Decreasing the water-binder ratio (w/b) or the inclusion of SCM's (supplementary cementitous material) is known to result in refinement of the pore structure, which has benefits of decreasing permeability of concrete to oxygen, moisture and chlorides. As SCM's are not pertinent to this study their influence will not be discussed further, but rather focus is given to the influence of w/b ratio on corrosion rates.

Mangat, Khatib & Molloy (1994) show how a lower w/b ratio results in lower corrosion rates. The highest corrosion rate of 2,16 µA/cm^2 was found in the concrete sample with w/b of 0,76, while the lowest corrosion rate of 0,13 µA/cm^2 was found in a sample with a much lower w/b ratio of 0,45. It is important to note that the sample that incurred the lowest corrosion rate has a higher chloride content than some of the samples with very high corrosion rates. This result reflects the notion that chloride content alone cannot be considered to be the only parameter indicating a structures service life (Otieno, 2008).

Table 2 - 3: Effect of w/b ratio on corrosion rates (Mangat, Khatib & Molloy, 1994)

w/b ratio	Cement content (kg/m^3)	I_{corr} (µA/cm^2)
0,45	430	0,13
0,58	430	0,65
0,76	430	2,16

2.3.3.1 Influence of w/b ratio on oxygen availability

In a similar way that increasing the cover depth leads to an increase in oxygen's travel path, the quality of the concrete cover also influences the ingress of oxygen. As early deterioration of concrete structures is strongly tied to the ingress of unfavourable agents, it follows that the quality

of the concrete cover strongly influences reinforced concrete's durability. Concrete considered to be of poor quality is associated with highly inter-connected pores that facilitate the rapid ingress of moisture and oxygen. A denser cement paste matrix leads to a reduction of the permeability of concrete and hence the movement of oxygen through the cover layer (Polder, 1996). This denser pore structure can be achieved through the inclusion of SCM's (supplementary cementitious materials) and/or a reduction of the w/b ratio.

Scott (2004) showed that the cover depth is more effective at reducing the corrosion rate via oxygen control than the quality of the cover. This was found to be true only for concrete that was cathodically controlled, such as concrete made from OPC.

2.3.3.2 Influence on moisture content

Ryu, Ko & Noguchi (2011) showed how the desorption isotherm is affected by w/b ratio of the concrete (Figure 2 - 10). These two graphs show the moisture content of uncracked specimens for w/b ratio of 0,3 and 0,6 respectively after drying for a given period of time. Two observations can be made, one of which is that of the moisture profile of both concretes before the start of drying is different. The relative moisture content of the concrete with w/b ratio of 0,6 is 100% at all depths except 90 mm, while the moisture content of the concrete with a w/b ratio of 0,3 does not reach 100% at any depth that exceeds 10 mm. This can be attributed to water struggling to permeate into the deep parts of the concrete with such a dense pore structure. The second observation is that of the change in relative moisture content upon drying. The reduction in the relative moisture content is smaller in the concrete with w/b ratio of 0,3 than the concrete with a w/b ratio of 0,6. This can be attributed to (i) the less amount of free evaporable water in the concrete and (ii) a more refined pore structure which inhibits the escape of moisture (Nilsson, 2002).

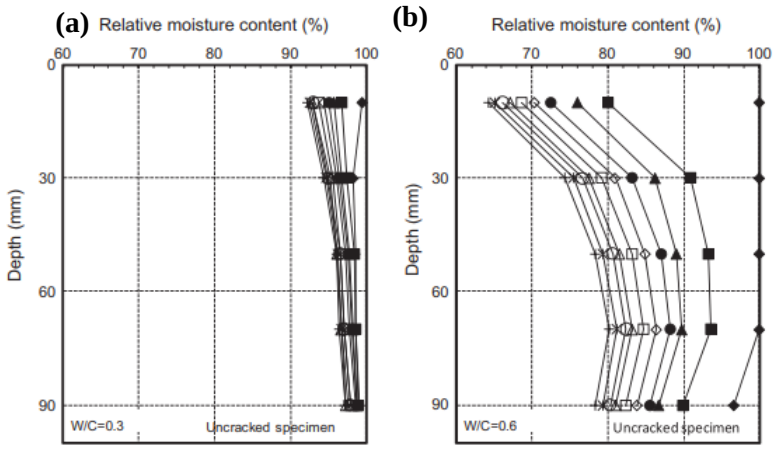

Figure 2 - 10: Moisture content profiles at different cover depths for (a) uncracked and (b) cracked specimens (Ryu, Ko & Noguchi, 2011)

2.3.4 Temperature

Tuutti (1982) showed that increase the temperature from 0 to 20ºC could increase the corrosion rate by a factor of 10. It is widely understood that an increase in temperature results in faster movement of the corrosion ions, leading to an increase in the corrosion rate. However, this effect is found to only be significant at RH greater than 85%, in which case the diffusion of oxygen is inhibited quite notably anyway (Soroka, 2003). This effect can be seen in Figure 2 - 11 that shows the amount of rust formed under different temperature conditions. Apart from the obvious effect temperature has on the anodic reaction, there is also research that attributes the effect of temperature change directly to oxygen availability and moisture content within concrete (See section 2.3.4.1 and 2.3.4.2 below).

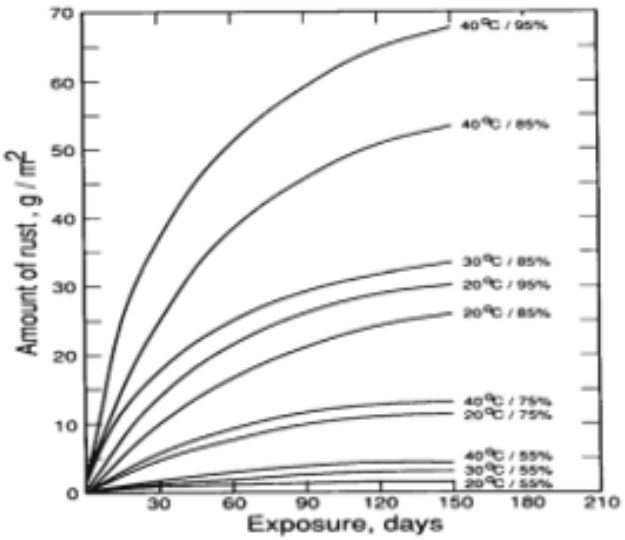

Figure 2 - 11: Corrosion current as a function of outdoor Temperature and RH (Soroka, 2003)

2.3.4.1 Effect of temperature on oxygen availability

Revie & Uhlig (2008) argue that an increase in temperature allows more of the dissolved oxygen in the concrete pores to be allowed to participate in the corrosion reaction at the steels surface. Although the corrosion rate increases with an increase in oxygen concentration present, there is a critical concentration of oxygen above which corrosion is actually reduced (Uhlig, Triadis & Stern, 1955). It is this critical concentration of oxygen that is increased with a rise in temperature, and the rationale behind Revie & Uhlig (2008) findings. This concept is illustrated in Figure 2 - 12 where an increase in temperature results in a higher critical concentration of dissolved oxygen.

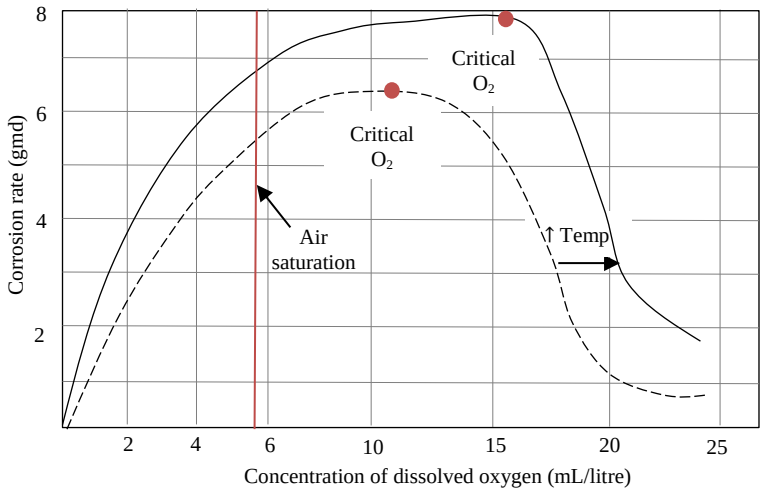

Figure 2 - 12: Effect of oxygen concentration on corrosion of mild steel in distilled water (After Uhlig, Triadis & Stern, 1955)

For a given oxygen concentration, the corrosion rate can double when subjected to a 30ºC rise in temperature (Skaperdas & Uhlig, 1942). However, in a closed system, above 80ºC the reduction in oxygen solubility in water eventually overshadows the accelerating effect of temperature alone, and the corrosion rate is remarkably reduced.

2.3.4.2 Effect on moisture content

Ryu, Ko & Noguchi (2011) showed that temperature had the biggest impact on the behaviour of drying of moisture in concrete. Given all other factors are equal, concrete dries out more rapidly at higher ambient temperatures. Since moisture transfer in the tidal zone is achieved through mechanisms of capillary tension, the effect of temperature on capillary tension (or sorption) is pertinent. Research by Ono (2005) has shown that as temperature increases, the physical properties of water will change (i.e. the surface tension of liquid water decreases). Considering the knowledge that surface tension plays a big part in influencing surface adsorption, it is evident that a lower surface tension (from a higher temperature) makes it easier for water to escape concrete. Additionally, higher ambient temperatures are also associated with an increased rate of evaporation of water in the surface pores of concrete (Ye, Nanguo & Xianyu, 2017). This has a knock on effect in that the concentration gradient present as a result of evaporation then facilitates diffusion of internal water towards the surface of concrete.

Hundt & Kantelberg (1978) investigated the effects of temperature on the desorption of moisture from concrete (Figure 2 - 13). It can be seen how at a fixed relative humidity the water content of the concrete decreases with increasing ambient temperature. In other words, there is comparatively greater moisture retention in concrete at a temperature of 20ºC than concrete at 70 ºC. Similar observations were made by Burgh & Foster (2017) through their investigation of both adsorption and desorption isotherms. Moreover, it can be observed that the change in moisture retention value as a result of an increase in temperature has a greater effect on concrete at relative humidity's of between 50 and 90%, and less of an effect on concrete with very high (>90%) or low (<40%) relative humidity's (Poyet & Charles, 2009).

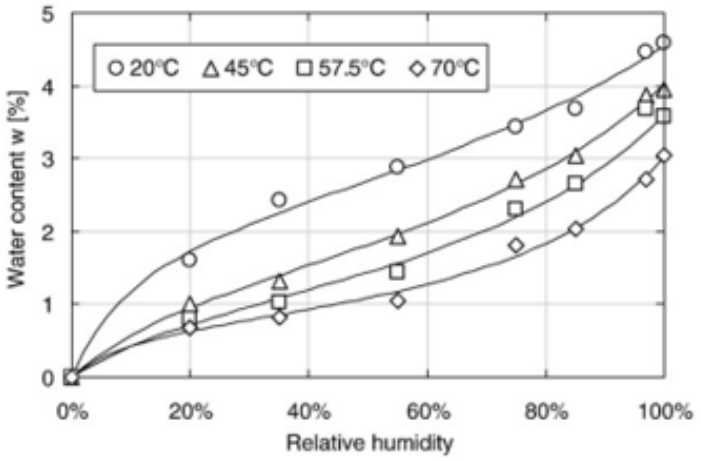

Figure 2 - 13: Desorption isotherm of a concrete for four temperatures (Hundt & Kantelberg, 1978)

Temperature has also been shown to have an effect of the adsorption of moisture, although the effects are significantly less than that of drying concrete. Higher temperatures result in a slower influx of moisture into concrete, particularly at RH of between 60 and 90% (Daian, 1988).

2.3.5 Chloride ion concentration

As already established, chloride ions are required in sufficient concentrations at the level of the steel in concrete in order for corrosion to be initiated. Although research tends to focus on the effects of chloride ions on the initiation of corrosion, the chloride concentration can also have appreciable effects on rate of corrosion propagation. These include but are not limited to the influence on the moisture of concrete and oxygen availability.

2.3.5.1 Effect of chloride content on oxygen availability

It has been shown that the concentration of salts in the concrete influences the solubility of oxygen. As the chloride concentration increases, the solubility of oxygen progressively decreases and hence stifles the corrosion rate. This is shown in Figure 2 - 14.a as the solubility of oxygen halves as the salt concentration increases from 0 to approximately 2,5 N (Foley, 1970).

At the same, the increased chloride ion concentration leads to an increase in the conductivity of concrete which encourages corrosion to proceed (Bamforth, 1994). Considering the dual effect of an increasing chloride ion concentration, there is an optimum value at 0,5 N (Normality) where the corrosion rate is maximised. This can be seen in Figure 2 - 14.b where the value of 0,5 N corresponds to the highest corrosion weight loss. Given the same temperature, any chloride concentration value higher than 0,5 N leads to a reduction in oxygen solubility and hence decreases the corrosion rate.

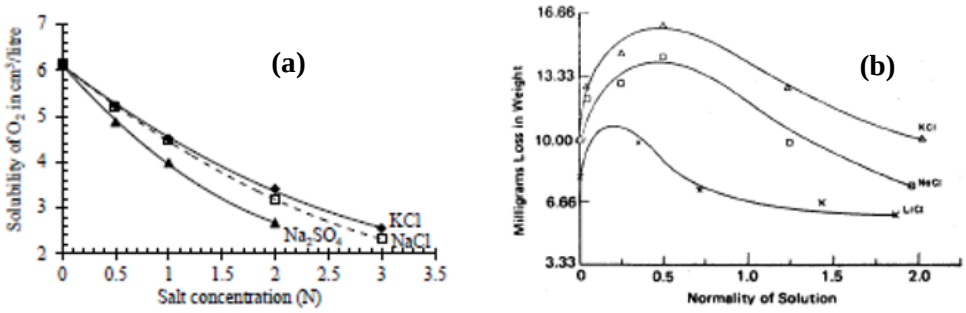

Figure 2 - 14: Effect of (a) salt concentration on oxygen solubility and (b) chloride content on corrosion rate (Foley, 1970)

2.3.5.2 Effect on moisture ingress

Chlorides can increase the moisture content due to hygroscopic properties of salts such as NaCl and $CaCl_2$. Hygroscopy is the affinity of salts to attract water molecules from the surrounding environment. The amount of moisture that is retained by salt is dependant firstly on the concentration of salt in concretes pores and secondly on the relative humidity of the surrounding environment Persons (2009). The effect of retaining extra moisture within the concrete could be favourable or detrimental for the corrosion rate, depending on the exposure conditions. For example, in the tidal zone where the duration of time the concrete is exposed to air is relatively small, the hygroscopic effects of chloride ions can inhibit the drying of the concrete cover and actually impede corrosion propagation. However, in cases where the concrete is not cathodically controlled, the increased moisture levels can foster further ingress of chloride ions through the bulk transfer of water and in this way hasten the process of corrosion initiation. (Hall, Najim & Keikhaei, 2012)

2.3.6 Concrete resistivity

The higher the resistivity of concrete the more difficult it is for ions to move through the concrete cover. When the resistivity is high enough, it can actually limit the maximum corrosion rate that can be obtained. This is more likely to occur in concrete that uses SCM's (supplementary cementitious materials) and not in PC concrete structures (See Figure 2 - 8) (Scott, 2004).

Apart from the inclusion of SCM's, there are other factors that can influence the resistivity of concrete, including w/b ratio, degree of pore saturation, presence of chlorides, and temperature. However, the degree of pore saturation or moisture content has been found to be the most influential factor (Hornbostel, Larson & Geiker, 2013). Results from Gjorv, Vennesland & El-Busaidy (1977) show that when the degree of saturation was reduced from 100 to 40%, the resistivity of concrete increased by 3 orders of magnitude.

Nevertheless, Saleem et al. (1996), who evaluated the effects of chloride concentrations on the resistivity of concrete, indicated that the presence of chlorides can also be highly influential in

increasing the electrical conductivity of concrete. This is particularly true at a high salt concentration (even in near dry concrete) where it was shown that the degree of pore saturation actually had little influence on the electrical resistivity of concrete.

2.3.7 Oxygen availability

Oxygen availability is influenced by a variety of factors such as relative humidity, chloride ion concentration, cover depth and concrete quality (some of which have already been discussed in detail). This section addresses the transport of oxygen with respect to different moisture conditions.

2.3.7.1 Diffusion of oxygen in relation to moisture conditions

The mechanisms for movement of a gas (such as oxygen) through a porous medium can be highly complex, and is governed mostly by diffusion. The diffusion of oxygen can vary significantly owing to the moisture content of the concrete. Oxygen moves rapidly through empty pores while water saturated pores can reduce the rate of flow of oxygen into the concrete by a factor of four (Hunkeler, 1995).

While there is limited research on the effect of moisture content on oxygen availability (especially on this relationship in the tidal zone), some attempt has been made by Hunkeler (1994) to relate these parameters (Equation 2-3)

Diffusion of Oxygen

$$D(0_2, C) = \frac{D_L\left(\frac{D_L}{D_W} - W\frac{D_L}{D_W} + 3\right)}{2W\left(\frac{D_L}{D_W} - 1\right) + \frac{D_L}{D_W} + 2} \quad (2\text{-}3)$$

Where $D(0_2, C)$ = oxygen diffusion coefficient in concrete in cm^2/s; D_L = oxygen diffusion coefficient in dry concrete in cm^2/s; D_W = oxygen diffusion coefficient in wet concrete in cm^2/s; W = water content of the concrete in % volume.

The relationship between oxygen availability and moisture content is also shown in Figure 2 - 15(a), where it can be seen that at a moisture content of 0%, a maximum oxygen diffusion coefficient of 28×10^{-4} cm^2/s is achieved. The figure also reflects that at a moisture content exceeding 75%, the diffusion coefficient of oxygen through concrete is approximately 0.

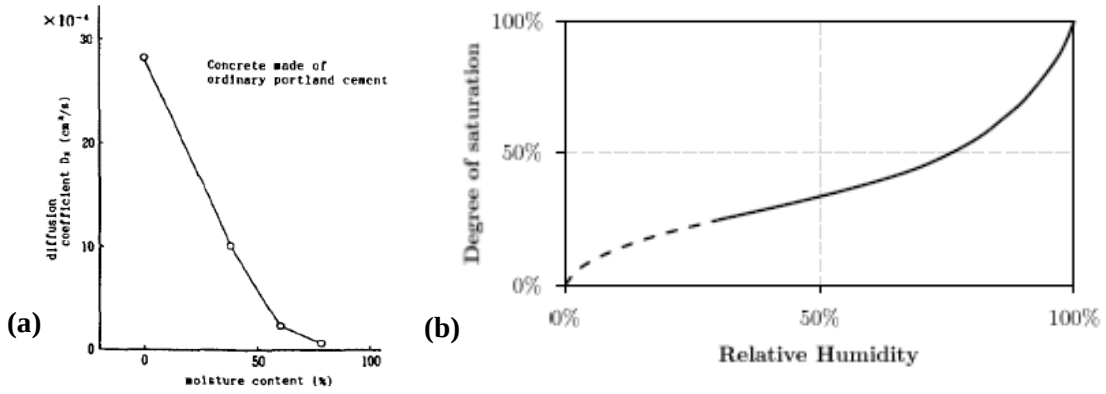

Figure 2 - 15: Graph showing (a) diffusion coefficient of oxygen at different moisture contents and (b) relationship between degree of saturation and relative humidity (Bertolini et al., 2013)

However, it is very difficult to measure moisture content in concrete owing to the complex microstructure and a lack of appropriate test methods. For this reason, the internal relative humidity is often measured and then a moisture condition inferred. For concrete in equilibrium with the environment, the relationship between relative humidity and moisture levels is a relatively simple one as can be seen Figure 2 - 15(b). However, this relationship is not suitable for concrete in the tidal zone, as the conditions in the tidal zone are constantly changing and concrete equilibrium with the external environment is not usually achieved.

A study which embedded steel in concrete and exposed the samples to different drying durations and relative humidity's (or moisture condition) showed that cathodically controlled corrosion rates are most predominantly influenced by the relative humidity itself. The study showed that concrete quality and cover depth also affect the oxygen availability in concrete, but to a far lesser extent than the relative humidity. Andrade, Alonso & Garcia (1990).

2.3.7.2 Oxygen availability in submerged conditions

When concrete is partially saturated with water from its environment and the majority of the pores are filled, oxygen accessibility can become limited at the steel surface. Substantial research has presented on influence of moisture conditions on the oxygen availability. Raupach (1996) showed that if concrete is permanently water-saturated, as long as the residual oxygen is consumed first, the corrosion rate becomes negligible. It was also shown that for long wetting cycles, the influence of oxygen on the corrosion rate is also predominant. This is true as long as (i) the concrete in the vicinity of the steels surface is saturated, and (ii) the residual oxygen has been consumed in the cathodic process. Once removed from submerged conditions the length of time for the corrosion rate to increase to its pre-wetting value depends on the thickness and quality of the concrete cover.

Hunkeler (1994) contributes to this idea further by assessing the time required for the residual oxygen to be depleted due to corrosion under constant submersion. As seen by Figure 2 - 16, for a w/b ratio of 0,5 and a cover of 40 mm it takes approximately 28 days for all the oxygen to be

consumed at the cathode and the corrosion rate to be consumed. This complies with Andrade, Alonso & Garcia (1990) whose findings also show that when using an electrochemical technique, the amount of oxygen available at the steel exceeds that required for the corrosion process, even up to day 30 of being submerged.

Hussain (2011) impressed corrosion currents in concrete under different environmental conditions and attempted to quantify the limiting corrosion current under water. Experimentally, the limiting corrosion current of concrete under saturated conditions was determined to be 0,04 µA/cm^2. Furthermore, it was also stated that oxygen is a limiting factor in corrosion when the concrete has a relative humidity of 95% and has sufficient cover depth and quality.

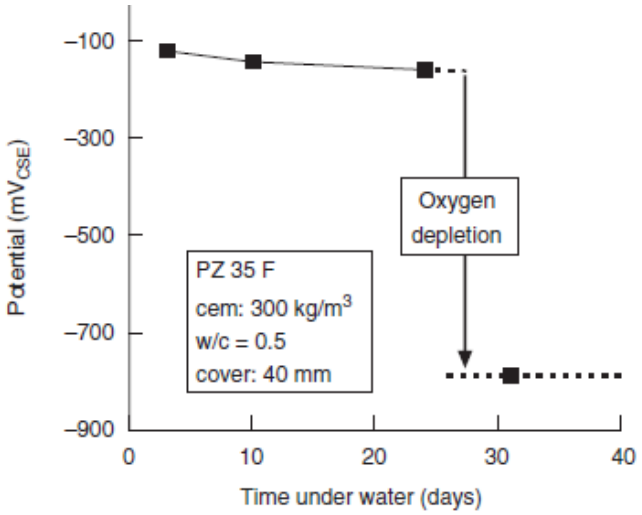

Figure 2 - 16: Potential change in concrete immersed under water (Hunkeler, 2005)

2.3.7.3 Anaerobic corrosion conditions

Once the residual oxygen at the steel has been depleted, the corrosion can continue to occur under conditions known as ‘anaerobic’ conditions. The type of corrosion product that is formed when the supply of oxygen is restricted is commonly referred to as black rust. Black rust is less expansive and can reduce the cross-section significantly more before causing delamination of the concrete cover, which makes it difficult to detect when performing any maintenance checks on a structure (O’Donovan et al., 2013).

There is not much literature available on how the corrosion of steel proceeds under anaerobic conditions, with only a few theories available on the corrosion mechanisms. These include cathodic depolarisation theory (Iverson, 1996), formation of iron/iron sulphide galvanic cells (King & Miller, 1971), and corrosive and volatile phosphorous compounds (Kuang et al., 2007) to name but a few. It is clear from the wide range of theories available that the corrosion mechanisms of black rust is still not well understood.

2.3.8 Marine fouling

Concrete structures in the marine environment are almost always covered in marine growth and include organisms such as sponges, sea weed, barnacles, mussels and tube worms (McLeish, 1994). The type of marine organisms and the thickness of the growth is influenced by factors such as dissolved oxygen concentration, water temperature, depth and light intensity to name but a few. In a study of a 34 year old structure in the marine environment, it was found that the tidal zone had a wide distribution of algae while barnacles were found in concrete in the lower tidal region. Mussels were attached from the mid tidal zone level and extended towards the concrete splash and spray zone (Taywood Laboratories, 1980).

There are conflicting ideas about the effects marine growth has on the durability of concrete. Fouling of concrete surfaces has been shown in some research to have a detrimental effect on the durability of concrete structures (Gaylarde & Morton, 1999). Acids and metabolites produced by microorganisms attached to the concrete surface have the ability to increase the concretes porosity and therefore decrease durability (Allsopp, Seal & Gaylarde, 2004). One study has shown that concrete with high porosity values are more vulnerable to the effects of microorganisms, while smooth and rounded fine aggregates can also favour the development of aquatic organisms (Hughes et al., 2013). While there is lots of research available on the mechanism of attack different aquatic organisms have on concrete, there is not much information available that quantifies these in terms of potential durability.

In contrast, research shows that the influence of marine growth on durability is favourable. Sharp (1979) states that a layer of marine fouling can act as a barrier to the diffusion of oxygen and chloride ions into the concrete layer. Similarly, investigation into the durability of the Tongue Sands Tower in Thames estuary United Kingdom, showed that a layer of marine growth on the surface of the structure actually inhibited corrosion (Taywood Laboratories, 1980). This could be accredited to a lower rate of drying in concrete with a marine layer which further inhibits the movement of oxygen. A study by Maruya et al (2003) showed that concrete covered in marine organisms (particularly barnacles) has a high resistance to chloride induced reinforcement corrosion. This was attributed to the basal membrane of a barnacle being significantly more dense than concrete, thereby slowing the ingress of chloride and oxygen. Apart from slowing the entry of oxygen and chloride ions, the marine organisms might also reduce the concentration of dissolved water in surface pores by utilising available oxygen in its own metabolic processes.

In addition to the positive effect marine organisms can have, there is also a strong interaction between cement hydrates and the ions in seawater. This leads to a 30 µm thick layer of brucite on the surface of concrete, which causes a significant reduction in the permeability of concrete. This effect only occurs on concrete immersed in real seawater and not in simulated sodium chloride solution (Beunfeld & Newman, 1986).

Although there is overwhelming evidence that the attachment of marine organisms to concrete is beneficial for the durability of a structure, the organisms are often removed as they are considered undesirable aesthetically (Kawabata, Kato & Iwanami, 2012). Furthermore, marine organisms are removed from the surface of concrete when inspections are carried out, as they impede visual investigations (Port and Airport Research Institute, 2007).

2.4 Transport mechanisms for corrosion inducing species

Deleterious substances move into concrete through the pores of the cement matrix, the interfacial transition zone (ITZ), and micro-cracks at a rate that is governed by the transport mechanisms involved. The characteristics of the transport process depends fundamentally on the extrinsic environmental conditions (such as temperature and ambient humidity), and the intrinsic properties of concrete like microstructure and binder type. Considering structures in the marine environment are exposed to a diverse range of environmental conditions (submerged, tidal, and splash and spray zones) it follows that structures in these varying microclimates will experience different mechanisms of ingress. Most often, the transport process of agents into concrete is a combination of various mechanisms. Understanding how damaging substances penetrate into the concrete cover under different exposure conditions is essential to further understanding and preventing corrosion, and developing durability assessment measures. In this section, the transport mechanisms of both moisture and chloride ions within each exposure zone are described.

2.4.1 Moisture transfer

It is essential for engineers studying corrosion to be able to predict the moisture movement in concrete in response to varying environmental conditions. The reason for this is that most deterioration mechanisms are a direct consequence of the movement of deleterious substances into concrete with moisture transfer (Fagerlund, 1975). Consequentially, the rapidity of moisture ingress into and out of concrete strongly influences the rate at which corrosion can proceed. Despite the importance of understanding moisture transport in concrete, the complexities of moisture particle's interaction with concrete pores and various environmental factors makes quantifying moisture movement a difficult task. Pores partial saturation during wetting is one of the many reasons moisture transfer is such a complicated concept (Ryu et al., 2007). However, some attempts have been made to elucidate the behaviour of moisture in concrete, although most studies focus on the initial drying conditions of concrete in relation to drying shrinkage (Powers, 1965)(Feldman, 1968).

2.4.1.1 Moisture ingress mechanisms

Moisture enters into concrete through transport mechanisms; permeability, diffusion, sorption, and wick action. Some exposure zones have more prevalent mechanisms, although a combination of any mechanisms can occur. Figure 2 - 17 presents (a) a summary of the transport mechanisms found in different exposure conditions, as well as (b) the approximate distribution profile of

moisture in different exposure zones. It can be seen that the moisture content of concrete is highest in the submerged zone and becomes subsequently less with increasing height of the concrete. Details of these various mechanisms of moisture ingress are discussed below.

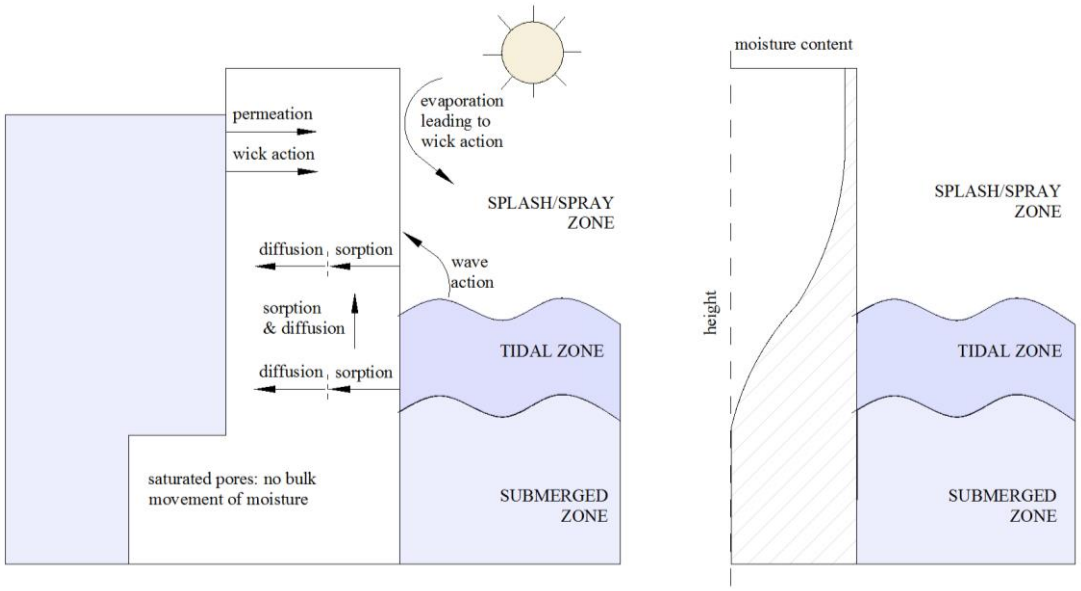

Figure 2 - 17: Schematic of (a) moisture transport mechanisms (after Alexander 2016) and (b) moisture content depth (after Hunkeler, 2005)

(i) Submerged zone

When concrete is immersed in water for a long period of time, the pores become fully saturated with water. In this state, there is no bulk movement of moisture through the concrete pores except for some of the dissipating wave energy from the tidal zone that can force water into surface pores. Andrade & Alonso (1996) investigated the time to saturation for concrete immersed in water for long periods of time and found that the core of a concrete with a w/b of less than 0,6 was only partially saturated.

Another mechanism of moisture ingress in the submerged zone is permeation, which is caused by a pressure difference that can occur if one side of a structure is submerged while the other side remains exposed to air (Claisse, 2005). The permeability of concrete is a measure of the rate of transfer of moisture under a pressure gradient, and is a function of the properties of the permeating fluid, the microstructure of the concrete and concretes moisture state (Ballim, Alexander & Beushausen, 2009). The penetration of a fluid as a result of permeation is given by Equation 2-4, which is governed by Darcy's Law.

Darcy's Law

$$v = \left(\frac{k}{n}\right)\left(-\frac{dh}{dx}\right) \tag{2-4}$$

Where v = velocity of the fluid in m/s; k = permeability coefficient in m/s; n = porosity of the concrete in %; h = hydraulic head in m; and x = distance parameter in m.

(ii) Splash zone

In the splash zone, water transfer into concrete can occur through a mechanism called water vapour diffusion which occurs when there is a higher concentration of water vapour in one region of concrete than another. In order to achieve a concentration equilibrium water will move from the pores at the surface with a high vapour concentration towards the internal pores with a low vapour concentration (Claisse, 2005). The modelling of the rate of diffusion of a fluid into a permeable materials such as concrete is given by Equation 2-5.

Fick's 1st law of diffusion

$$J = -D_{eff}\left(\frac{dC}{dx}\right) \quad (2\text{-}5)$$

Where J =mass transport rate in g/m^{2}s; D_{eff} = effective diffusion coefficient in m^2/s; C = concentration of fluid (g/m^3); and x = distance in m.

Sorption, which is discussed in more detail in the next section, is another transport mechanism which occurs in the splash zone. Sorption is prevalent only in the surface layer of concrete and occurs either when large quantities of water are splashed onto the concrete surface, or when the concrete is exposed to rain. Given a specific set of circumstances, wick action can also facilitate the movement of moisture into concrete. When one concrete face is exposed to drying while one face is wetted with an ionic solution, wick action can occur. The evaporation of moisture on the drying side facilitates the ionic solution to be drawn into the concrete member and deposits moisture deeper into the concrete (Hearn, Hooten & Nokken, 2006).

In the splash zone, the depth of the moisture ingress into concrete is a strongly related to the quantity of water splashing on the element. Moreover, the cover zone of concrete has significant amounts of moisture while the internal regions remain relatively dry.

(iii) Tidal zone

Moisure enters the tidal zone through many mechanisms such as diffusion, sorption, permeation and wick action, each of which performs under a unique set of conditions. Moisture enters the surface layer of concrete through capillary suction (or sorption). Sorption describes the rate of movement of the wetting front into dry or partially dry concrete. The surface tension of water encourages molecules to adhere to the pore walls and in this way penetrate into the concrete. The sorptivity is affected mainly by the pore size distribution, pore connectivity and degree of saturation (Ballim, Alexander & Beushausen, 2009). Sorptivity is considered uni-directional and can be described by Equation 2-6.

Sorptivity

$$S = \frac{Fd}{M_{sv} - M_{s0}} \quad (2\text{-}6)$$

Where S = sorptivity in mm/√hr; F = slope of mass loss against the square root of time (g/h^2); d = specimen thickness in mm; M_{sv} = vacuum saturated mass in g; and M_{s0} = dry mass (g) at the initial time of 0 sec.

The interior region of concrete has a different transport mechanism. At high tide, a pressure head is created between the concrete and the environment allowing moisture to permeate into the concrete. Moisture can also diffuse into concrete as a result of the different vapour concentrations in the outer and inner regions of the concrete. As discussed before diffusion occurs as a result of a concentration gradient. Additionally, the moisture concentration difference between the submerged and tidal zones can facilitate the diffusion of moisture up the structure.

Wick action is another mechanism that performs a significant role in the ingress of moisture in the tidal zone .This occurs frequently in relatively thin concrete members (such as a pile), where only one side is exposed to sunlight on one face.

2.4.1.2 Drying of concrete

In a porous material such as concrete, moisture (which includes water in the liquid or vapour phase) is transported from the wetter part to the drier part (Comings & Sherwood, 1934). The movement of water out of concrete is driven by the same transport mechanisms that transfer water into concrete. Moisture movement takes place mainly as the (i) diffusion of water vapour in air-filled pores with vapour pressure gradient as the driving force or as (ii) capillary suction (or sorption) in water-filled pores with a water pressure gradient as the driving force. As there is no drying phase for concrete in the submerged zone drying mechanisms for the submerged zone cannot be presented below.

(i) Tidal zone

At the onset of drying, the liquid water in near saturated pores exits the concrete through capillary action, which is the movement of liquid under capillary pressure from surface tension. As such, the movement of moisture in the tidal zone is dominated by capillary transport of water (Figure 2 - 18(a)). As the drying time proceeds, the water in the pores become discontinuous and capillary desorption is only present in the regions where the water is still continuous (Figure 2 - 18(b)). As shown in Figure 2 - 18(c), in pores where the water is not continuous, the main transport process is diffusion (Maekawa, Ishida, & Kishi, 2008).

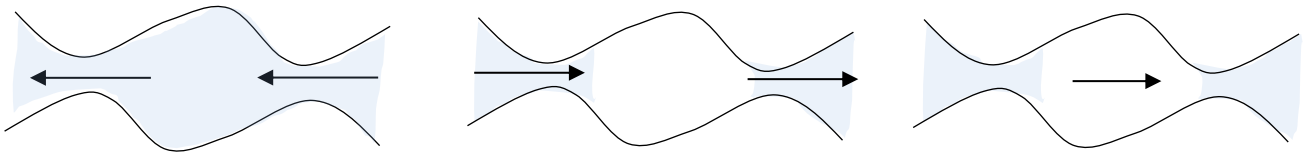

(a) Capillary absorption **(b)** Capillary desorption in saturated pores **(c)** Diffusion in unsaturated pores

Figure 2 - 18: Illustration of capillary transport and evaporation-condensation in a single pore (After Maekwa, Ishida & Kishi, 2008)

It is acknowledged that the moisture content in concrete is different in the both the wetting and drying stages. Figure 2 - 19 shows how once the wetting period ends and the concrete starts to experience drying (i.e during low tide in a tidal cycle), some of the water is retained in the concrete (Šelih, Sousa & Bremner, 1996). In other words, the rate of water ingress is greater than the rate of water exiting the concrete. One theory known as the ink-bottle effect provides a possible reason for this (Zhang, 2015).

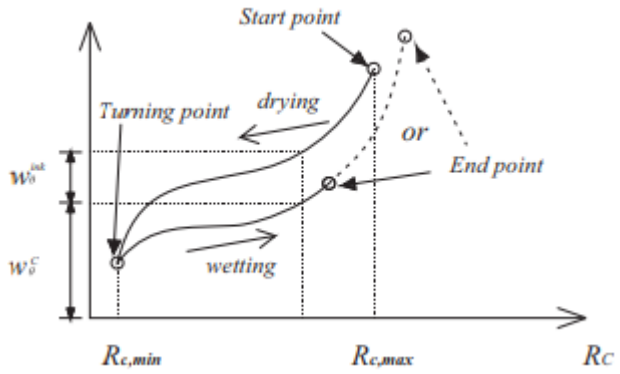

Figure 2 - 19: Ink-bottle effect of entrapped water in concrete (Šelih, Sousa & Bremner, 1996)

As illustrated in Figure 2 - 20, the ink-bottle effect proposes that when a saturated pore is connected to external empty pores only through pores of a smaller dimension, the saturated pore cannot empty (Burgh, Foster & Valipour, 2016). This occurs when water in the neck of the pore evaporates first and then evaporation continues in the internal pore. However, when the humidity reaches a value below that of the external empty pore, the internal pores remain filled with liquid and the structures exhibits drying retardation (Duroudier, 2016). This concept of pore blocking mechanisms is one of the explanations for the difference in curves for the sorption and desorption isotherms of porous mediums.

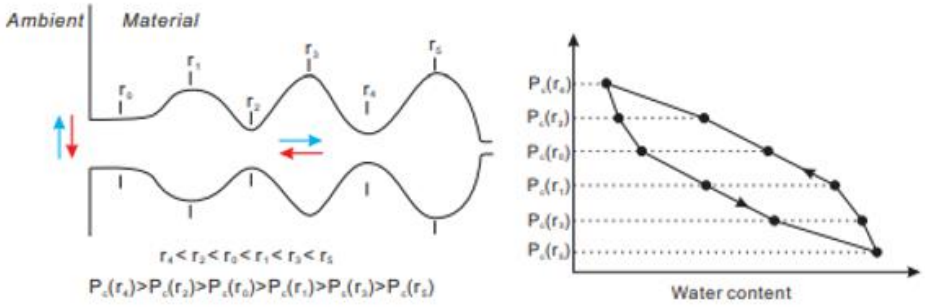

Figure 2 - 20: Ink-bottle effect showing (a) moisture transport in one pore and (b) the corresponding sorption isotherm (Burgh, Foster & Valipour, 2016)

It is insufficient to just have knowledge of the moisture distribution in concrete in order to assess the corrosion potential of reinforced concrete structures. Rather, it is important to consider the time dependant change of moisture over time, i.e. the rate of change of moisture of the moisture distribution. This is particularly true for concrete in the tidal zone that only has a finite amount of time for which to dry to the level of reinforcing. Figure 2 - 21 shows desorption isotherms for a disc of cement paste that is left to dry at 25ºC for a duration of 170 days (Grudemo, 1976). It can be seen that even at 5 weeks (35 days) the concrete has still not reached equilibrium and more evaporable water continues to escape from the concrete (Nilsson, 1980). Although it can be seen that it takes a significant amount of drying time for concrete to reach equilibrium with the environment, this information does not indicate the distribution of moisture in the concrete cover, which is crucial when attempting to understand corrosion results.

(ii) Splash zone

While there is not sufficient research about how the splash and spray zone dries, the effect of rainfall on the drying of concrete can be used to understand how splashing from wave's influences the moisture distribution in concrete.

Andrade, Sarria & Alonso (1999) investigated the effects of rainfall in concrete both exposed directly to rainfall and sheltered from the rain. For concrete that is exposed directly to rain, concrete is absorbed at the concrete surface and penetrates through capillary action into the interior of the structure.

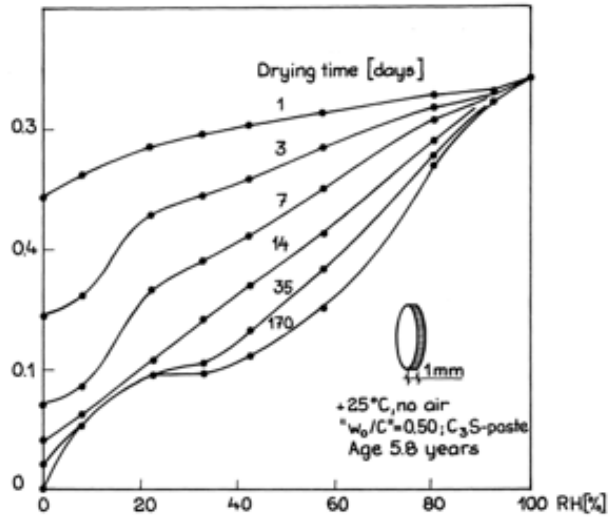

Figure 2 - 21: Time course at determining the desorption isotherm for C_3S paste (Grudemo, 1976)

When drying out, some water at the concretes surface evaporates out while some diffuses further into the concrete towards the steel (not all the water that entered during the rain period is dried out again). This is represented in Figure 2 - 22(a) where the concrete is saturated throughout the rain cycle and starts to lose moisture slowly at the onset of drying. The gradient of this drying curve is

dependent on many factors including, the temperature, season, time of the day, and the properties of the concrete itself. In the case of concrete that is sheltered from the rain (Figure 2 - 22(b)), the internal moisture content may increase due to the increase in relative humidity that occurs in the environment. This influence is small and can sometimes be negligible. These same mechanisms of drying can be applied to concrete that has direct and indirect exposure to spray from wave action.

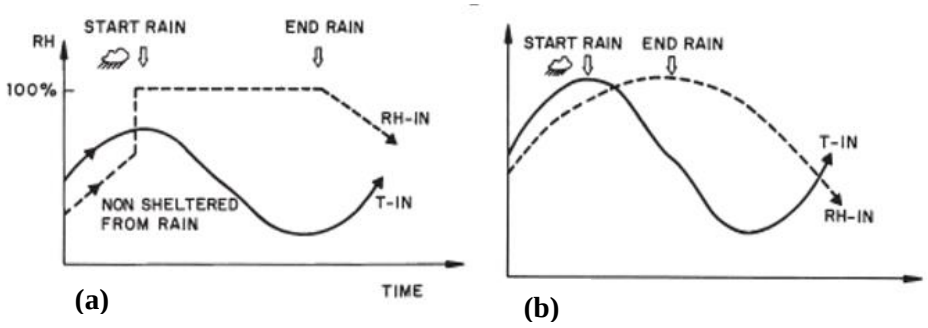

Figure 2 - 22: Change of RH in concrete due to rain in (a) unsheltered concrete and (b) sheltered concrete (Andrade, Sarria & Alonso, 1999)

Ryu, Ko & Noguchi (2011) also studied this concept and proposed that the duration of rainfall is more crucial in keeping concrete at high moisture contents than the amount of rainfall. This infers that structures exposed to prolonged periods of rainfall will have a lower drying rate than structures exposed to short bursts of heavy rainfall. With regards to the effect of splash and spray of seawater, this research also implies that concrete exposed to large waves that occur infrequently dries faster than concrete exposed to low intensity but constant splashing.

Apart from the research mentioned above, there is not enough data on the quantity of splashing needed to effectively influence the relative humidity (or moisture content) at the level of the steel.

2.4.2 Chloride ingress

The deposition of chlorides into concrete occurs as a consequence of movement of moisture into the concrete pores. Hence chlorides can ingress through bulk movement of ionic solution, ionic diffusion, and convection. Each zone is exposed to different conditions and thus chlorides will follow different transport mechanisms of ingress. In the submerged zone chloride will ingress primarily through diffusion; while chloride in the tidal and splash zones will enter through a combined absorption, diffusion and convection process. Figure 2 - 23 provides (a) a summary of the various chloride ingress mechanisms that can occur, as well as (b) an approximation of the change in chloride content with height.

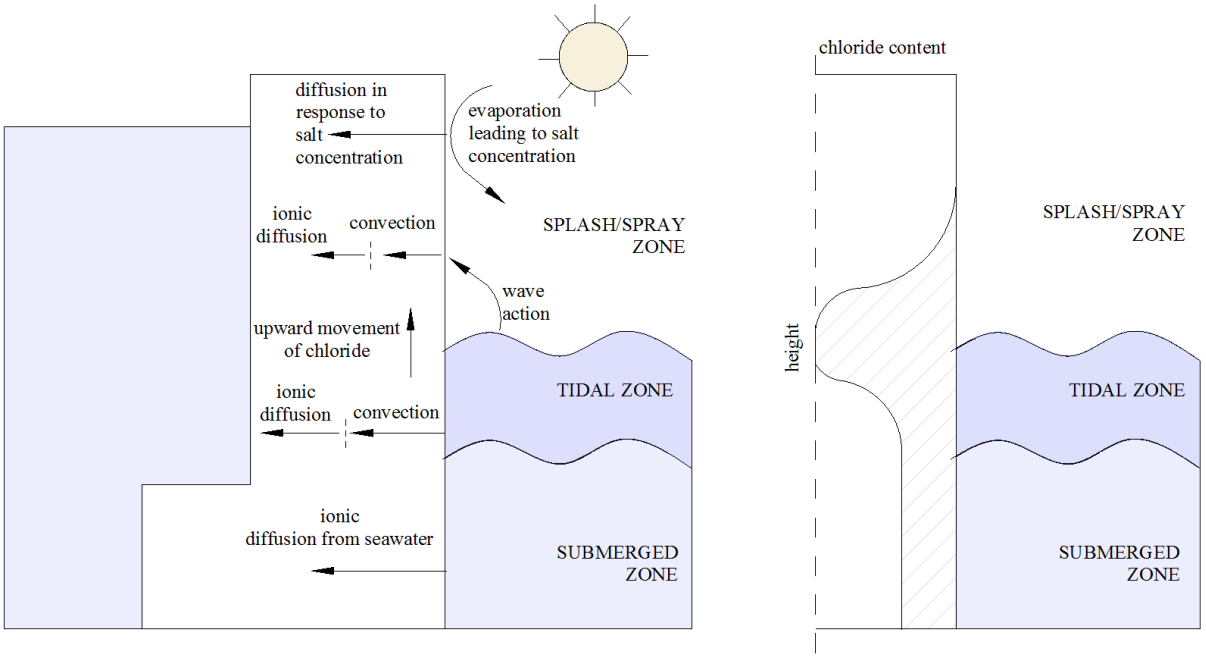

Figure 2 - 23: Schematic of (a) chloride transport mechanisms (after Alexander 2016) and (b) chloride content depth (after Hunkeler, 2005)

2.4.2.1 Submerged zone

As water in concrete pores are static under submerged conditions, chloride ions cannot ingress with the bulk movement of water (as water is not moving), but rather manoeuvres through the water itself (McLeish, 1994). This process is referred to as ionic diffusion and comprises dissolved chlorides moving from a high concentration to a low concentration along a water path in order to achieve equilibrium. Fick's second law of diffusion Equation 2-7 describes the rate of change of chloride concentration with respect to time and distance, and can be used to estimate the chloride profiles in concrete (Hellmich & Bernhard, 2015). The profile produced using Fick's law shows that chloride content increases with time of exposure but decreases with depth into the concrete.

Fick's 2nd law of diffusion

$$\frac{dc}{dt} = D\frac{d}{dx}\left(\frac{dc}{dx}\right) \tag{2-7}$$

Where dc/dt = mass transport rate in kg/m^3; D = diffusion coefficient in m^2/s; c = concentration in kg/m^3; and x = distance in m.

The solution to this differential equation is given by Crank's error function (Equation 2-8). Constraints for this solution are that: no chlorides are present in the concrete at the start of exposure ($C_x = 0$ at $t = 0$); and the concentration of chlorides on the surface of the concrete remains constant throughout duration of exposure ($C_x = C_s$ at $x = 0$). (Kim et al., 2016)

Crank's error function solution

$$C_{x,t} = C_s\left[1 - \text{erfc}\left(\frac{x}{2\sqrt{D_a t}}\right)\right] \quad (2\text{-}8)$$

Where $C_{x,t}$ = concentration of chlorides at depth x and time t in mass %/cement; C_s = chloride content on the concrete surface in mass %/cement; erfc = error function; x = depth into concrete in m; D_a = apparent chloride diffusion coefficient in m^2/s; and t = time in s.

2.4.2.2 Splash zone

In the splash zone, the primary mechanism of chloride into concrete is through convection. This describes the transport of chlorides into concrete due to the bulk movement of water, which typically occurs in partially saturated or unsaturated concrete. The movement of chloride ions is most rapid in concrete that is experiencing moisture ingress caused by capillary suction of sea water i.e. convection (see Section 2.4.1).

Convection

$$\left(\frac{\partial C}{\partial t}\right) = -v\left(\frac{\partial^2 C}{\partial x^2}\right) \quad (2\text{-}11)$$

Where v = the average velocity of a vector fluid in m^3/sec; C = the concentration of solute at depth x after time t.

Chloride ions can further diffuse into concrete as a result of the chloride concentration gradient. Wick action can also lead to the deposition of chloride ions when moisture evaporates from within the concrete member. This can occur when the one face is 'damp' from sea spray and shielded from the sun, and the other face is dry owing to evaporation. Wick action can increase the rate of chloride beyond that predicted by diffusion (Hearn, Hooten & Nokken, 2006).

2.4.2.3 Tidal zone

As shown for the submerged zone, the primary mechanism for the transport of chloride ions is diffusion. Comparatively, chloride ingress in the tidal zone can be described by a combination of both convection and diffusion. The concrete's exposure to cycles of wetting and drying results in dissolved chlorides moving in and out of the surface layer of concrete with the bulk movement of seawater (i.e. convection). This convection zone does not follow Fick's Second Law of diffusion and can be of varying depths (Δx) depending on the drying properties of the concrete (Figure 2 - 24). Beyond the convection zone, chloride ions manoeuvre into concrete primarily through diffusion as a result of the concentration gradient between the convection zone and deeper regions of the concrete.

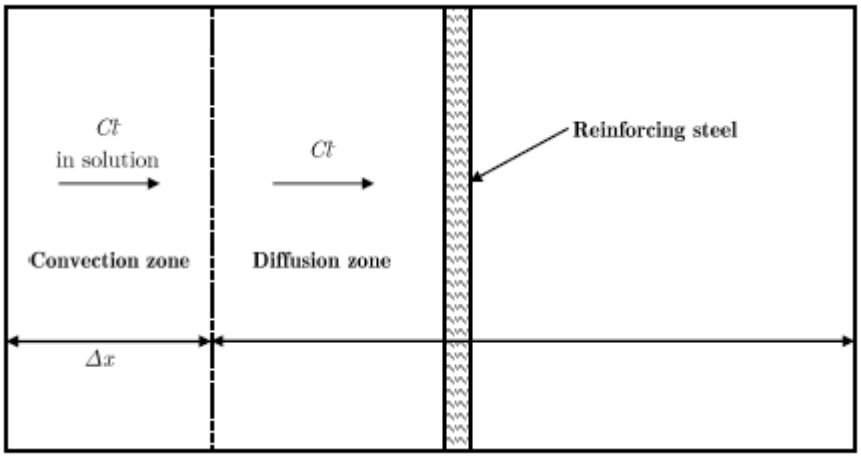

Figure 2 - 24: An illustration of the convection and diffusion zones controlling the ingress of chlorides under cyclic wetting and drying (Golden, 2015)

Gehlen (2000) modelled the ingress of chlorides in the tidal zone (Equation 2-9) by incorporating the concept of a convection zone into Crank's existing error function solution.

Gehlen's error function solution

$$C_{x,t} = C_i + (C_{\Delta x} - C_i) \cdot erfc\left[1 - \frac{x - \Delta x}{2\sqrt{D_a(t)\left(t - t_{exp}\right)}}\right] \quad (2\text{-}9)$$

Where $C_{x,t}$ = chloride concentration at depth x and age t in wt %cement; C_i= initial chloride background level in weight % cement; $C_{\Delta x}$ = chloride content at depth Δx in wt %cement; D_a = time dependent apparent diffusion coefficient in m^2/s; t_{exp} = time until first exposure to chlorides in s; t = concrete age in s; $erfc$= error function

Water and chlorides often move upwards in a structure from where the pores are saturated to the zone where the water can evaporate (wick action). In the evaporation zone when water is removed from the concrete, chloride ions remain behind. For this reason, the highest chloride concentrations are found above the water level (Hunkeler, 2005). This is illustrated Figure 2 - 23, which shows the maximum concentration of chloride ions just above the submerged zone. Roy, Chye & Northwood (1993) did an experiment into the chloride profiles obtained in the different exposure zones of the marine environment. It can be seen that the tidal and submerged zones have similar chloride profiles, while the atmospheric zone has significantly smaller values for the same cover depth (Figure 2 - 25).

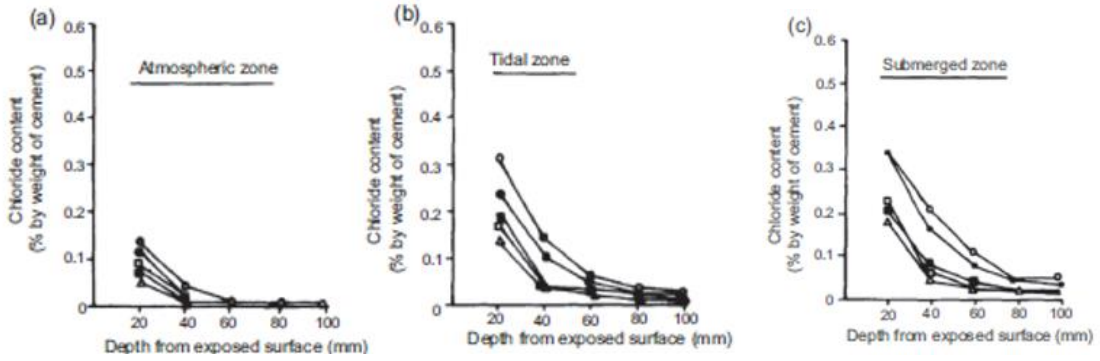

Figure 2 - 25: Difference in the chloride profiles obtained for the different zones (Roy, Chye & Northwood, 1993)

2.5 Review of exposure classes in international standards

Premature deterioration of concrete structures as well as the need for a sustainable approach to construction and design, has led to the inclusion of durability design provisions in standards around the world. Consequentially, many countries have developed durability designs that are stringent and durability focused. This section reviews the durability provisions provided by international standards by presenting the chloride corrosion related exposure classes and their associated limiting property values.

2.5.1 European Standard EN 206-1: 2013

The European Standard (EN 206-1:2013) categorises the exposure classes based on different degradation mechanisms. One of these mechanisms, categorised by the symbol XS, is corrosion induced by chlorides from sea water, and is further divided into 3 sub-classes as shown in Table 2 - 4. These exposure conditions are very well defined when compared to that of some of the other standards.

Table 2 - 4: Corrosion induced by chloride from sea water in reinforced concrete (EN 206-1: 2013)

Class	Description of environment	Example where exposure classes may occur	Maximum w/c ratio	Minimum strength class	Minimum cement content (kg/m^3)
XS1	Exposed to airborne salt but not in direct contact with sea water	Structures near to on the coast	0,50	C30/37	300
XS2	Permanently submerged	Parts of marine structures	0,45	C35/45	320
XS3	Tidal, splash and spray zones	Parts of marine structures	0,45	C35/45	340

Several prescriptive requirements are given for the different exposure conditions, including maximum w/c ratio, minimum strength class and minimum cement content (Table 2 - 4). EN 206-1(2013) has adopted a prescriptive requirement approach, as it is stated that performance requirements are still underdeveloped. However, performance related parameters are allowed if they conform to the durability rules.

2.5.2 Australian Standard AS 3600: 2009

The Australian Standard defines 6 main exposure classes and 17 sub-classes, of which the chloride induced corrosion related classes are given in Table 2 - 5. In this table Class A represents the most benign conditions while Class C represents the worst condition. Class U refers to concrete exposed to an environment of unknown severity. The characteristic compressive strength as well as the minimum period of curing is stipulated for these different exposure conditions (Table 2 - 6)

Table 2 - 5: Exposure classification according to AS 3600:2009

Surface and exposure environment	**Reinforced or prestressed concrete members**	**Plain concrete members**
Surfaces of members in above ground exterior environments in areas that are:		
(a) Near-coastal (1 km to 50 km from coastline) any climatic zone	B1	A1
(b) Coastal (up to 1 km from coastline but excluding tidal and splash zones) (Note 5), any climatic zone	B2	A1
4 Surfaces of members in water		
(a) In sea water		
(i) Permanently submerged	B2	U
(ii) In tidal or splash zones	C	U

The difference between this standard and others is that it geographical location is also considered as a variable. A map of Australia is included and divides the country into three zones, namely tropical, arid and temperate. The requirements change depending on these 3 locations.

2.5.3 Canadian Standard CSA A23.1: 2009

The Canadian Standard Association's main standard on concrete is CSA A23.1 and consider five major exposure classifications. Similarly to the European standards, each of these 5 classes is broken down into sub-classes and explained using typical examples (Table 2 - 7).

Table 2 - 6: Concrete requirements according to AS 3600:2009

Exposure class	f'_c MPa	Curing requirement	
		Intitial continuous curing*, days	Average compressive strength at completion of curing, MPa
A1	Not less than 20	3	Not less than 15
B1	Not less than 32	7	Not less than 20
B2	Not less than 40	7	Not less than 25
C**	Not less than 50	7	Not less than 32
U	Concrete shall be supplied to ensure durability under the particular exposure environment		

*Provisions will not apply for concrete cured by accelerated methods. However, average compressive strength requirement at the completion of accelerated curing will govern.
**Where the strength requirement for Class C cannot be satisfied due to inadequate aggregate strength, concrete with f_c' not less than 40 MPa may be used, provided that cement content of the mix is not less than 470 kg/m^3 and cover requirements are increased by 10 mm.

Prescriptive limiting values for each exposure condition is given in Table 2 - 8. Some exposure zones in the Canadian standard consider the 56 day compressive strength instead of the usual 28 day compressive strength. The Canadian Standard was also among one of the first to consider the results of the chloride ion permeability test (ASTM 1202) for extreme exposure conditions.

Table 2 - 7: Exposure classes of Canadian Standard CSA 23.1:2004

Class	Definitions of classes pertaining to chloride exposure
C –XL	Structurally reinforced concrete exposed to chlorides or other severe environment with or without freezing and thawing conditions, with higher durability performance expectations than the C-1, A-1 or S-1 classes.
C-1	Structurally reinforced concrete exposed to chlorides with or without freezing and thawing conditions. Example: Bridge decks, parking decks and ramps, portion of marine structures located within the tidal and splash zones, concrete exposed to seawater spray, and salt water pools.
C-2	Non-structurally reinforced (i.e. plain) concrete exposed to chlorides and freezing and thawing. Examples: garage floors, porches, steps, pavements, sidewalks, curbs and gutters.
C-3	Continuously submerged concrete exposed to chlorides but not to chlorides and freezing and thawing. Examples: underwater portions of marine structures.
C-4	Non-structurally reinforced concrete exposed to chlorides but not to freezing and thawing. Examples: underground parking slabs on grade.

Table 2 - 8: Requirements for specifying concrete based on exposure classes (CSA A23.1:2004)

Class of exposure	Maximum water to cement ratio*	Minimum specified compressive strength (MPa) and age (d) t test*	Air content (for 20 mm aggregate shown here)	Curing type Normal concrete (Not high volume SCM)	ASTM C1202 chloride ion penetrability test requirement and age at test**
C-XL	0.37	50 within 56 d	4 – 7% or 5 – 8% if exposed to freezing	Extended	<1000 coulombs within 56 d
C-1 or A-1	0.40	35 at 38 d	4 – 7% or 5 – 8% if exposed to freezing	Additional	<1500 coulombs within 56 d
C-2 or A-2	0.45	32 at 28 d	5 – 8%	Additional	
C-3 or C-4	0.50	30 at 28 d	4 – 7%	Basic	
C-4**** or A-4	0.55	25 at 28 d	4 – 7%	Basic	

**** The requirements for air-entrainment should be waived when steel troweled finish is required. Interior ice rink slabs and freezer slabs with a steel trowel finish have been found to perform satisfactorily without entrained air.

2.5.4 North American Standard ACI 318: 2014

In 2008 the American Concrete Institute (ACI) restructured their building code requirements to include more refined durability exposure classes. These exposure classes have remained similar with only a few changes to the 2014 version. The classes are divided into four categories which incude: (i) Class F for concrete vulnerable to freezing and thawing; (ii) Class S for concrete vulnerable to sulphates; (iii) Class C for concrete vulnerable to corrosion; and (iv) Class W for concrete in contact with water. These four categories are subdivided further into sub-classes as given in Table 2 - 9. A ‘not applicable’ sub-class is given per category so that the design engineer can make an appropriate decision for a structure that is not exposed to the relevant class. Furthermore, the standard also instructs designers to consider each structural member individually when more than one exposure class is involved.

Each sub-class is given limiting values for the maximum w/b ratio, minimum compressive strength and in certain categories cover depth and chloride ion content (Table 2 - 10). The standard is mainly prescriptive, with only concrete exposed to sulphates having a performance based requirement (ASTM C1012). In the standard it also states that for concrete in an environment that requires low permeability, the rapid chloride permeability test should be performed (ASTM C1202).

Table 2 - 9: Exposure classes specified in ACI 318:2014

Exposure class	Sub-class
C Corrosion	C0 (Not applicable): Concrete that will be dry and protected in service
	C1 (Moderate): Concrete exposed to moisture but not to an external source of chlorides
	C2 (Severe): Concrete exposed to moisture and an external source of chlorides

Although the cover depth is provided based on the quality of the concrete, there is no direct link between cover depth and the exposure classification. The minimum cover depth is provided in the standard and it is suggested that the cover depth be suitability increased for corrosive environments.

Table 2 - 10: Requirements for concrete vulnerable to corrosion (ACI 318:2014)

Exposure class	Max w/c	Min f_c MPa (psi)	Chloride ion limit (water soluble chloride by % wt. of cement)	Additional minimum requirements
Reinforced concrete				
C0	-	17	1.00	
C1	-	17	0.30	
C2	0.40	34.5 (5000)	0.15	Cover
Prestressed concrete				
C0	-	17	0.06	-
C1	-	17	0.06	-
C2	0.40	34.5 (5000)	0.06	Cover

2.5.5 South African Standard SANS 10100-2: 2009

SANS 10100-2 (2009) covers materials and execution of work completed for construction of concrete used structurally and does not include concrete made with high alumina cement. General exposure conditions are classified in the standard such as mild, moderate and severe depending on the type of environment the concrete is exposed to (Table 2 - 11).

Table 2 - 11: Minimum cover depth to reinforcing steel in SANS 10100-2 (2009)

Condition of exposure	Description of member/surface to which the cover applies	Minimum cover, mm				
		Grade of concrete, MPa				
		20	25	30	40	50
Moderate	All	50	45	40	30	25
Severe	- All exposed surfaces - Surfaces on which condensation takes place - Surfaces permanently under running water - Surfaces in contact with soil	NA	50	45	40	35
	Cast in situ piles: (a) Wet cast against casing (b) Wet cast against soil (c) Dry cast against soil	50 75 75	50 75 75	50 75 75	50 75 75	50 75 75
Very severe	- All exposed surfaces of structures within 30 km from the sea - Surfaces in rivers polluted by industries - Cast in situ piles, wet against casings	NA NA NA	NA NA NA	NA NA NA	60 60 80	50 50 80
Extreme	- Surfaces in contact with sea water of industrially polluted water - Surfaces in contact with marshy conditions	NA	NA	NA	65	65

The limiting values for all exposure conditions is that the maximum binder content may not exceed 550 kg/m^3. A maximum w/b ratio of 0.53 for concrete vulnerable to freeze/thaw attack and 0.5 for concrete requiring low permeability. 0.2% by mass of cementitious materials is the chloride ion limit when expecting additional chlorides from an external environment, while 0.4% is given where no additional ingress is expected. The type of cement or SCM's used is not restricted, as long as they comply with the relevant standard. The minimum cover depth to reinforcement is provided based on the grade of the concrete for each different exposure condition (Table 2 - 11). The exposure conditions are still too ambiguous and restrictive. Furthermore, concrete cover reduces with increasing concrete strength which is problematic as concrete strength is considered not to be an indicator of durability.

2.5.6 Criticisms of the current approach

The categories that are given in all the above standards are quite arbitrary and restrictive, and should be expanded to include a wider range of exposure sub-classes. There should be sub-classes that force the design engineer to consider the mechanisms of attack. Furthermore, a no risk option should also be included in the standards, as it allows for engineers to be unambiguous in their design decisions.

Most of the standards and requirements for concrete durability tend to be prescriptive in nature. While it is mostly agreed that performance based requirements are a superior method to ensuring as built quality, a lack of adequate tests and specification limits make them underutilised. Some efforts at providing performance based specifications have been made, for example, SANRAL who has adopted Durability Index (DI) tests for oxygen permeability, water sorptivity and chloride conductivity to improve national infrastructure (Nganga, Alexander & Beushausen, 2017).

Additional exposure classes can be considered for the marine environment. Firstly, it is too vague to have one exposure category for 1 – 50 km from a coastline, as the severity of reinforced concrete changes dramatically across this distance. Secondly, the splash and spray zone, and tidal zone have been found to have very different corrosion severities, despite them having the same design requirements. Furthermore, structures themselves can form different micro-climates. For example: the space under an enclosed jetty results in more wet concrete, whereas concrete exposed to direct sunlight will be dryer. These micro-climates can have varying effects on the degradation mechanism. This too should be considered.

2.6 Techniques for accelerating corrosion initiation and propagation

Techniques that encourage steel corrosion that is faster than a corresponding natural one, is referred to as accelerated corrosion. Natural steel corrosion is a slow process that needs years to cause reasonable corrosion damage. (Castel et al., 2003) and (Vidal, Castel & François, 2007) had to wait for 4 - 5 years for their specimens to start corroding naturally and a further 6 – 7 years after corrosion had been initiated for the onset of cracking, time not afforded in laboratory tests. For this reason, accelerated corrosion is used to try and simulate the actual corrosion mechanism and predict the induced damage in reinforced concrete structures. Miyagawa (1985) listed principal requirements for accelerated corrosion tests and stated that the tests should: (i) simulate corrosion mechanisms of natural corrosion; (ii) be faster than the natural corrosion process; (iii) have a wide application and; (iv) be easy to conduct. A crucial point missing from this list is the need for consideration of the type of corrosion products formed in accelerated tests, and whether these simulate corrosion products formed under natural conditions. Although using accelerated corrosion methods shorten the time of testing, it is difficult to find a method that satisfies all four requirements and is representative of the natural corrosion process. The different techniques for accelerating

corrosion are reviewed below in order to assist with selecting an appropriate method to meet this study's objectives. Such techniques include, use of an impressed current, admixing chlorides, wetting and drying and use of temperature or humidity, some of which accelerate the corrosion initiation phase, propagation phase or in some cases both.

2.6.1 Impressed current

This method involves the application of a current to the embedded steel from an external power source. The impressed current is applied to the anode (the steel under investigation), and a separate cathode, and increases the flow of electrons that flow. As more electrons are forced to move, there is an increase in the oxidation and reduction rate at the anode and cathode respectively. Consequently, the corrosion is accelerated to a rate faster than that of the natural corrosion process. (Ahmad, 2009)

Although a popular method, there are many criticisms of the impressed current technique. The corrosion mechanism occurring as a result of the impressed current is very different to the de-passivation of steel in natural conditions. Research conducted by Poursaee & Hansson (2009) and Yuan, Ji & Shah (2007) show that the chemical composition of the corrosion products formed using the impressed current technique and under natural conditions are different. In naturally corroding steel, the inhomogeneous ingress of chlorides into concrete leads to localised areas of corrosion, while the impressed current technique forces corrosion to occur over the whole surface of the steel bar. There is also much debate about the acceptable levels of impressed current densities that should be used to accelerate corrosion. El Maadawy & Soudki (2003) recommend a limiting impressed current density to 200 $\mu A/cm^2$.

2.6.2 Admixing chlorides

Another way to accelerate the depassivation of steel is to mix chlorides into concrete prior to casting of the specimens. As mentioned previously, the alkaline environment of concrete protects embedded steel by surrounding it with a passive layer. This passive layer can be destroyed by a sufficient quantity of chlorides penetrating into the cover layer, which can take years to occur. Mangat & Elgarf (1999) and El Maaddawy & Soudki (2003) aimed to immediately de-passivate the steel by the inclusion of chlorides ranging from 1% – 5%. This was found to significantly reduce the time taken for specimens to begin actively corroding. As this method of accelerating corrosion is simple and requires no expensive equipment it is a relatively common.

The main disadvantage of this technique, as highlighted by Poursaee & Hansson (2009), is that the steel will not have an opportunity to develop a passive protective layer, which is contrary to mechanisms that occur under natural conditions. They also showed that contaminating concrete with chlorides when mixing can affect the cement hydration and hence porosity of the concrete, as well as increase the conductivity of the pore solution. This leads to a change in the resistivity of the concrete, as well as the change in the rate of ingress of elements like oxygen and water that

facilitate corrosion. As with the impressed current technique, the inclusion of chlorides at mixing of concrete leads to a homogenous distribution of corrosion agents around the steel. This is contrary to natural conditions where an inhomogeneous distribution of causes localised areas of corrosion (Malumbela, Moyo & Alexander, 2012).

2.6.3 Wetting and drying

In this method of accelerating corrosion, reinforced concrete specimens are exposed to repeated cycles of wetting and drying in chloride solution. The effect of this is twofold:

i) Firstly, the cycles of wetting and drying cause the chloride solution to penetrate the concrete through capillary sorption instead of diffusion that occurs in natural conditions. This means that the chlorides are penetrating deeper into the concrete more rapidly as shown by (Moukwa, 1990) and Hong (1998). This effect leads to an early de-passivation of the embedded steel and the onset of active corrosion.

ii) Secondly, the drying phase, if sufficiently long, allows oxygen to penetrate through the cover layer and be replenished at the steel surface. Sufficient concentrations of oxygen allow the cathodic reaction to proceed, and prevent the corrosion reaction from being cathodically controlled and hence stifled.

Different techniques exist for accelerating corrosion using the concept of wetting and drying. Yuan, Ji & Shah (2007) proposed the application of a salt spray to be uniformly distributed around the concrete specimens. It was found that after cycles that included 1 hour of spraying with salt water and 7 hours exposed to infrared light, the corrosion characteristics of the steel bar in the artificial environment was representative of natural corrosion mechanisms. Other researchers like Chang, Cherry & Marosszeky (2008) fully or partially immersed specimens in a chloride bath and then dry them for a predetermined amount of time. Standards like ASTM G109 (used to assess the effect of chemical admixtures on the corrosion of specimens) recommend ponding chloride solution on the top face of specimens. This ponding technique is the most commonly used wetting and drying method applied in research, and best replicates the corrosion mechanisms of natural exposure conditions.

2.6.4 Elevated temperature

Exposing specimens to elevated temperatures or elevated humidity is another way to accelerate corrosion propagation. Živica et al. (1997) found that when the ambient temperature was increased, the corrosion rate also increased significantly. As corrosion can be considered electrochemical in nature, and increase in energy results in more rapid movement of electrons. However, the latter was only found to be true for temperatures of less than 40 ºC. This is attributed to the decrease in oxygen solubility with an increase in temperature, and accordingly cathodic control of the corrosion rate. In addition to this effect, high temperatures also dry concrete and decrease the moisture

content, which in turn increases the concretes resistivity. If the resistivity of concrete is too high, the ionic current flowing from the cathode to the anode is opposed and the corrosion current is reduced (Beushausen & Alexander, 2009).

This method's simplicity is advantageous, but is criticized as elevated temperatures have been shown to lead to microstructural damage of the concrete. Microstructural damage is significant as it affects the transport properties of the concrete and hence has an influence on the progression of corrosion of embedded steel. Kanna, Olsen & Jennings (1998) showed that as temperatures became more severe (i.e. 150 ºC), the damage to the microstructure also increased. Temperatures as low as 60 ºC were also found to alter the microstructure of hardened cement paste Gallé (2001). For the aforementioned reasons, increasing temperatures as a way to accelerate corrosion rates is not implemented often.

2.7 Techniques for corrosion assessment in concrete

In addition to testing of field reinforced concrete, laboratory techniques are also important for the development of the test methods used in the field and also to analyse corrosion protection systems (Berke, Shen & Sundberg, 1990). The polarization resistance method and the macrocell corrosion method are commonly used electrochemical techniques, and are reviewed in this section in order select an appropriate method for the laboratory-based experimental programme. These tests require substantial understanding on the topic of corrosion theory and electrochemistry. In addition to these two electrochemical techniques, parameters such as cover depth to embedded steel, resistivity and half-cell potential are often used as corrosion rate indicators (Alexander, Beushausen, & Otieno, 2012). These parameters considered together give an indication of the corrosion risk of steel and are not quantitative measures of the corrosion rate. In comparison, the corrosion rate indicators are easy to implement and do not require extensive knowledge of corrosion mechanics. All three methods are reviewed.

2.7.1 Polarization resistance method

Corrosion rates can be monitored using polarization resistance techniques, which is particularly useful for giving an indication of the corrosion resistance of materials in aqueous environments. Unlike the half-cell potential measurement that only gives the probability of corrosion (See Section 2.7.3.2 later), polarization resistance measurement provides a direct measurement of the instantaneous corrosion rate (Halabe, Kavi & GangaRao, 2016). As a consequence, more informed maintenance and repair decisions can be implemented.

The test method itself considers the findings of Stern & Geary (1957) that current versus potential is linear around the corrosion potential of reinforced concrete. A very small potential perturbation is applied (usually around 10 mV) and the resulting change in current is measured between the working and counter electrode. Alternatively, a small current can be applied and the potential shift

measured. The relationship between the current and potential change can then be converted to corrosion current density (Yang, 2008).

Various equipment is available to measure corrosion rate, including the use of a potentiostat or a guard ring electrode. The benefit of this corrosion monitoring technique is that it is relatively easy to perform (Institution of Structural Engineers, 2010). However a very good understanding of corrosion theory is required before measuring and interpreting results.

2.7.2 Macrocell corrosion method

Corrosion in structures exposed to chloride rich environments often succumb to macrocell corrosion (Section 2.2.2.3). Macrocell corrosion is characterised as a mechanism where there is a distinct separation between the anode and the cathode, and occurs when an actively corroding steel bar is electrically connected to a passive steel bar as a result of different environments (and hence potential). This potential difference between the anode and cathode creates a current flow, the rate of which is proportional to the rate of steel corrosion.

In order to represent this circuit, corrosion cells called macrocells can be cast that measure the galvanic current between steel embedded in an upper and lower layer. A resistor is connected to the upper steel anode and lower steel cathode so that the voltage drop across the resistor of known value can be determined (Figure 2 - 26). Results of laboratory based concrete specimens are not equivalent to results obtained from field structures, and thus can be used semi-qualitatively and for comparisons as opposed to absolute data (Nygaard, 2008).

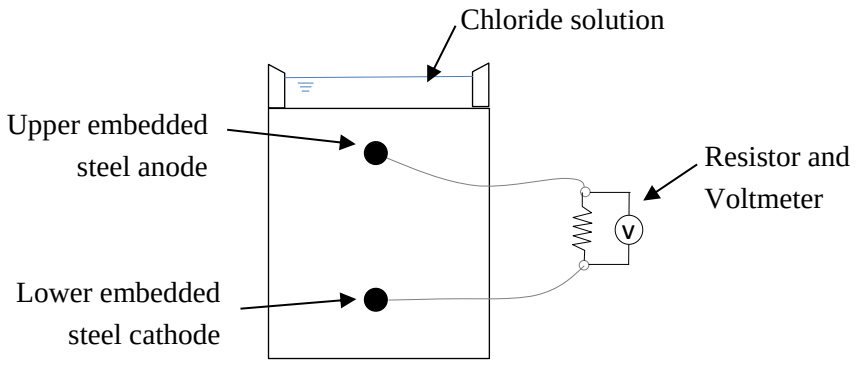

Figure 2 - 26: A macrocell as described by ASTM G109 and Southern Exposure method

Some of the laboratory tests that make use of the concept of macrocell corrosion currents to monitor corrosion activity include ASTM G109 and the Southern Exposure method (Trejo, Halmen & Reinschidt, 2009). ASTM G109 has made use of the concept of a macrocell to establish the effect of corrosion inhibiting admixtures on the corrosion of steel in concrete. It states that 3% chloride solution should be cyclically ponded, and the voltage drop recorded over a 100Ω resistor. The integrated macrocell current, measured in Coulombs, can then be established to give an indication

of the total amount of corrosion that has occurred in the macrocell. The Southern Exposure Test method is similar to that of ASTM G109 and uses larger macrocell specimens. The specimens are exposed to cyclic ponding at low relative humidity under accelerated drying conditions. In reality, marine environments do not achieve such low relative humidity and this test method might present different characteristics of corrosion to that of specimens in natural exposure conditions (Baboian, 2005).

The sensitivity of this method should be noted. In experiments comparing the polarization resistance technique to the macrocell corrosion technique (Berke, Shen & Sundberg, 1990), it was found that the corrosion in macrocell inferences was always detected by the polarization resistance technique, but not always by the macrocell technique. Furthermore, as the macrocell corrosion technique does not take into account localized (or microcell corrosion), the corrosion rates can be underestimated. Nonetheless, the simplicity of this technique of monitoring corrosion makes it widely used for comparing different set-ups in a laboratory environment.

2.7.3 Corrosion rate indicators

A combination of resistivity readings, half-cell potentials and cover measurements act as indicators for the likelihood of corrosion. None of these indicators should be considered in isolation, but rather be used to complement each other. The operating principle is given for each set of test equipment.

2.7.3.1 Resistivity

The electrical resistivity of concrete can be related to the (i) initiation period as a result of rate of chloride penetration and (ii) the propagation period as a consequence of the corrosion rate, and is a way to quantify the conductive properties of concrete. The 4-point Wenner probe is equipment commonly used to determine the resistivity of concrete (Figure 2 - 27). When the four equally spaced probes are placed in contact with the concrete surface, a current is applied across the two outer probes while the resulting potential difference between the two inner probes are used to determine the resistivity (Gower & Millard, 1999).

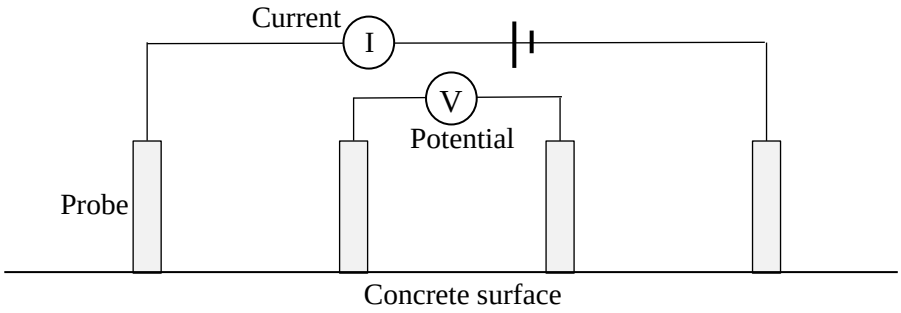

Figure 2 - 27: Schematic of 4 point wenner probe (After Alexander, Beushausen & Otieno, 2012)

Assessment criteria to classify potential corrosion activity in terms of resistivity has been widely investigated as given chronologically in Table 2 - 12. The variability in the critical values of resistivity among different researchers can be attributed to the experimental set-up, mix design and cause of corrosion (Hornbostel, Larson & Geiker, 2013). For instance, Morris et al. (2002) investigated criteria for the corrosion risk level in terms of chloride induced corrosion and obtained higher threshold values than Hope & Manning (1985) and Smith, Schokker & Tikalsky (2004) who investigated criteria for a general cause of corrosion. Furthermore, lower resistivity values were obtained for concrete made of OPC as shown by Hope & Manning (1985), while blended cements tended to have higher results. As a single relationship between concrete resistivity and the potential risk of corrosion cannot been established and applied to all cases, factors including binder type and exposure environment should also be taken into account before selecting a preferred approach with respect to interpreting resistivity values.

Table 2 - 12: Resistivity and associated risk level (After Hornbostel, Larson & Geiker, 2013)

Risk Level	Resistivity (Ω m)		
	Hope & Manning (1985)	*Morris et al. (2002)*	*Smith, Schokker & Tikalsky (2004)*
High	< 65	< 100	< 80
Moderate	65 - 85	100 - 300	80 - 120
Low	> 85	> 300	> 120

2.7.3.2 Half-cell potential

Half-cell potential measurements are of the most widely used methods to assess the probability of steel corrosion occurring in reinforced concrete. The steel's potential is measured using a half cell reference electrode (either saturated copper/copper sulphate or silver/silver chloride) and a high impedance voltmeter. The positive terminal of the voltmeter is connected to the steel embedded in the concrete, while the negative terminal is connected to the reference electrode which is in turn in contact with the concrete surface (Figure 2 - 28). (Forde, 2009) Through the voltmeter the potential difference between the metal in the reference electrode (copper or silver) and the steel in the concrete is measured.

The operating principles of the half-cell equipment make it most suited to chloride induced corrosion of steel that tend to form distinct cathodic and anodic regions in the corrosion process. In contrast to chloride induced corrosion, it is not recommended for half-cell potential mapping to be done on concrete with corrosion caused by carbonation where there are no clearly defined anodic regions (Raupach & Buttner, 2014).

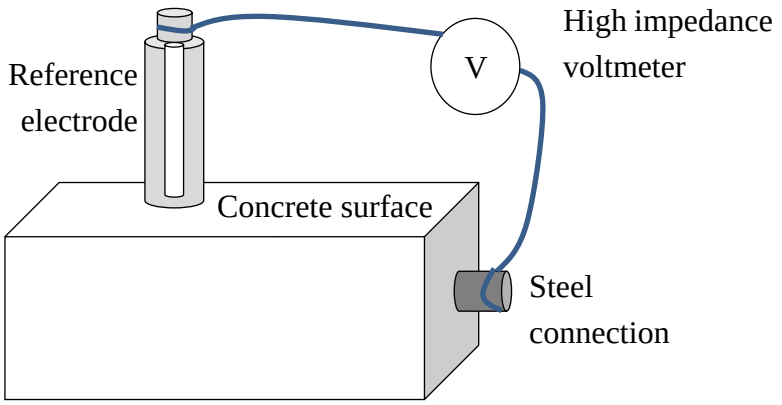

Figure 2 - 28: Reference electrode circuitry (ASTM C876 - 15)

Half-cell potentials only locate possible areas of corrosion activity and do not evaluate the degree of corrosion that has occurred or the rate of corrosion (Beushausen & Alexander, 2009). The half-cell potential data should also be validated with other measurements like resistivity values and cover measurements before an interpretation of corrosion likelihood can be made. ASTM C876-15 guidelines for interpreting results are given in Table 2 - 13 where the more negative the potential is the higher the probability of corrosion.

Table 2 - 13: Guidelines for interpreting half-cell potentials (ASTM C876 – 15)

Copper/copper sulphate electrode potential (mV)	Silver/silver chloride electrode potential (mV)	Risk of corrosion
> – 200	> – 106	Low chance of corrosion (< 10%)
– 200 to – 350	– 106 to – 256	Uncertain
< – 350	< – 256	High chance of corrosion (> 90%)
< – 500	< – 406	Severe corrosion

2.7.3.3 Cover depth measurement

Insufficient cover depth results in steel corrosion and an overall reduction in the performance of the structure. Therefore, it follows that identifying the location and cover depth of the steel is crucial to evaluating the risk of corrosion (NACE International, 2011).

Cover depth measurement is usually a non-destructive test that produces reliable and accurate results. However the accuracy of cover depth equipment can decrease with the depth of the cover. Evidence of this is seen in research conducted by Sivasubramanian (2013) where the error percentage was found to be significantly higher at depths larger than 60 mm.

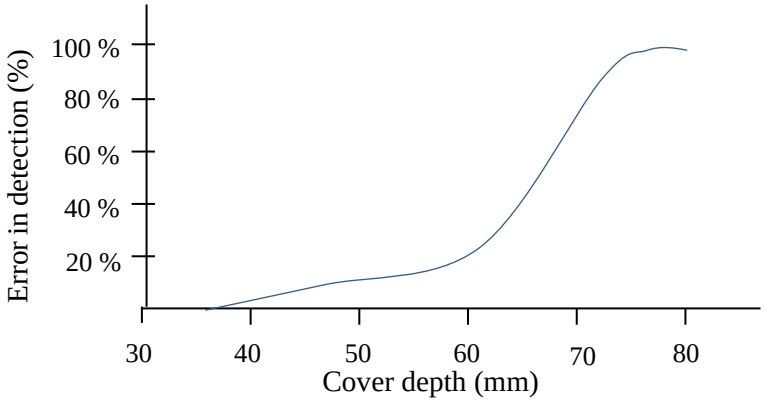

Figure 2 - 29: Reliability of non-destructive cover depth testing (After Sivasubramanian, 2013)

The concrete quality was not a factor in this study, however the trend observed in Figure 2 - 29 is dependent on concrete quality. Cover depth measurements in conjunction with resistivity and half-cell potential measurements are a useful tool to assess the potential durability of reinforced concrete.

2.8 Closure

This chapter presented the fundamentals of chloride induced steel corrosion. Specifically, the transport properties of moisture and chlorides in concrete, and initiation and propagation phases of the corrosion process. Corrosion of steel in the marine environment, after depassivation has occurred, are directly related to the availability of water and oxygen. While this concept is widely accepted, the availability of oxygen under different tidal conditions has not been investigated. Various techniques for assessing corrosion rates and accelerating corrosion phases were also presented. It can be concluded that each technique has its own unique set of advantages and disadvantages that should be considered.

Considering the review of literature, it is clear that studies have failed to adequately show the relationship between oxygen availability and rate of steel corrosion in reinforced concrete in the tidal zone. It is also evident after considering different standards, that the exposure classifications for the marine environment could be improved to more adequately reflect real life scenarios.

3 Field structures in Southern African harbours

This chapter presents comments on the long term exposure conditions of various field structures along the coast of Southern Africa. Six different structures along the coast of Southern Africa were assessed. A visual inspection of each structure was conducted after which both the horizontal and vertical steel cover depths were recorded. The resistivity was also taken at relevant locations on the structures surface. Table 3 - 1 and Table 3 - 2 below gives a summary of the six structures assessed, along with the cover depth values. The height of the test area given in the exposure column is the height relative to the mean sea level, information which is crucial to evaluate the influence of the exposure zone on durability conditions of a structure.

Table 3 - 1: Condition assessment of field structures along Southern African coast

Structure	Age	Test area	Exposure Zone	Minimum cover depth (mm)	Condition
Jetty 1, Walvis Bay	+ 60 years	Coping Beam; Direct wave action	(+0,1 m) Tidal	61	No visible corrosion damage
			(+2 m) Splash	73	Delamination
		Concrete sheet pile sea facing; No direct wave action	(+0,5 m) Tidal	87	No visible corrosion damage
			(+1 m) Upper Tidal	81	No visible corrosion damage
			(+2 m) Splash	84	Hairline cracks/rust stains
		Precast deck soffit	Splash	>90	No visible corrosion damage
Repair Jetty, Walvis Bay	44 years	Side of service beam	Splash	71	No visible corrosion damage
			Splash	60	Rust stains
		Service beam soffit	Splash	68	Delamination
		Precast bearing piles	(+ 0.3 m) Tidal	81	No visible corrosion damage
			(+ 1 m) S&S	85	No visible corrosion damage
		Deck soffit	S&S	57	Spalling and Delamination

Table 3 - 2: Condition assessment of field structures along Southern African coast

Structure	Age	Test area	Exposure Zone	Average cover depth (mm)	Condition
Caisson, Saldanha Bay	40 years	Sea facing wall	S&S	50	Cracking and rust staining
			Tidal	46	No visible corrosion damage
Small Craft Harbour, Saldanha Bay	33 years	Sea wall; sheltered from wave action	S&S (+1,5 m)	44	Extensive spalling with signs of rebar corrosion
			Tidal (+0.5 m)	42	No visible corrosion damage
Strandfontein	13 years	Tidal pool wall	Tidal	100	Hairline cracking and corrosion
Hangklip, Pringle Bay	46 years	Public launch ramp	Tidal	55	Severe reinforcement corrosion
			Submerged	55	Cracking and rust staining

3.1.1 Jetty, Walvis Bay Namibia

The jetty located in Walvis Bay Namibia, consists of a precast deck supported by a reinforced concrete sheet pile on one side and piles on the other (Figure 3 - 1). The side with reinforced concrete piles rocks filling the spaces that would be open to the environment and is landlocked (i.e. no ship is able to dock along the length of this side of the jetty). A coping beam is situated on the land end of the jetty, which experiences splashing from the movement of vessels in the harbour but is otherwise protected from direct wave action.

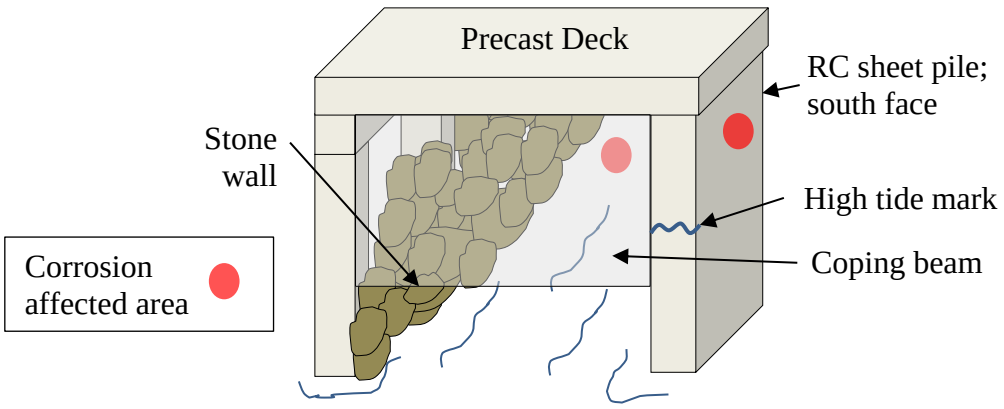

Figure 3 - 1: Schematic of jetty located in Walvis Bay, Namibia

The outside of the sheet pile appeared to have damage as a result of durability issues. Cover depths of concrete in both exposure zones are similar (± 80 mm), yet deterioration can only be seen in the splash and spray zone while the upper tidal zone remains unaffected. Usually in structures, the upper tidal zone experiences corrosion as there is longer time for the concrete to dry out to the level of steel to facilitate corrosion. In this case however, the cover is quite significant and the concrete requires an even longer drying duration for the cover to dry 80 mm to the level of the steel. Furthermore, there could be some movement of moisture up within the concrete itself from the lower tidal level to the upper tidal level as a result of wick action. This further addition of moisture in the upper tidal zone could contribute to the extended critical drying time required for oxygen to reach the steel, which explains why even the upper parts of the tidal zone have remained unaffected by corrosion.

The coping beam also displayed this trend, where concrete in the tidal zone with a cover depth of 61 mm showed no signs of corrosion. However, the splash and spray zone showed significant delamination despite actually having a higher cover depth of 73 mm. Once again, this can be attributed to the availability of both oxygen and moisture at the level of the embedded steel in the splash and spray zone.

3.1.2 Repair jetty, Walvis Bay Namibia

The repair jetty located in Walvis Bay Namibia, and is made up of a deck supported by precast bearing piles. On each side there are coping beams where rubber fenders are attached for docking of large vessels. There is also a service beam that runs along the length of the jetty that is accessible via a metal covering on the top of the deck (Figure 3 - 2). Unlike the jetty discussed above, this jetty experiences more direct wave action.

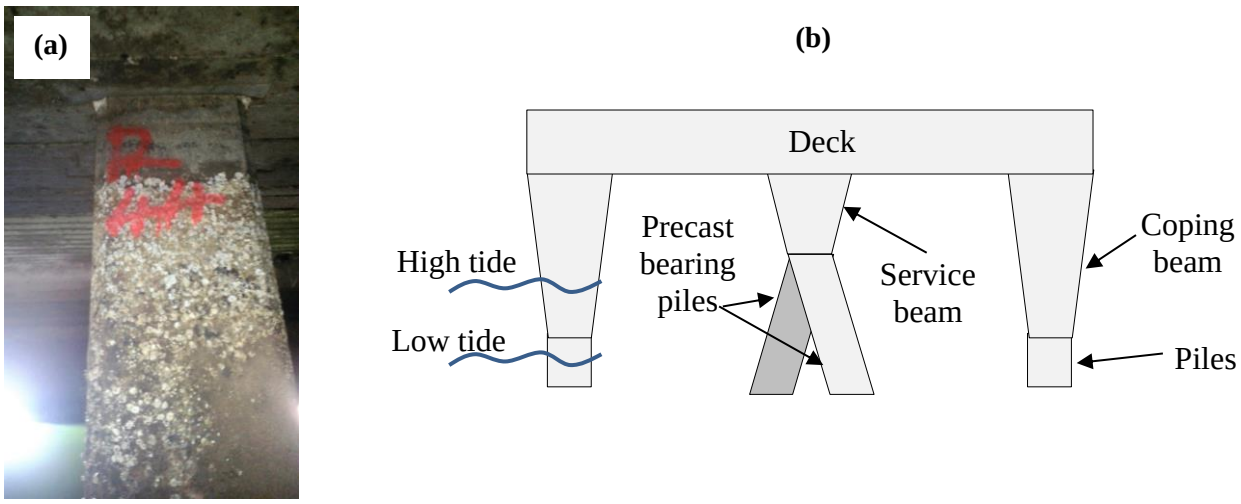

Figure 3 - 2: Cross-section and (b) undamaged pile of repair jetty in Walvis Bay, Namibia

Since this fixed berthing structure is used for fishing vessels and offshore service vessels, the top of the deck is usually wetted when offloading fish and the deck washed down with sea water after repairing vessels. This typically results in intense steel corrosion on the decks of the jetty.

While there isn't any evidence of corrosion on the top of the deck, there was significant spalling and delamination in sections of the deck soffit. In the areas where corrosion was occurring, the cover depth of the slab was 57 mm. Corrosion is to be expected considering the age of the structure despite meeting the 60 mm cover depth requirement as recommended by Alexander & Mackechnie (2003). Moreover, heavy loading on the jetty from repair equipment can result in cracks forming on the underside of deck allowing rapid ingress of chlorides and hence significant corrosion to proceed (Otieno, 2014).

Along the side of the service beam two different locations were investigated, one where there was some rust stains evident (cover depth here was 60 mm) and another where the beam was still in good condition (cover depth was 71 mm). Considering both locations on the beam are made from the same mix and experience the same exposure conditions, this example exhibits how larger covers can retard corrosion initiation of steel.

The service beam soffit showed moderate corrosion in places despite having a similar cover depth (68 mm) when compared to the sides of the beam. A possible explanation for this could be that the soffit experiences appreciably more direct splashing, especially as waves hit the piles located underneath the beam itself. This could lead to rapid ingress of chlorides and a shorter corrosion initiation time.

The precast bearing piles were mostly situated in the tidal zone, with only about 20 cm extending above into the splash zone. Neither parts of the pile located in the tidal zone nor the lower splash zone had any signs of corrosion damage, despite high levels of chlorides located here. It can be assumed from the high chloride content (0,7 %) that the steel has depassivated, and the lack of corrosion here can only be attributed to insufficient quantities of corrosion inducing species at the level of the reinforcing.

Although the piles had recently been cleaned, one could see there was previous presence of marine biofilm on all piles in the tidal zone. This marine layer, along with the large cover depth and high quality associated with precast concrete, could in combination prevent the concrete from drying out. As discussed before, a high moisture content in the cover layer of concrete notably limits oxygen's accessibility to the steel, which in turn limits the propagation of corrosion.

3.1.3 Caisson, Saldanha Bay

A sand filled caisson located at the end of an ore jetty in the port of Saldanha Bay was also investigated (Figure 3 - 3). The outer faces of caisson units usually experience many micro-climates, from submerged to cyclic wetting and splashing conditions. As this caisson was located on the end of a particularly long jetty that reaches the boundaries of the harbour, it experiences

frequent wave collisions of great wave amplitude. Even at low tide, the large recurrent waves are keeping the upper tidal zone permanently wet.

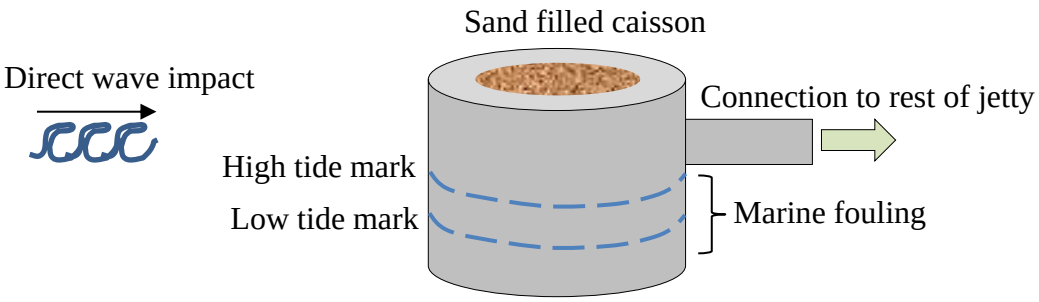

Figure 3 - 3: Schematic of caisson located in Saldanha Bay

The wall of the caisson facing the sea showed rust stains and evidence of some corrosion induced cracking. Evidence of a repair mortar could be seen at the top of the reinforced concrete wall, presumably to cover up steel that had been affected by corrosion (See Figure 3 - 4). The corrosion induced damage was found to only occur in the splash and spray zone with a cover depth of 50 mm, while the tidal zone with a cover of 46 mm once again remained in good condition. This could only be assumed to be a direct consequence of the different exposure environments, as the cover depths and quality of cover are relatively similar.

Corrosion occurs at a relatively lower cover depth in this structure than that of the structures discussed in Section 3.1.1 and 3.1.2. This could be due to the direct wave impact that forces a faster ingress of chlorides and the direct sunlight which facilitates a faster drying rate.

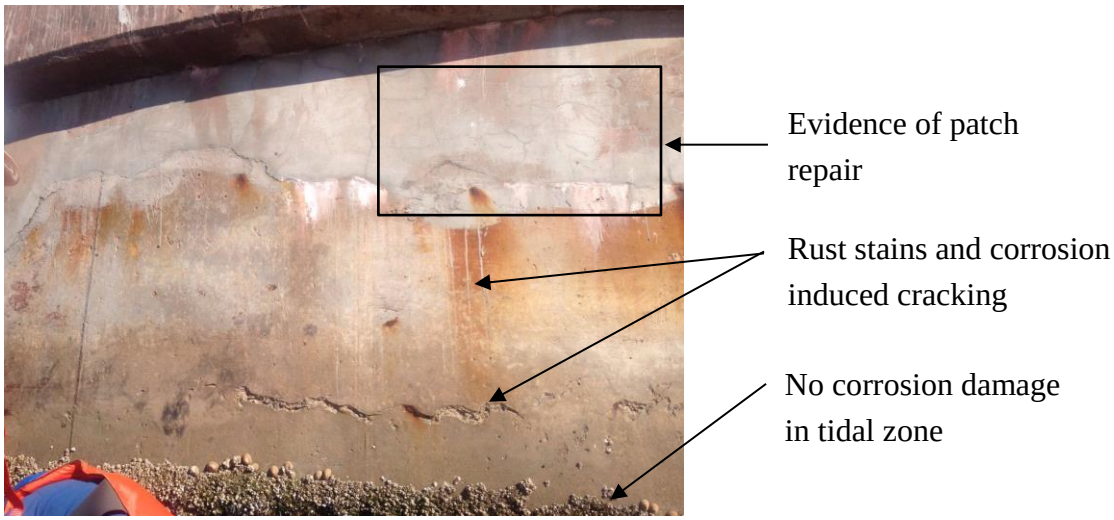

Figure 3 - 4: Image taken of caisson exposed to direct impact of waves, Saldanha Bay

3.1.4 Small Craft Harbour, Saldanha Bay

The wall of a small craft harbour, not exposed to any direct waves, was investigated. As shown in Figure 3 - 5, significant spalling occurred in the splash and spray zone of the wall. After removal of some of the marine fouling layer, no evidence of corrosion could be found in the tidal zone.

The chloride profile of the concrete in both the splash and tidal zone was determined using potentiometric titration (Figure 3 - 5). The chloride content in the splash zone, which corresponds to a 44 mm cover depth (at the level of the rebar) is approximately 1,1% by mass of cement. As expected, this value exceeds the critical chloride threshold and successfully depassivates the steel, allowing corrosion to propagate if O_2 is present. Evidence of this is the large areas where spalling and corrosion can be seen.

Furthermore, the chloride content at the level of reinforcing in the tidal zone has a similar value of 0,95 % per mass of cement. According to literature, it is highly likely that this value exceeds the critical chloride threshold value, and that the passive layer around the steel has been destroyed. Despite this, there is no evidence of chloride induced corrosion anywhere in the tidal zone. This shows how in this case, the cover depth has not limited the onset of corrosion initiation, but rather limits the corrosion propagation (which is largely affected by lack of available oxygen).

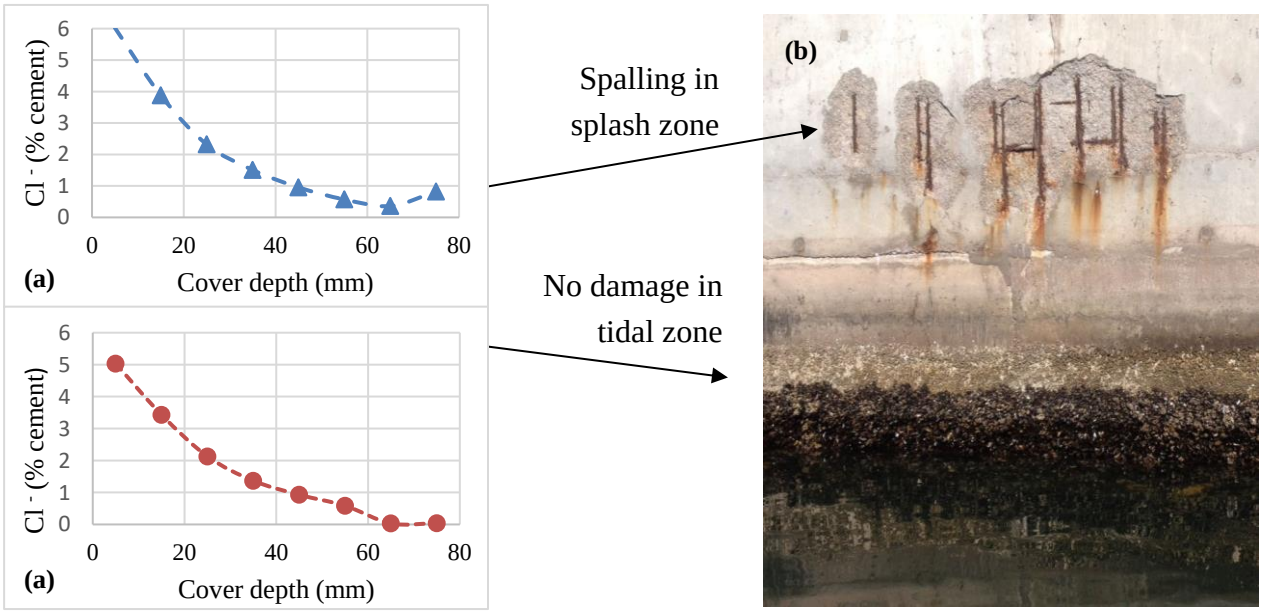

Figure 3 - 5: (a) chloride profiles of splash and tidal zone and (b) photograph of a small craft harbour in Saldanha Bay

3.1.5 Tidal pool, Strandfontein

Tidal pool walls are structures that are permanently submerged on one side, while the other side cycles between wetting and drying during high and low tide respectively.

Although today most tidal pools are constructed using mass concrete, in the past some tidal pools along South Africa's coast were made using reinforced concrete. One such cases includes the southern hemispheres largest tidal pool, situated in Strandfontein roughly 8 km east of Muizenberg. As this tidal pool has since been reconstructed, the information presented is secondary data that was obtained from a study completed in 1994 (Strohmeier, 1994). At 13 years old, and a cover depth exceeding 100 mm, the corrosion damage was extensive.

This finding contradicts the four case studies discussed above where the tidal zone has no evidence of corrosion. This could be because the tidal pool walls get chloride exposure from both the outside and inside wall. The inside wall is continuously exposed to chlorides, which can migrate to the outside wall through diffusion, permeation, and to some extent absorption. This would result in a high chloride content but not necessarily corrosion. Most likely, the steel on the inside wall surface and the steel on the outside wall surface form a corrosion cell, where the outside steel acts as the anode and the inside steel as the cathode. Even if corrosion is slow due to limited oxygen at the cathode, the corrosion cell effect will be strong enough to corrode the external steel.

3.1.6 Launch ramp, Hangklip

A 1970's public launch ramp located near Hangklip lighthouse about 2 km outside of Pringle Bay was investigated. Much like the tidal pool wall, this structure is fully submerged at high tide. Part of the structure is permanently submerged while part of the structure experiences cyclic wetting and drying. This high tide mark was established by considering the location of drift seaweed on the shore.

As shown in Figure 3 - 6 (image taken at low tide), severe corrosion of the steel is apparent in the concrete located in the tidal zone. The concrete in this zone has been eroded over time which is made noticeable by the exposed aggregate surface. The extent of corrosion damage to the launch ramp appears to become less and less from the upper tidal to the submerged zone. As opposed to the tidal zone that shows significant spalling, only cracking and delamination could be observed in the lower tidal and submerged zone. Both areas have similar cover of approximately 55 mm.

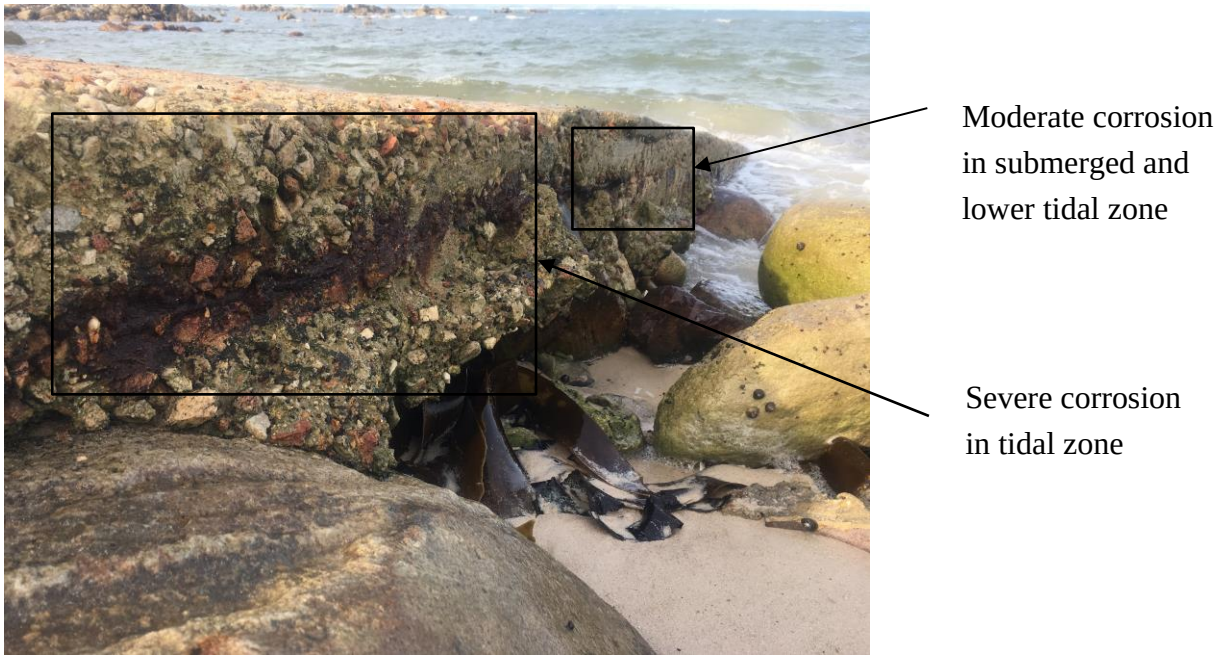

Figure 3 - 6: Photograph of launch ramp in Hangklip showing corrosion

Firstly, structures such as tidal pool walls and launch ramps are not protected from the direct force of waves in the same way that jetty's located in protected harbours are. This large wave impact often leads to abrasion of the wall surface and an overall reduction in the depth to embedded steel, allowing corrosion to develop prematurely.

Secondly, in submerged conditions, there is not much oxygen available to drive the cathodic process. Consequently, structures that are fully submerged show no sign of corrosion, despite being depassivated. However, when the depassivated zone is linked to a part of the structure that has conditions that make the cathodic reaction viable, a macrocell corrosion cell forms and corrosion proceeds (As shown in Figure 3 - 7). The parts of the structure where this occurs is the splash zone which is sufficiently aerated, and the tidal zone (given certain cover depths). McLeish, 1994

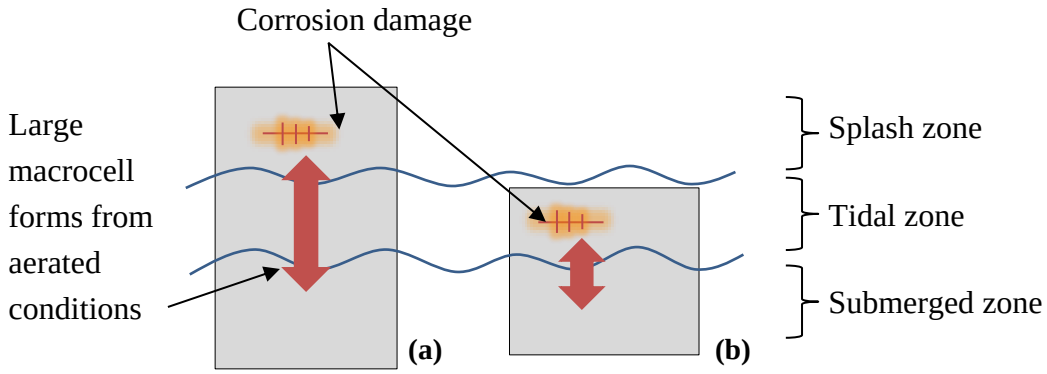

Figure 3 - 7: Potential difference in concrete that extends to (a) all 3 exposure zones and (b) 2 exposure zones

For concrete that does not extend above the high tide mark, a lack of reinforced concrete in the splash zone means that the cathodic process cannot proceed. In a similar mechanism as described above, steel within the tidal zone has a higher potential than that of steel within the submerged zone, leading the reinforced concrete in the tidal zone to be the preferential anode for corrosion (Figure 3 - 7.b). This could explain why corrosion is more prevalent in the tidal zone of structures that only exist within the tidal and submerged exposure classes. Nonetheless, it can still be assumed that the limited oxygen supply in the tidal region notably reduces the corrosion rate of steel, if there is sufficient cover depth and quality.

3.1.7 Cover depth versus level of deterioration

Each section of the 6 structures investigated was assigned a level of deterioration based on its condition (Table 3 - 3) which was plotted against cover depth. As established in the experimental data, the relationship between the corrosion current and the cover depth is dependent on the exposure conditions. For this reason, data points from the splash zone and tidal zone were plotted as separate datasets. It must be noted that this figure is just an indication, as all the structures are grouped together into a single data pool, despite there being many difference between them. However some trends can be identified.

A regression line was drawn for the two exposure categories as indicated on Figure 3 - 8. The points of intersection between the 2 regression lines occur at 83 mm cover depth, which indicates that for concrete with a cover depth of less than 83 mm, the condition of concrete in the tidal zone will be better than the same concrete located in the splash zone. The smaller the cover depth becomes, the higher the difference in deterioration is between structures. As the quality of the cover was unknown, no inferences can be made with regard to this. More data points and structures should be included in order to refine and further clarify the relationship between structures located in different micro-climates.

Table 3 - 3: Value assignments based on level of deterioration of site element

Number assignment	Level of deterioration
1	no damage
2	some cracking
3	delamination
4	spalling
5	severe damage

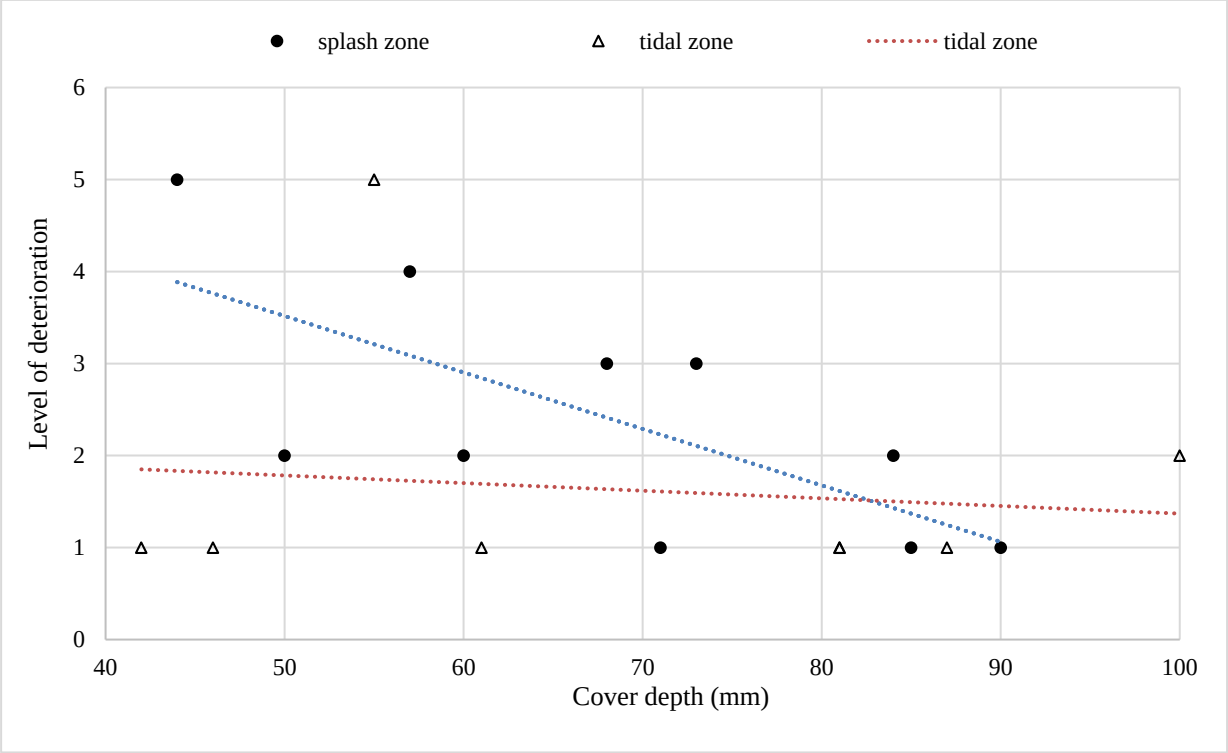

Figure 3 - 8: Scatter plot of level of deterioration versus cover depth for concrete located in the splash zone and tidal zone

3.2 Closure

From the case studies, it is clear that the current classification of marine environmental conditions is highly over simplified. Marine structures tend to have a wide range of deterioration conditions depending on the location, exposure condition and function of the structure.

Reinforced concrete structures exposed directly to ocean waves and the wake of large vessels tend to show more deterioration than that of structures surrounded by calmer waters. This could be as a result of the physical abrasion from waves in rougher seas, as well as increased ingress of moisture and chlorides into the concrete which accelerates corrosion. In this way, the location of the structure is important.

It is also suggested that the type of structure be considered when investigating durability concerns. For examples, reinforced concrete structures that are continuous across all three exposure zones (i.e. piles or quay walls) tend to show damage in the splash zone, while the tidal zone remains relatively unaffected. Conversely, structures that only exist in the tidal and submerged zone (i.e. tidal pool walls) tend to corrode significantly faster than they would if they had concrete in the splash zone. One other reason there is usually no damage in the tidal zone (apart from lack of available oxygen) is that the steel in the splash zone protects the steel in the tidal zone by acting as a sacrificial anode.

The function of the structure is also crucial, as a jetty slab that is used to offload fish or hold heavy repair equipment might experience further deterioration problems as opposed to a slab that is used for small craft mooring and recreational activities. This is because heavily loaded structures experience more micro-cracks, which accelerate deterioration.

The main finding from the case studies presented in this chapter is that the splash and tidal zone of a structure deteriorate at different rates. The tidal zone usually has no corrosion while the slash zone does. This is probably owing to the lack of available oxygen at the reinforcing steel in the tidal zone, which limits the cathodic (and hence overall corrosion) reaction. This concept is assessed further using the experimental methodology as set out in Section 4.

4 Research methodology

4.1 Introduction

This chapter presents the details of experiments performed in this study. Explanations of the variables selected are given as well as details of the sample preparation, test techniques and frequency of testing. The objective of this research is to determine the extent to which oxygen availability in the tidal zone limits the corrosion rate of embedded steel. The influence of the cover depth and quality of the cover on the oxygen availability, and hence the corrosion rate was investigated.

4.2 Variables

The influence of the concrete cover, w/b ratio, and exposure environment were investigated for their effects on the corrosion rate. The binder type, and wetting and drying durations remained constant throughout the experiment. The details of the three variables are given below.

4.2.1 Concrete cover depth

The distance from the surface of the concrete to the steel was varied to attempt to correlate the depth of the cover layer to the drying time of concrete. A high cover depth could result in concrete located in the tidal zone not drying out sufficiently at low tide, thus lessening the amount of oxygen available. On the other hand, concrete with a lower cover depth in the tidal zone at low tide could have sufficient time to dry out, thus allowing oxygen to reach the steel and facilitate corrosion. Different cover depths were therefore represented in the laboratory samples.

A minimum cover of 40 mm is normally recommended for reinforced concrete structures exposed to a marine environment (SANS 10100-2), although a negative tolerance of 5 mm is often achieved in practice (Newman & Choo, 2003)(Clark et al, 1997). However, smaller cover depths than these were chosen to accelerate chloride and oxygen ingress under laboratory conditions. Consequently, cover depths of 10, 20 and 30 mm were chosen for this study.

4.2.2 Water/binder ratio

Water/binder (w/b) ratios were varied in order to determine the effect of the microstructure of concrete on the drying time and hence the corrosion rate. A decrease in the w/b ratio is known to reduce the penetrability of the concrete, as the hydration products have a higher level of particle interlocking (Grieve, 2009). In order to adequately test the effect of the w/b ratio on oxygen availability and reinforcement corrosion rates, two w/b ratios were selected. One mix was designed to produce concrete that facilitates the easy absorption of water and chlorides, while the other mix was designed to have a lower porosity and thus minimize the ingress of water and chlorides. With this in mind, w/b ratios of 0,5 and 0,8 were selected.

4.2.3 Exposure conditions

As the purpose of this investigation was measure corrosion in the tidal zone (and hence infer oxygen availability as a controlling parameter), the concrete specimens were exposed to 6-hour cycles of wetting and drying. This duration was applied in order to simulate the natural exposure conditions in the tidal zone.

The same experiment was repeated with identical concrete specimens exposed to splash and spray conditions and submerged conditions. As there is sufficient literature available on the effect of these two exposure zones on oxygen availability (Hussain, 2011) (Raupach, 1996), the results of these experiments served as a control. Details of the set-up of the 3 exposure zones are given in Section 4.4.

4.3 Specimen details

4.3.1 Mix design

The selection of 2 different w/b ratios required 2 different concrete mix designs. The Cement and Concrete Institute's (C&CI) volumetric mix design was followed as outlined in Addis & Goodman (2009). The results are summarised in Table 4 - 1 below. Detailed procedures of the calculations are given in Appendix A: Laboratory mix design.

Table 4 - 1: Concrete mix designs

Material (kg/m^3)	**Mix 1**	**Mix 2**
	PC (w/b 0.5)	**PC (w/b 0.8)**
Cement (CEM I 52.5N)	380	238
Fine aggregate (Crusher sand)	492	553
Fine aggregate (Dune sand)	492	553
Coarse aggregate (13.2 mm Greywacke)	878	878
Water	190	190

4.3.2 Material selection

CEM I 52,5N was selected as the binder for this research, as it most closely represents the binder that would have been used in the construction of the aged structures found along the coast today. For this reason, the results of this study are limited to plain PC structures. Also, the size of the coarse aggregate was selected to be 13,2 mm instead of the popular 19 mm. This was chosen in an attempt to try and reduce as far as possible the effect of the Interfacial Transition Zone (ITZ) on

the permeability of the concrete cover (Wu et al. 2016). A polycarboxylate superplasticiser (Chryso Premia 310) was used to make the concrete mix workable for easy placement and compaction.

4.3.3 Casting

The materials for each mix design were weighed to the nearest 5 grams using a calibrated scale. Owing to the fact that only 6 corrosion cell moulds were available, only 6 corrosion cells could be produced at a time (details of corrosion cells are given in Section 4.4.5). This resulted in the corrosion cells being cast over a period of 6 days. In addition, the moulds had to be manually adjusted to accommodate for different cover depths. For this reason, all the casting required for a given cover depth was completed before commencing with a new cover depth.

The variables of the specimens cast such as w/b ratio, cover depth and slump values are given in Table 4 - 2.

Table 4 - 2: Casting dates and measured slump

Reference letter	Specified w/b ratio	Specified cover depth (mm)	Slump (mm)
C10-50	0,5	10	75
C10-80	0,8	10	80
C30-50	0,5	30	85
C30-80	0,8	30	90
C20-50	0,5	20	75
C20-80	0,8	20	85

Each mix was made in 48 litre batches, and was used to cast 6 corrosion cells, specimens for moisture profiles (See Section 4.4.6), 3 cubes for compressive strength testing and the specimens required for Durability Index (DI) testing. The corrosion cells required half of the mould to be filled with chloride contaminated concrete, and the other half to be filled with chloride free concrete. Each layer of the corrosion cell specimens were then mechanically vibrated for approximately 10 seconds. This concept is discussed further in Section 4.4.5.

4.3.4 Curing

After casting, all the specimens were covered with polythene sheets for 24 hours before being demoulded. The cubes to be tested for compressive strength and durability were placed in a 23 $\pm$ 2 ℃ water bath for 28 days. The specimens for measuring the corrosion rate and moisture profiles were allowed to dry for 2 weeks in a 50% relative humidity (RH) environment, before being sealed with epoxy on all but one face. After 2 cycles of ponding in 5% NaCl salt solution, the corrosion

cells were set-up in their respective exposure environments. By allowing the specimens to dry before applying the epoxy, the initial exposure to chlorides will be more severe, thereby promoting ingress of chlorides and facilitating the onset of corrosion (ASTM G109).

4.3.5 Manufacture of corrosion macrocell

This section details the approach to producing a macro cell device (also called a corrosion cell). A modified version of the corrosion macrocell outlined in ASTM G109 was used.

4.3.5.1 Overview of corrosion cell

A total of 36 corrosion cells were cast with dimensions 120 × 122 × 380 mm (Figure 4 - 1). The exact dimensions of the mould fittings and rebar location are given in Appendix B-1: Dimensions of mould fittings. Two 10 mm diameter stainless steel rebar (of Grade 316) were embedded in the specimen at varying cover depths (10, 20 and 30 mm) at the bottom of the prism. These serve the function of the cathode in the cell and are set in chloride free concrete. A 10 mm diameter reinforcing steel rebar was then embedded in chloride contaminated concrete in the upper part of the prism to act as the anode. Electrical wire attached to the end of the top and bottom rebar was left to protrude out from the side of the specimen during casting. These wires were then used to create a connection from the anodic steel to the cathodic steel. The ratio of the area of the cathode to the anode was 2:1 to ensure that the surface area of the stainless steel (cathode) did not limit the oxygen reduction rate.

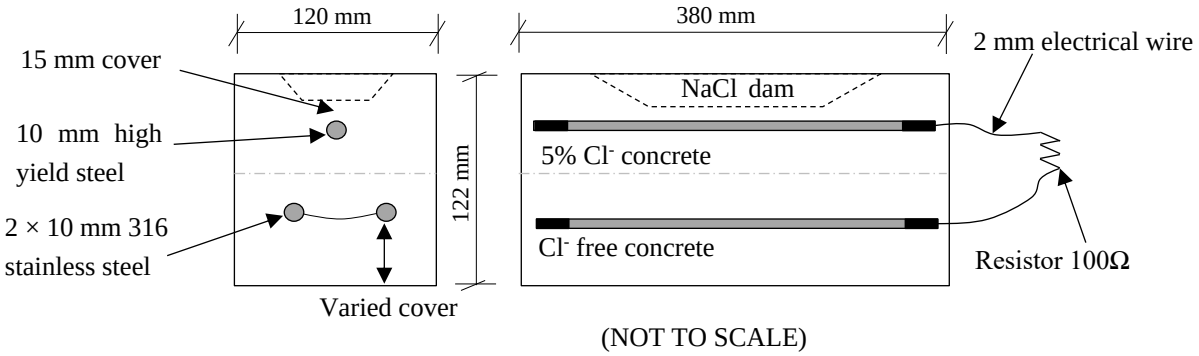

Figure 4 - 1: Schematic of macro cell corrosion prism

4.3.5.2 Preparation of steel bar

Before the rebar was placed in the mould, it needed to be prepared. Insulated electrical wire was connected to one end of each bar. This was done by drilling a hole on one end of each bar and soldering the 2 mm copper wire into place. The ends of the steel bars were then sealed with shrink wrap and insulating tape in order to protect the electrical connection. The other ends of the bars were also sealed to eliminate the chance of oxygen entering the corrosion cell erroneously and influencing the corrosion rate. The connection and shrink wrap seal are shown in Figure 4 - 2.

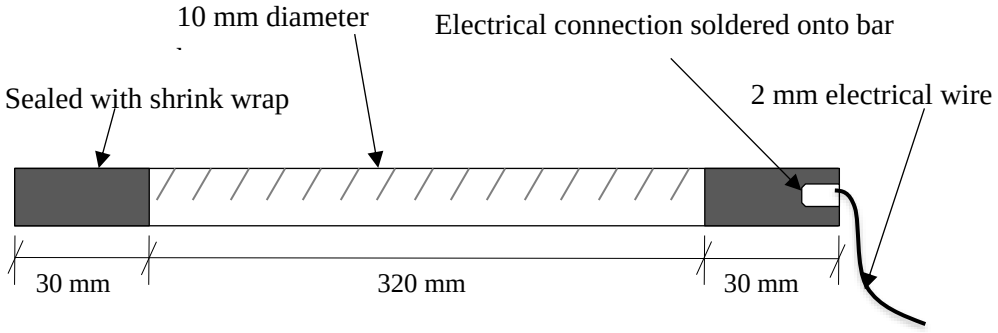

Figure 4 - 2: Set-up of steel rebar

It was important to ensure that the reinforcing bar and the electrical wire had a proper connection. In order to verify the connection, a closed circuit was made by touching one side of a battery to the rebar and the other side of the battery to the electrical wire. An LED light was also included in the circuit. If the electrical connection at the steel/wire interface was unsatisfactory the LED would not light up (See Appendix B-1 for details).

4.3.5.3 Placement in exposure zones

After the corrosion cells were cast and cured, five of the faces were sealed with epoxy (included in this is the edges of the face with the ponding feature). The bottom surface of the cell was left unsealed as well as the ponding feature. The corrosion cells were then placed in plastic containers in a controlled room (temperature set to 22ºC and RH to 50%) on two non-conductive supports. The supports were narrow as to allow air flow under most of the specimen (Figure 4 - 3).

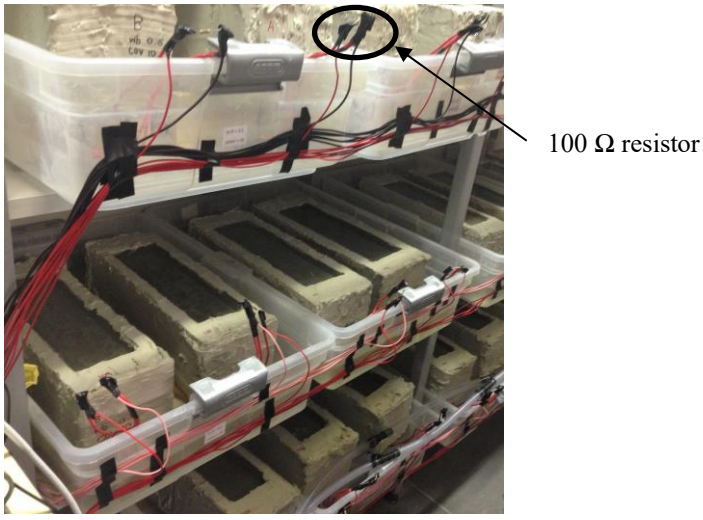

Figure 4 - 3: Set-up of corrosion cells with ponding features and electrical connections

All possible combinations of parameters were assigned to each exposure zone. Two replicates per combination were made, as the equipment used to measure potential drop restricts the number of

total specimens that can be connected to 40. In order to have the recommended three replicates per combination, the amount of parameters would have had to be reduced.

4.3.5.4 Connecting corrosion cell to data acquisition unit

Once the corrosion cells were set-up in their relevant exposure zones, 100 Ω resistors were connected to each specimen as shown in Figure 4 - 3. The electrical connections were protected with insulating tape.

To determine the potential difference across a resistor, a voltage reading device was connected in parallel across each macro cell. This is done to prevent the internal resistance of the voltmeter itself influencing the value of the current recorded, which would lead to an incorrect interpretation of results. A data acquisition unit (HP 34970A) with a 40 channel multiplexer was used to measure the voltage across the resistor in each corrosion cell. This information was used to calculate the current flow between the anode and cathode as explained further in Section 4.5.2.

4.3.5.5 Activation of corrosion

Two techniques for activation of corrosion were considered. The first technique involves casting the cathode in chloride free concrete, and the anode in concrete with a 5% chloride content. This will result in the anode being depassivated and allow the onset of active corrosion.

The second technique, the impressed current technique, involves applying a current to force the steel into an active state of corrosion. The impressed current technique was found to be problematic in some experimental work (Golden, 2015). Hence this technique was not selected, and the method of casting chlorides into the concrete was selected.

In order to provide a continual supply of chlorides to the anode, a ponding feature was incorporated into the corrosion cell (Figure 4 - 1). Each specimen was initially exposed to cycles of 4 days wetting and 4 days drying as a way to accelerate the corrosion (ASTM G109). Owing to time constraints, this cycle was only repeated twice before the pond was kept permanently saturated (this needed to be done to ensure that oxygen was not entering the specimen through the empty ponding feature). NaCl solution in the ponding feature uses sorption and diffusion to force the flow of chlorides into the concrete and encourage further corrosion. A plastic cover was placed over the ponding feature to minimise evaporation of the solution.

4.3.5.6 Electrochemical theory of corrosion cells

This section attempts to provide justification for the design of the macrocells by describing the corrosion process in relation to the actual specimen's features. Further information on the corrosion process is presented in Section 2.1 of the literature review.

The corrosion process ordinarily forms electrochemical cells with areas of anodic (oxidation) and cathodic (reduction) reactions on the surface of the steel. This requires the existence of an anode (reinforcing steel), cathode (stainless steel), route for ion conduction (concrete pore solution), and

connectivity of cathode and anode (the steel itself). The first half cell reaction occurs at the anode (high yield rebar) where electrons (e^-) are passed into the electrical wire as a result of iron being oxidised. These electrons then move along the electrical wire, through the resistor and into the cathode (stainless steel rebar). Electrons and oxygen (which progress from the environment through the cover layer) are then consumed at the cathode in order to form hydroxide (OH^-). This is the second half cell reaction. The hydroxide (OH^-) is transported through the concrete pore solution from the cathode to the anode where expansive rust product is formed. The flow of ions and electrons through the corrosion cell is illustrated in Figure 4 - 4.

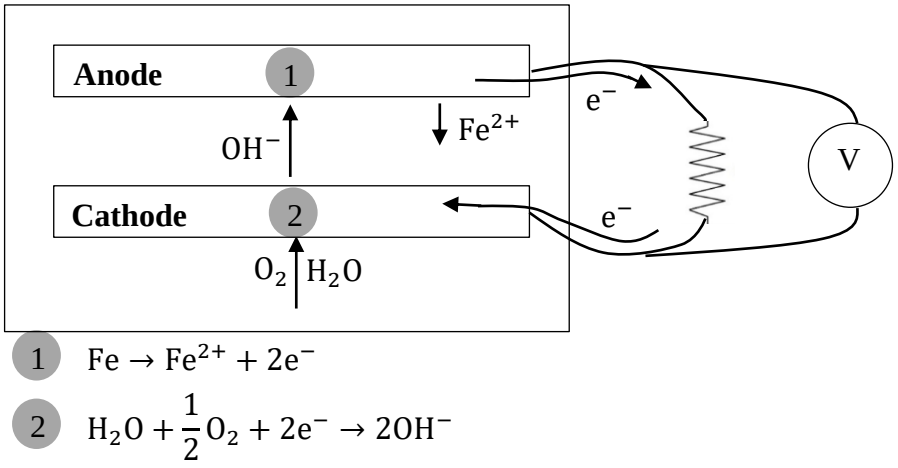

Figure 4 - 4: Half-cell reactions and flow of electrons in corrosion cell

Although these 2 half reactions were described separately, in reality they occur simultaneously. Accordingly the amount of electrons transferred across the concrete-steel interface has to be balanced across the whole system. Consequently, for this particular set-up, the quantity of electrons being transferred is limited only by the availability of oxygen at the cathode. This in turn is affected by the cover depth and the quality of the cover of the corrosion cell. In order to make sure that the reaction of oxygen was not curbed by the ratio of the cathode to anode surface area; two stainless steel bars were incorporated into the design of the corrosion cell instead of one. Also, stainless steel was chosen as the cathode material so that it will remain passive no matter the conditions of the concrete. The current flow between the top and the bottom steel gives an idea of the corrosion rate, which is controlled by the anodic or cathodic reactions.

4.3.6 Manufacture of moisture specimens

Three companion moisture specimens were cast per mix in order to establish moisture profiles in the different exposure zones. The specimens were made by inserting steel rods into the moisture mould prior to casting at a height of 10, 20 and 30 mm. The steel rods were coated in a lubricant and removed during the demoulding process. The effect of the lubricant on the moisture measurements was deemed negligible. This left voids in the concrete in which a 5 mm moisture

probe (HC2 – P05) could be inserted. These voids were closed with a rubber seal and a plastic cap, to ensure that any moisture detected is from the exposed surface and not from moisture entry into the void itself (See Figure 4 - 5). This technique was preferred to that of Akita, Fujiwara & Ozaka (1995) that uses a gravimetric method as using a moisture probe is more accurate for small increments in cover depths. The sides were sealed so that only one face (the bottom face) was exposed to the environment allowing unidirectional ingress of moisture. The effect of sealing was confirmed by sealing all sides of one sample, and measuring the weight gain when submerged for 72 hours (Appendix B-3). The percent change in mass was less than 0,1 %, which is considered insignificant.

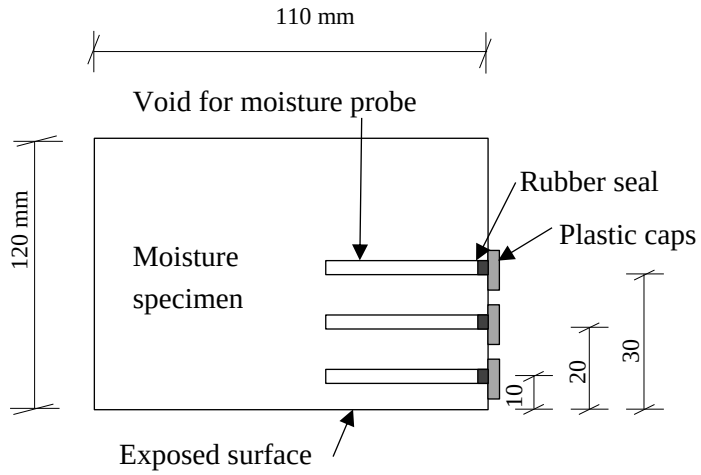

Figure 4 - 5: Specimens used for moisture profiles

4.4 Exposure zone set-up

All the specimens were kept in a control room where the humidity and temperature of the environment was regulated and monitored. The experimental set-up for the different exposure zones are given below.

4.4.1 Submerged Zone

In order to simulate the submerged environment, the cover zones of the specimens were permanently saturated with a 5% NaCl solution. For practical reasons, the specimens were not submerged to their full height. However, as long as the path from the exposure surface to the site of the cathode (i.e. the cover layer) remained submerged, the diffusion of oxygen through the covercrete would be hindered and mimic that of the submerged zone (Figure 4 - 6). Furthermore, the ponding feature on the top face of the specimen will allow the upper part of the specimen to remain wet. The results from this experiment should be comparable with that of the works of Hussain (2011), Andrade, Alonso & Garcia (1990) and Raupach (1996) who show in their work that the corrosion rate is thwarted as a result of diminished oxygen levels when submerged.

4.4.2 Splash and Spray Zone

Concrete specimens were placed in a controlled environment with regulated temperature and relative humidity, and manually sprayed with 750 ml of 5% NaCl solution every Monday, Wednesday and Friday. This was done to simulate the spray of sea water. Exposure to air will result in the concrete having sufficient levels of oxygen at the steel concrete interface to facilitate the cathodic reaction, while also having sufficient moisture and chlorides to facilitate completion of the circuit. These specimens are intended to serve as a benchmark for comparing the results in the simulated tidal zone.

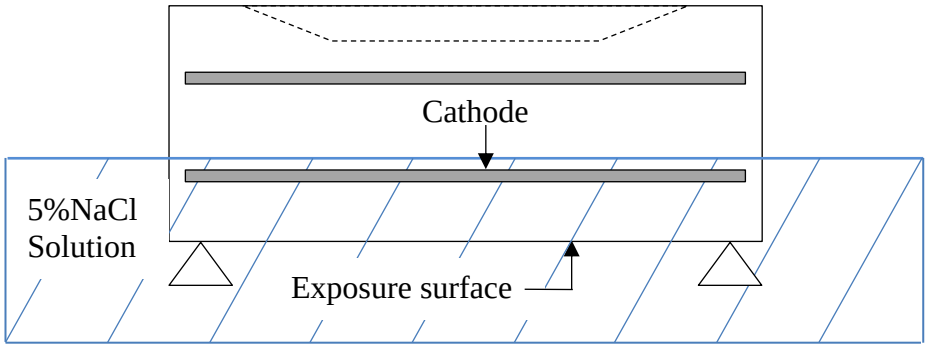

Figure 4 - 6: Corrosion cell in the submerged zone showing exposure surface fully covered

4.4.3 Tidal Zone

The remainder of the concrete specimens were exposed to cyclic wetting and drying in order to clarify the role oxygen plays in the corrosion process in the tidal zone. To simulate the natural tidal zone as much as possible, 12 hour cycles consisting of 6 hours wetting and 6 hours drying were selected. In order to achieve this, a pump with a timer was utilised and set to switch on every 12 hours. This transferred 5% NaCl solution from the reservoir into the containers holding the specimen, thus raising the tide. Another pump with a timer was used and set at a delay of 6 hours from the first pump (Figure 4 - 7). This allowed the transfer of the 5% NaCl solution back into the reservoir, thus lowering the tide. In this way, specimens were exposed to consistent cycles of wetting and drying.

Adjustable irrigation valves were attached to the ends of the pipes in order to control the water flow, and thus the rate at which the tide increased or decreased. The flow was controlled so that the time taken for the water level to change from low tide to high tide, and vice versa was approximately 10 minutes. In addition, in order to prevent the water from siphoning back through the water pipe as a result of filled water pipes, an orifice was made in the tubing. This orifice stops the flow of water, and allows the reservoir and the containers holding the specimens to remain at different water levels until the onset of the next tidal cycle.

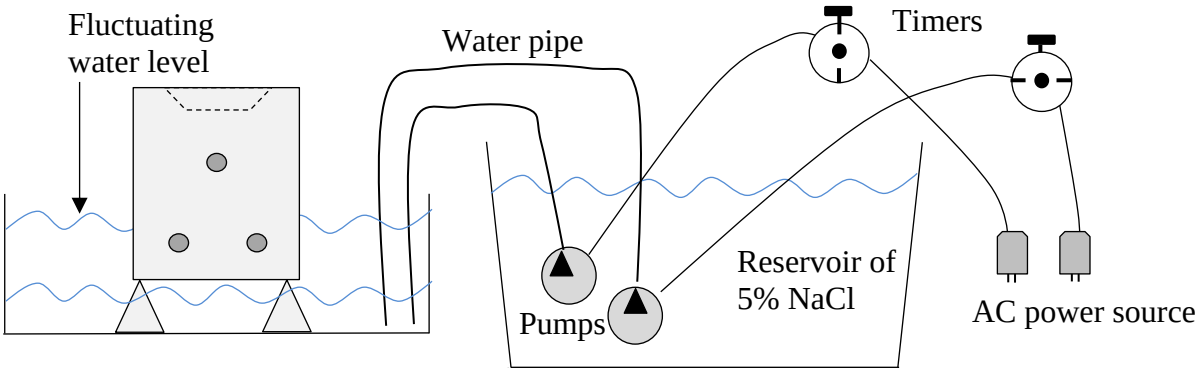

Figure 4 - 7: Experimental set-up for tidal exposure environment

4.4.4 Chloride Solution

The 5% NaCl solution was prepared by mixing salt into warm 40ºC potable water. This was done to allow more salt particles to be dissolved between the water molecules. The solution was then allowed to cool to room temperature before being used in the experimental set-up. Furthermore, the reservoir of NaCl solution was stirred once a week to ensure a consistent concentration of salt throughout.

4.5 Monitoring of specimens

This section addresses how data was collected, and the frequency at which the tests were performed. Data was collected for this project over a period of 23 weeks.

4.5.1 Cover measurements

As the experiments require knowledge on the effect of the moisture content on the corrosion rate for a wide range of cover depths, it was important to ensure the required cover thickness was achieved. After curing of the corrosion cells, cover measurements were taken across three sections of the specimen and the average recorded. This had to be done before the corrosion cells were placed in their final configuration, as the surface to be tested was difficult to reach once set-up. An elcometer with a standard cover head was used to take the readings. Detailed cover depth measurements are given in Appendix E.

4.5.2 Corrosion performance

All 36 corrosion cells were connected to the data-logger (Figure 4 - 8). The reading of the voltage was taken at the end of the drying cycle. This was done to correspond to the relative humidity results of the specimens. Once the voltage was measured, the current (in Ampere) flowing through

the circuit could be determined using Ohm's law. Ohm's law states that the current across a conductor is proportional to the voltage and inversely proportional to the resistance in that circuit (Equation 4-1). (Rauf, 2017)

$$\mathrm{I(macrocell\ current)} = \frac{\mathrm{V(voltage)}}{\mathrm{R(resistance)}} \tag{4-1}$$

The resistance of the circuit is known (100 Ω) and the voltage is obtained from the data logger. Thus the macrocell current (and therefore the corrosion rate) can be determined. Voltage readings were taken once a week.

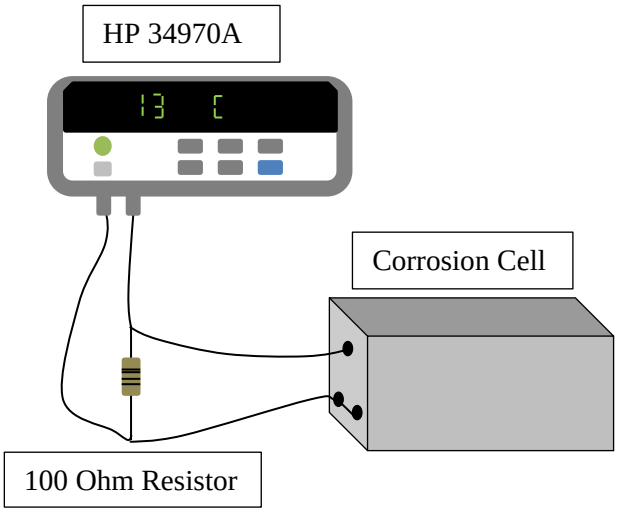

Figure 4 - 8: Connection from corrosion cell to data acquisition system

Furthermore, the integrated corrosion current can be calculated for each corrosion cell using equation 4-2 (ASTM G109). Effectively, this formula allows the total area under the current versus time graph to be determined, which indicates the gross corrosion that has occurred.

$$TIC_j = TIC_{j-1} + \left[\left(t_j - t_{j-1}\right) \times \frac{(i_j + i_{j-1})}{2}\right] \tag{4-2}$$

Where TIC = total integrated current in coulombs; t_j= time in seconds; and i_j= macrocell current at time t_j in amps.

Note that when integrating the current, the unit changes from ampere to coulomb. This is because the value in ampere is equivalent to one coulomb per second, and when integrated over time gives the total charge that has passed through the circuit (i.e. coloumbs).

4.5.3 Moisture profile

A moisture probe was used to establish the relative humidity at various cover depths. The moisture probe was left for 20 minutes to adjust to the relative humidity of the room. The humidity reading from the probe was compared to that of the actual humidity value of the room. This information

was then used to calibrate any results obtained from the moisture specimens. The relative humidity readings were taken at 5 different times during the duration of the experiment (day 60, day 80, day 102, day 120 and day 145).

Although other methods such x-ray diffraction exists to obtain moisture profiles, the technology is expensive and difficult to operate. The equipment required is confined to specialist laboratories and therefore was not available for this investigation.

4.5.4 Durability tests

Durability index tests were required for each mix. The durability index tests were conducted at 28 days and followed the procedure as outlined in the DI Test Manual (2018). Companion cubes were cast and then cored and cut into 70 × 30 mm discs as per the requirements (SANS 3001-CO3-1). Three durability indicators were assessed for each concrete mix, namely:

- OPI (Oxygen Permeability Index) (SANS 3001-CO3-2)
- WSI (Water Sorptivity Index) (SANS 3001-CO3-4)
- CCI (Chloride Conductivity Index) (SANS 3001-CO3-3)

From these tests, reliable index values were produced which helped to characterise the concrete and predict its performance. Each test relates to a transport mechanism in the covercrete such as permeation, absorption and diffusion.

Details of the test procedure followed and the DI results are given in Appendix D: Detailed durability indices.

4.5.5 Compressive strength

The compressive strength of each mix was also determined by preparing standard 100 mm cubes. Specimens were tested at 28 days according to the procedure outlined in SANS 5863. A manually operated AMSLER machine was used and a loading rate of 0,3 MPa/sec was applied until failure. The compressive strength of each cube was determined by dividing the failure load by the cross-sectional area. Detailed compressive strength results are given in Appendix C.

4.6 Timeline of experimental programme

Corrosion cells cast → 2 weeks drying 50% RH → 2 cycles ponding (4 days wet 4 days dry) → set-up in exposure zones and then commencement of test → Results recorded weekly for 23 weeks

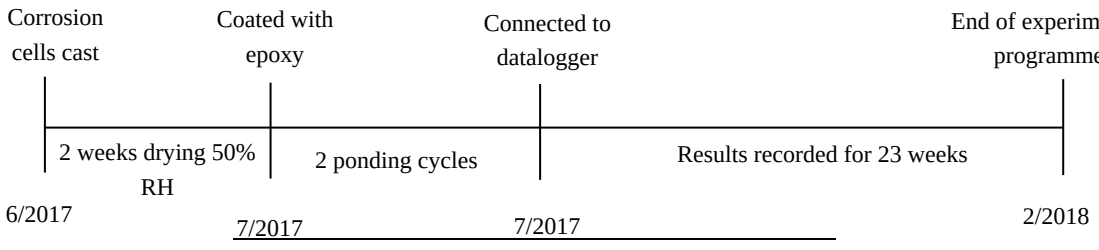

Figure 4 - 9: Timeline of experimental programme

5 Results and discussion of experimental testing

This chapter presents the results and findings of the experimental testing phase of this research. As stated previously, concrete that is exposed to chloride ions and high moisture contents allow for anodes and cathodes to be separated (commonly referred to as macrocell corrosion). This makes it possible to mimick the behaviour of chloride induced reinforcement corrosion in properly designed macrocell specimens. This chapter presents the results of these microcells' current in relation to time, cover depth, cover quality, and relative humidity.

5.1 Time variant corrosion current (I_{corr})

Figure 5 - 1 to Figure 5 - 6 show the 3-point moving average corrosion rate (I_{corr}) for macrocell specimens with varying cover depth and w/b ratio. These figures also depict the influence of different exposure conditions (tidal, splash and submerged) on I_{corr}. While general observations relating to I_{corr} to the exposure time are given below, a more detailed discussion between corrosion rate and parameters such as cover depth, cover quality and moisture content is presented later in the chapter.

5.1.1 3-point moving average

The 3-point moving average was calculated for each specimen in order to smooth the data and get an idea of overall trends of a data set. This was done by replacing a data point with the average of that point under consideration and its neighbouring data points (Equation 5 - 1).

$$3\ point\ average\ I_{corr} = \frac{I_j + I_{j-1} + I_{j+1}}{3} \qquad (5 - 1)$$

Where I_j = corrosion current at the j^{th} data point; I_{j-1} = corrosion current before the j^{th} data point; and I_{j+1} = corrosion current following the j^{th} data point.

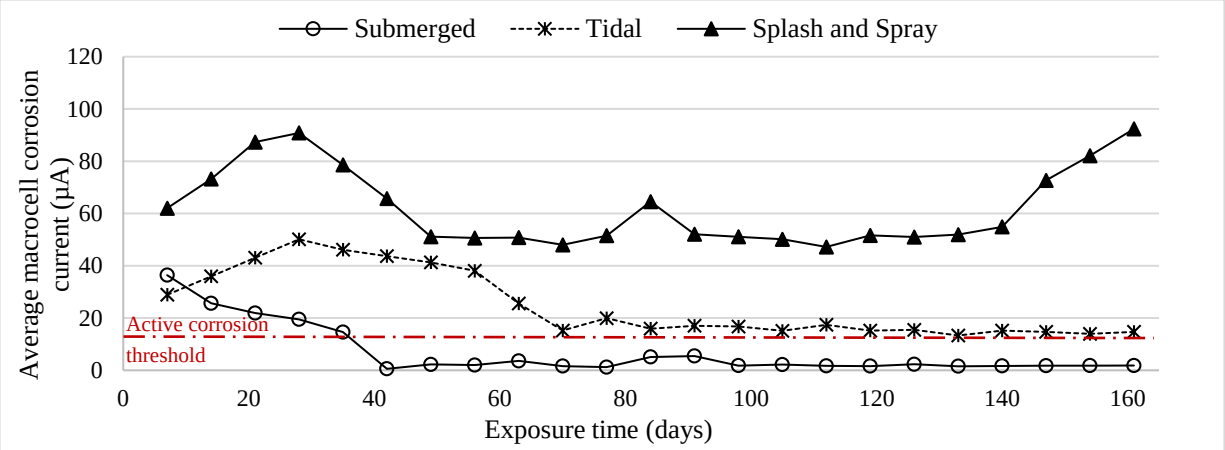

Figure 5 - 1: Moving average corrosion current for specimens C10-50

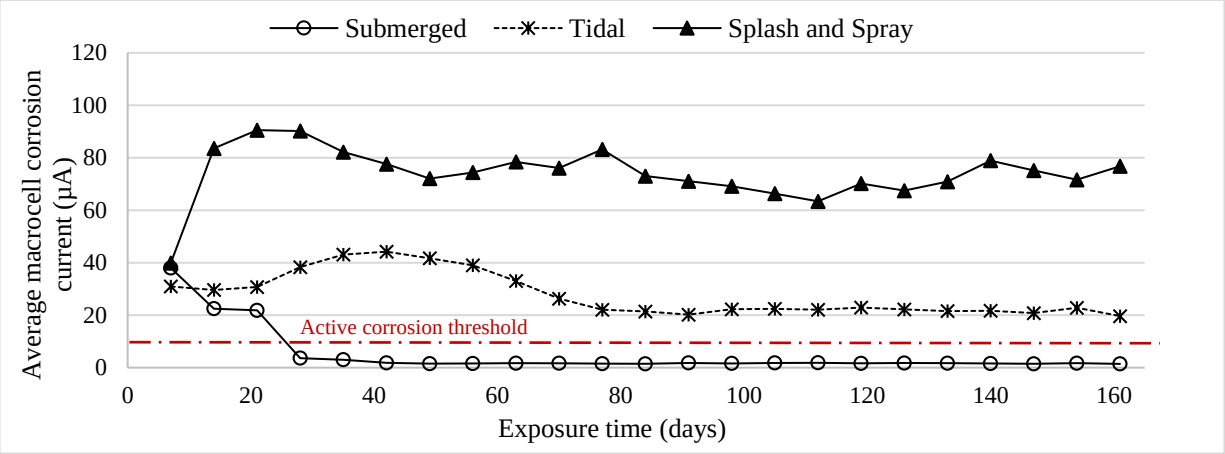

Figure 5 - 2: Moving average corrosion current for specimens C10-80

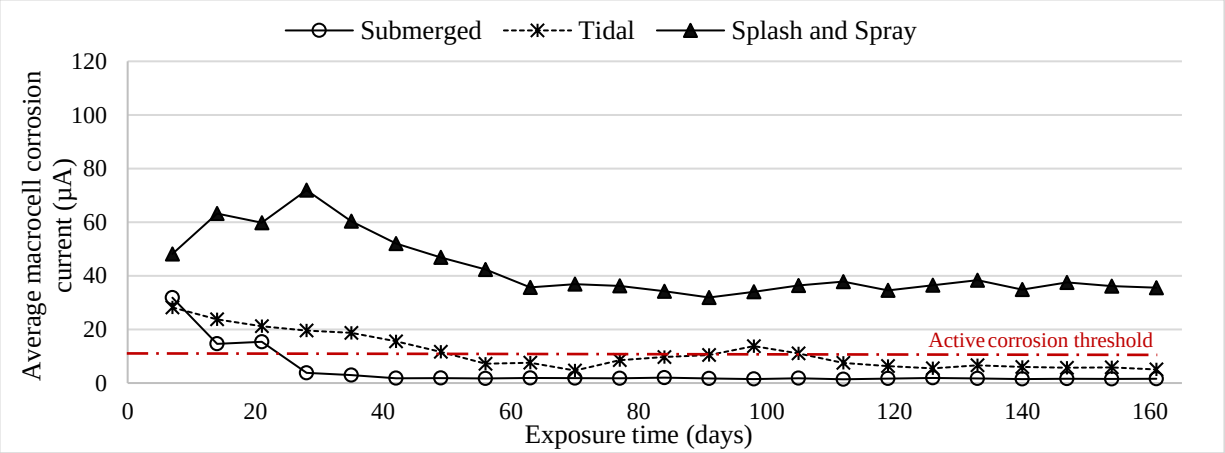

Figure 5 - 3: Moving average corrosion current for C20-50

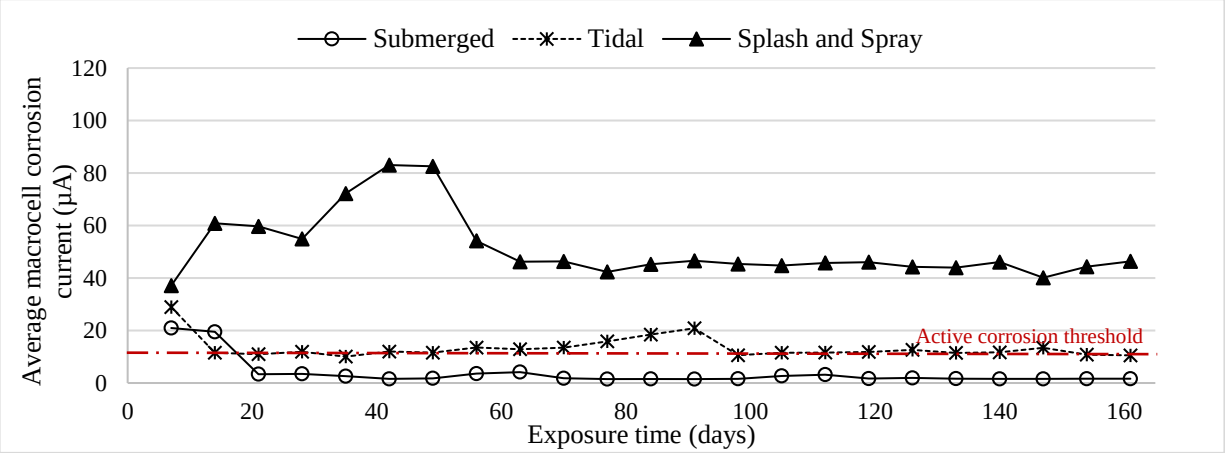

Figure 5 - 4: Moving average corrosion current for C20-80

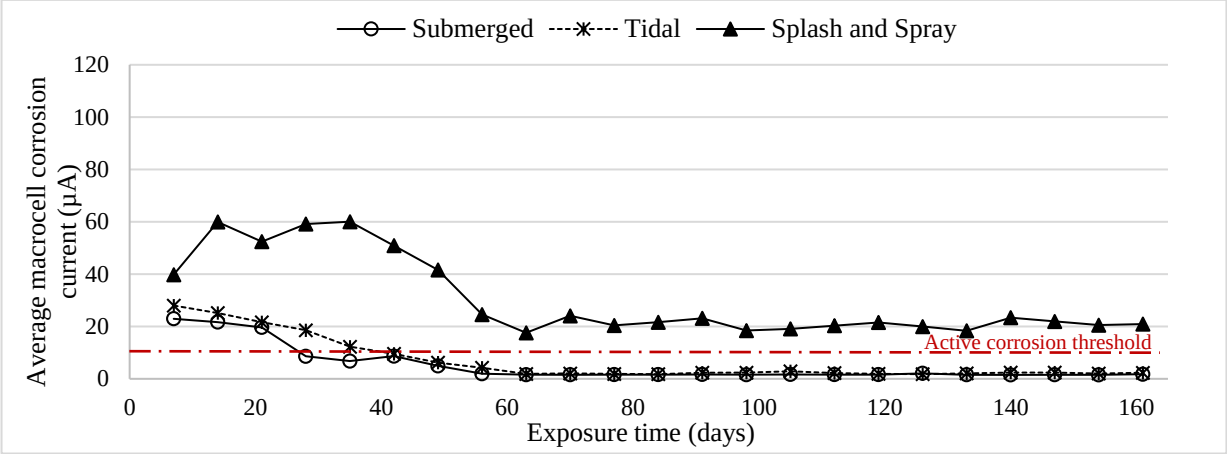

Figure 5 - 5: Moving average corrosion current for C30-50

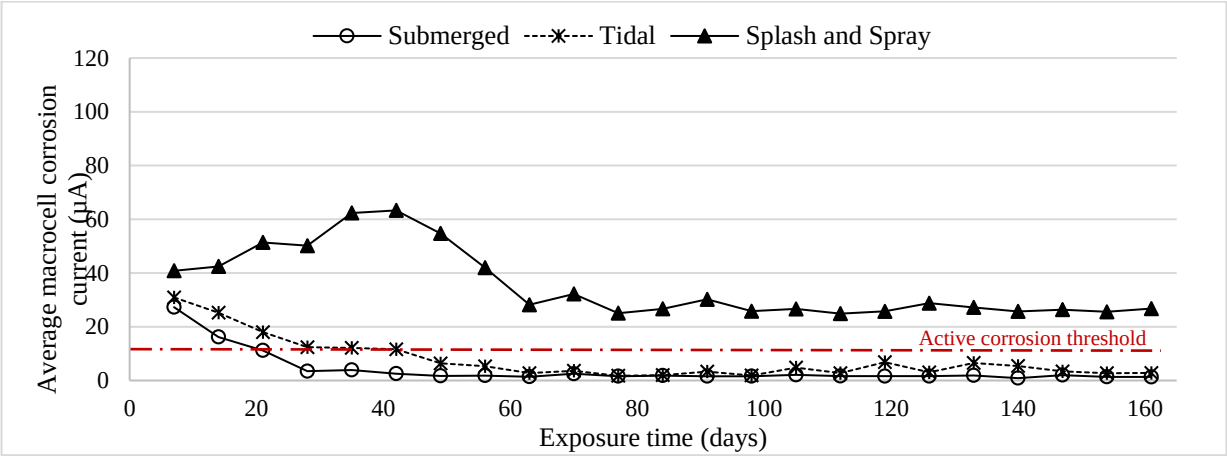

Figure 5 - 6: Moving average corrosion current for C30-80

A macrocell corrosion current of 10µA is indicated in Figure 5 - 1 to Figure 5 - 6 as it is often considered to be the point where there is sufficient corrosion to ensure the presence of corrosion for visual evaluation (ASTM G109). Many laboratory control specimens showed that for corroding G109 macrocell specimens, the integrated macrocell current was 150C or greater. This was found to be equivalent to 10 µA over 6 months (G109). This is a conservative value, as generally active corrosion is considered to occur at 0,1 µA/cm^2, which translates to 2,5 µA. Nonetheless, 10µA was chosen as the benchmark for active corrosion for the G109 macrocell corrosion specimens, in order to align with the values set out in the ASTM G109 standard (Valipour, Shekarchi & Ghods, 2014).

5.1.2 Observations about time variant corrosion current

Only the time variant observations about the corrosion current (I_{corr}) are presented below. The effect of parameters such as cover depth, w/b ratio and exposure condition are discussed in greater detail later.

5.1.2.1 Fluctuation of early age corrosion current

From day 0 to day 60, the corrosion current fluctuates quite significantly. Other studies also show variation in early age corrosion currents (Yuan, Ji & Jiang, 2009), and is attributed to time needed for equilibrium between the internal environment of the concrete and the artificial environment to be achieved.

5.1.2.2 Time variant corrosion current explained considering corrosion product layer

The rate of corrosion also appears to generally start off high and descend in most specimens during the first 60 days. After this, the corrosion current stabilises in the specimens from day 60 to the end of experimental monitoring at day 160. An exception to this is specimen C10-50, whose corrosion current ascends again at day 140 up until day 160. This behaviour can be explained by considering research on the mechanisms of the growth of the corrosion layer (Yuan, Jiang & Peng, 2010).

a. Phase 1: Descending corrosion current

During this phase, the ITZ (around the steel begins to fill with dense corrosion product. This corrosion product layer prevents air and moisture from accessing the steel and this the anodic reaction is inhibited and the corrosion current reduces (Figure 5 - 7). This is the reason why all the specimens show a descending corrosion current value from the onset to day 60.

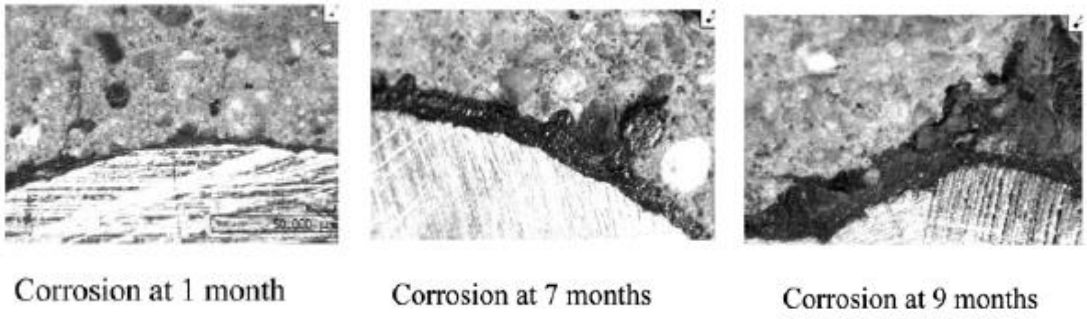

Figure 5 - 7: Corrosion layers in macrocell current as determined Yuan, Jiang & Peng (2010)

b. Phase 2: Steady corrosion current

During this phase, equilibrium is achieved between the access and consumption of water and oxygen, and the formation of the corrosion product layer. This is owing to the rate of the corrosion layer formed slowing down as a result of (i) less oxygen and moisture to fuel corrosion and (ii) more corrosion product required to cover a greater surface area as the volume of corrosion product expands. The equilibrium then leads to stable corrosion current values, as seen in all the specimens from approximately day 60 to the end of the experiment at day 160.

c. Phase 3: Ascending corrosion current

Once the corrosion product creates sufficient internal tension for the concrete to crack, the corrosion current tends to increase. This crack forms a new access route for oxygen and moisture to easily reach the steel. The increased availability of these resources result in an increase the corrosion current, as was observed in specimen C10-50 from day 140. If the corrosion current had continued to be monitored further, it is expected that the ascending phase would eventually stabilise again as the corrosion products fill up the cracks.

5.1.2.3 Size of ITZ's influence on duration of phase 2

Literature shows that concrete with a lower w/b ratio will stifle the corrosion current more than that of a concrete with a high w/b ratio as it inhibits the movement of moisture and oxygen through the concrete cover. This is reflected by looking at the values of the stable corrosion current for specimen C10-50 and C10-80 (w/b ratio of 0,5 and 0,8 respectively). The corrosion current of the higher w/b ratio of 0,8 is higher than that of the lower w/b ratio of 0,5. Nonetheless, the specimen with the lower w/b ratio (C50-10) and lower stable corrosion current, has a crack that runs parallel with the reinforcing steel, whereas the specimen with the higher w/b ratio (C80-10) doesn't. It is unsure why this crack has occurred, and this specimen has been excluded from the experimental results.

5.1.2.4 Time variant corrosion current for submerged zone

Another reason for the initial descent (phase 1) of the corrosion current for specimens in tidal and submerged conditions, can be explained by considering the residual oxygen in the pores from when the specimens were exposed to air before placement. Only once this residual oxygen has been used up in the corrosion process will there be a measurable fall in the current. This result was found in other studies (Andrade, Alonso & Garcia, 1990) and (Hussain, 2011) which show that the corrosion current of submerged specimens initially descended before reaching a stable value. Once the concrete is saturated and the residual oxygen has been consumed, the only limiting factor of the corrosion current is the rate of diffusion of oxygen through the pore solution. From Figure 5 - 1 to Figure 5 - 6, it can be seen that the point at which all residual oxygen has been used up occurs at different days of submersion. These values are given in Table 5 – 1 and shows that the time taken for residual oxygen depletion in the submerged zone varies from 28 to 42 days with no apparent relationship to cover depth and w/b ratio. It is important to note that oxygen depletion was not measured directly in the experiment, but rather inferred from corrosion rate measurements.

Table 5 – 1: Time to oxygen depletion inferred from corrosion rate in different specimens

Specimen	Time to oxygen deprivation (days) inferred from corrosion current measurements
C10-50	42

C10-80	28
C20-50	30
C20-80	21
C30-50	28
C30-80	35

The stabilising corrosion current from specimens in the splash zone is not from consumption of residual oxygen, as the concrete remains aerated in these conditions. This may be untrue for concrete in the splash zone with large cover depths (>60 mm). However, this lies outside of the research scope as the specimens all had relatively small cover depths of 10, 20 and 30mm.

5.1.2.5 Simulated chloride solution versus real seawater

As discussed in the literature review, owing to the formation of a thin brucite on the surface of concrete immersed in real seawater, the permeability of the surface of concrete is significantly reduced (Beunfeld & Newman, 1986). However, as the specimens in this experiment were immersed in a simulated sodium chloride solution, this surface skin would not have developed (Kawabata, Kato & Iwanami, 2012).

5.1.2.6 Consideration of the initiation phase

The time to initiation of corrosion has been excluded from this study by the virtue of inclusion of cast in chlorides. In reality, the initiation of corrosion can take years to occur. All specimens started with the same high chloride value at the reinforcing as the same concentration of chlorides was cast in each specimen. In natural exposure conditions, the specimens in different exposure conditions would have different governing transport properties, and different rates of ingress of chlorides. In general, concrete exposed to cyclic wetting and drying has higher chloride concentrations than submerged concrete or even splash concrete. When considering this there is no doubt that the initiation of corrosion in the tidal zone happens faster than for specimens in the submerged or the splash and spray zone. This must be taken into account when interpreting the corrosion propagation results which do not take consider time to initiation.

5.2 Total Integrated Current

While the corrosion current development (I_{corr}) over time is useful to consider, the total integrated current that has occurred for the duration of the experiment can also present interesting conclusions. For this reason, the total integrated current (TIC_{corr}) was evaluated for all 36 macrocell specimens using the method given in Section 4.5.2, and gives an indication of the total current passed through

a corrosion cell over 160 days. It should be noted that when integrating the current over time, the unit changes from µA to coulomb.

The total integrated current (TIC_{corr}) was determined for each combination of parameters and plotted in the bar graph below (Figure 5 - 8). From this graph, the following observations can be made:

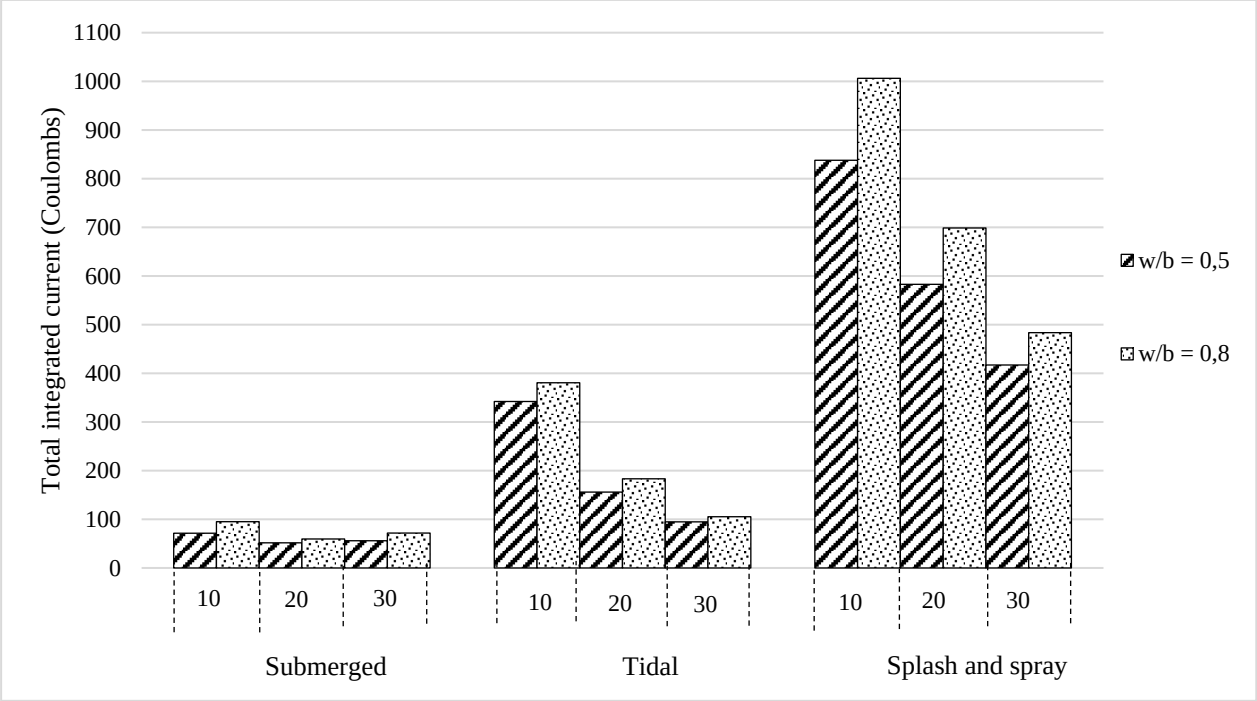

Figure 5 - 8: Total integrated current in specimens in 3 marine exposure conditions

5.2.1 Comparison of TIC_{corr} in different exposure conditions

The specimens with the most current passing through it in 160 days were the C10-80 specimens in the splash zone. This value of 1006 C is far above the 150 C value set to indicate the change over from active to passive corrosion. The next 5 highest TIC_{corr} values were all specimens in the splash zone (ranging from 1006 to 417 C), indicating that the most current passed through specimens in this exposure zone. These high corrosion values are attributed to oxygen in the external environment having sufficient time to reach the steel, and encouraging the cathodic reaction.

Specimen C20-50 in the submerged zone had the lowest TIC_{corr} of 52 C. This was closely followed by specimens C30-50 and C20-80 with values of 56 and 60 C respectively. All the specimens in the submerged zone had a very small TIC_{corr} over 160 days, with values ranging from 52 to 95 C. This range is well below that of the splash zone (1006 to 417 C) showing the significant different in specimens when comparing the splash and submerged zone. This result is as expected, and is owing to the slow rate of diffusion of oxygen through water. As the pores are saturated in the

submerged specimens, oxygen reaches the embedded steel at a very slow rate, and thus limits the cathodic reaction rate.

The range of specimens in the tidal zone had TIC_{corr} over 160 days vary from 381 to 95 C, where specimen C10-80 had the highest TIC_{corr}, and C30-50 had the lowest TIC_{corr}. This overall range was lower than the TIC_{corr} range of specimens in the splash zone (1006 to 417 C), although the upper limit in the tidal zone of 381 C (specimen C10-80) is close to the lower limit of 417 in the splash zone (specimen C30-50). The TIC_{corr} values in the tidal zone are higher than TIC_{corr} values of specimens in the submerged zone. The upper range of TIC_{corr} in the submerged zone (specimen C10-80) is the same as the lower limit of the C30-50 specimen in the tidal zone, with a value of 95 C. These results show that for certain combinations of parameters (high cover and w/b 0,5), specimens exposed to cyclic wetting and drying behave similarly to those that are submerged. This is as a result of oxygen deprivation at the steel owing to slowly diffusing oxygen through the cover layer. Specimens with low cover depths and w/b of 0,8 have higher corrosion values, as a result of oxygen being able to move faster through the concrete cover, and facilitate the cathodic reaction.

The suggestion that oxygen deprivation is the reason for varied corrosion rates in different exposure conditions can be reinforced by considering the moisture profiles in the specimens. The results of the actual moisture profiles obtained are discussed further in Section 5.3.

5.2.2 Comparison of TIC_{corr} for specified cover depths

When making a comparison amongst the specimens within the splash and spray zone alone, it is seen that the TIC_{corr} decreases with an increase in the cover depth. For example, considering specimens with a w/b ratio of 0.8, C10-80 has a TIC_{corr} of 1006 C, whereas C20-80 and C30-80 have values of 698 C and 484 C respectively. A similar trend appears when considering specimens with a w/b ratio of 0,5 in the splash zone. As the cover depth increases (C10-50, C20-50 and C30-50), TIC_{corr} decreases (838 C, 583 C and 417 C respectively). These findings were expected as literature shows that higher cover depths impede the ingress of harmful substances the propagate corrosion.

The same can be said when comparing all specimens within the tidal zone. TIC_{corr} decreases from 381 to 183 and 105 C (for specimens C10-80, C20-80 and C30-80 respectively) as the cover depth increases. For specimens with a lower w/b ratio of 0,5, TIC_{corr} also decreases with an increase in cover depth. This is evident from C10-50, C20-50 and C30-50, that have TIC_{corr} values of 342, 156 and 95 C respectively. High cover depths result in concrete needing far more time to dry out between cycles to allow oxygen to penetrate easily through the cover surface. This illustrates how bigger cover depths can retard oxygen ingress into the concrete cover layer, and hence stifle corrosion. There is not much literature available to validate this claim, which is why considering the moisture profiles of the specimens is useful (See Section 5.3).

The specimens in the submerged zone have a different pattern when increasing the cover depth. When increasing from 10 to 20 mm cover depth (C10-50 to C20-50), the TIC_{corr} decreases from 71 C to 52 C. Then as the cover depth increases further (C20-50 to C30-50) the TIC_{corr} increases slightly from 52 C to 56C. The same pattern can be observed in the specimens with w.b ratio of 0,8 (C10-80, C20-80 and C30-80 have TIC_{corr} of 95 C, 60 C and 72 C respectively). This shows that the cover depth does not have a significant influence on the corrosion rates in submerged conditions. Without oxygen supplied to the steel (i.e. in the submerged zone), corrosion is very low, which is independent of cover. Interestingly, in the tidal zone, cover does tend to have an influence, indicating that oxygen does get supplied to the steel at different amounts (cover depending). From Figure 5 - 8 a cover of 30 mm effectively converts the tidal zone into the submerged zone, as these specimens have very similar corrosion rates.

5.2.3 Comparison of TIC_{corr} for specified w/b ratios

When comparing the TIC_{corr}in specimens with different w/b ratios (given the same cover depth and exposure conditions), the w/b ratio of 0,8 yields larger TIC_{corr} than w/b ratio of 0,5. For specimens in the splash zone with a cover of 10 mm, the TIC_{corr} increases when w/b ratio changed from 0,5 to 0,8 (C10-50 and C10-80 have TIC_{corr} of 838 C and 1006 C respectively). The same was observed in specimens with a cover of 20 mm (C20-50 and C20-80 have TIC_{corr} of 583 and 699 C) and a cover of 30 mm (C30-50 and C30-80 have TIC_{corr} of 417 and 484 C). The reason for this result is that a higher w/b ratio of 0,8 is associated with a less dense pore structure and lower resistivity values. The low resistivity values allows the corrosion reactions to proceed at a faster rate. Higher corrosion rates in concrete with higher w/b ratios is probably also related to higher oxygen availability. Firstly, concrete dries out faster at a higher w/b ratio, which allows for oxygen to penetrate, and secondly, oxygen penetrates faster to the reinforcing steel when the permeability is higher.

In the tidal zone, specimens with a higher w/b ratio also yielded larger TIC_{corr} (given the same cover depth). Specimens with cover depth of 10 and w/b ratio of 0,5 and 0,8 (C10-50 and C10-80) had TIC_{corr} of 342 and 381 C respectively. The TIC_{corr} also increased when increasing the w/b ratio from 0,5 to 0,8 for a cover of 20 mm in the tidal zone (C20-50 and C20-80 has TIC_{corr} of 156 and 183 C). Similarly, for cover of 30 mm and w/b of 0,5 to 0,8 (C30-50 to C30-80), TIC_{corr} increased from 95 to 105 C. Specimens in the tidal zone with a low w/b ratio have a more dense pore structure, and will take longer to dry out, resulting in suppression of the cathodic reaction through oxygen deprivation. This explains the trend observed in the specimens in the tidal zone.

In the submerged zone, the increase in TIC_{corr} when changing the w/b ratio is less prominent. For example, specimens with a cover of 10 mm have TIC_{corr} increase from 71 to 95 C for w/b of 0,5 and 0,8 respectively (C10-50 to C10-80). Similarly, TIC_{corr} changes from 52 to 60 C (C20-50 and C20-80) and 56 to 72 C (for C30-50 and C30-80). This shows that rebar corrosion is stifled in the

submerged zone, due to a lack of oxygen, independent of other factors that usually influence rebar corrosion (such as w/b ratio and cover depth).

5.3 Effect of moisture content on TIC_{corr} corrosion rate

5.3.1 RH results from moisture specimens

The RH was recorded at 5 different times during the duration of the corrosion cell experiment (day 60, day 80, day 102, day 120 and day 145). The results from the tests across these 5 days for different parameters are given in Figure 5 - 9, Figure 5 - 10 and Figure 5 - 11 for cover depths of 10, 20 and 30 mm respectively.

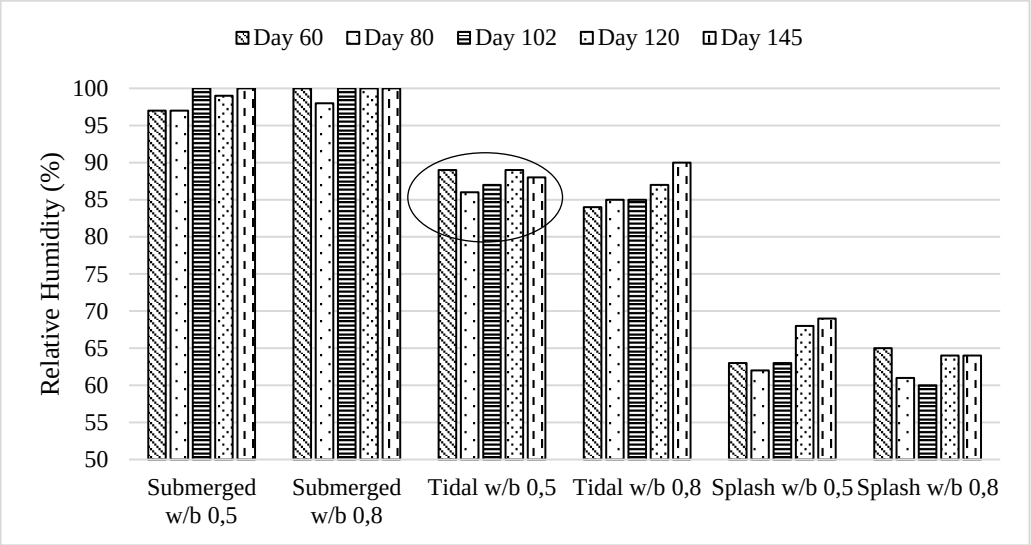

Figure 5 - 9: RH values for specimens with a cover depth of 10 mm

Hypothesis testing was used to compare the data sets across the 5 days to determine if there was any significant statistical difference (Appendix F: Statistical Analysis). At 5% level of significance ($\alpha = 0{,}025$), the critical t value was determined to be 4,3. From this information it was determined with 95% confidence that the RH profiles do not change over time (for example, there is no significant difference between the values circled in Figure 5 - 9). For this reason, the RH profile can be averaged and simplified to include only one RH value per unique set of w/b ratio, cover depth and exposure conditions.

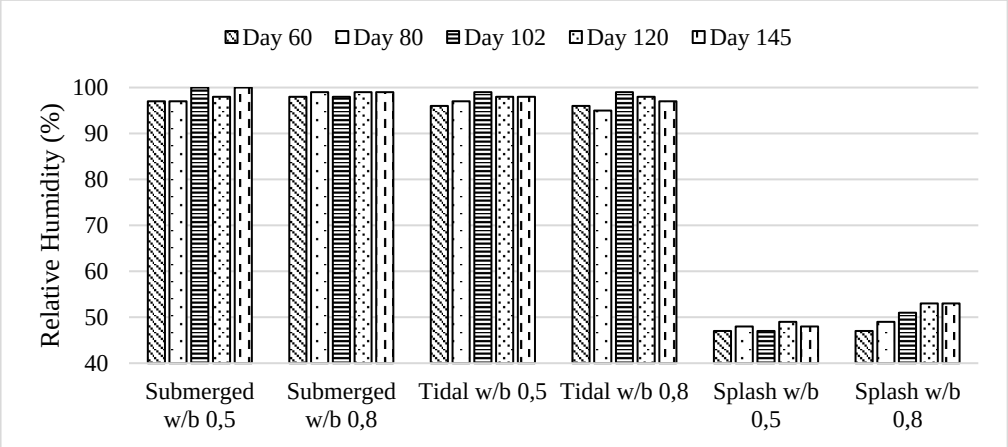

Figure 5 - 10: RH values for specimens with a cover depth of 20 mm

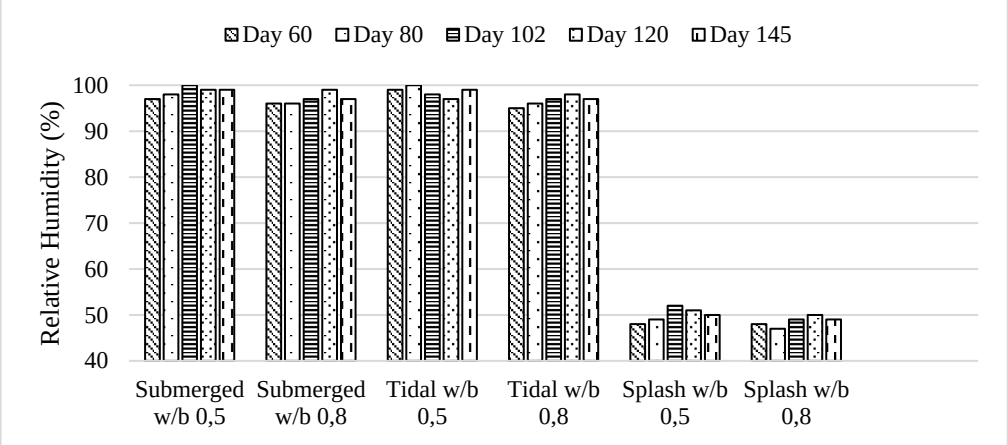

Figure 5 - 11: RH values for specimens with a cover depth of 30 mm

5.3.2 Submerged zone

The RH profiles and the total integrated current profiles for different cover depths were plotted on the same graph. A total integrated value of above 150 Coulombs over 160 days was assumed to be approximately where the corrosion can be considered active corrosion (Trejo, Halmen & Reinschidt, 2009).

Figure 5 - 12 shows the relative humidity profile for concrete specimens with w/b ratio of 0,5 and 0,8 respectively in submerged conditions. Two observations can be made about the relative humidity profiles of the specimens at cover depths of 10, 20 and 30 mm. Firstly, the relative humidity exceeds 97% for all cover depths of 10, 20 and 30 mm. This is to be expected as specimens in the submerged zone are saturated or partially saturated with water. The second observation is that at a w/b ratio of 0,5 the relative humidity reduces to 97% at a cover of 30 mm, whereas at 10 and 20 m cover depth the relative humidity was ± 100%. The same was not observed for specimens with a w/b ratio of 0,8, that had relative humidity's of ± 100% at all the cover depths. This can be attributed to water struggling to permeate into the deep parts of the concrete with such

a dense pore structure. The same was found by Ryu, Ko & Noguchi (2011) who showed that the moisture content of the concrete with a w/b ratio of 0,3 does not reach 100% at any depth that exceeds 10 mm.

Figure 5 - 12 also shows the corresponding TIC_{corr} for all 3 cover depths which are well below the 150 Coulombs limit of active corrosion, for both a w/b ratio of 0,5 and 0,8. The TIC_{corr} value for specimens with a w/b of 0,8 is slightly higher overall than the specimens with a w/b of 0,5. The difference is so small (< 20 Coloumbs) that any observed changed in TIC_{corr} in specimens is not statistically significant and therefore not discussed further.

An important observation when comparing the relative humidity profile to that of the TIC_{corr} is that high relative humidity values in specimens produce low TIC_{corr} values. It is likely that the high relative humidity (or moisture content) in the concrete is stifling the supply of oxygen to the steel, and hence preventing active corrosion. When concrete is partially saturated with water from its environment and the majority of the pores are filled, oxygen accessibility can become limited at the steel surface. This is because oxygen has a substantially lower diffusion coefficient in saturated concrete than it does in air. Furthermore, Gjorv (1972) stated that the concentration of oxygen in air is 210ml/litre, whereas the maximum concentration of dissolved oxygen in seawater is only 5-10 ml/litre. This shows how concrete that has fully saturated pores in the submerged zone has lower oxygen concentration, which further minimises it's availability for the electrochemical corrosion process at the cathode. These results conform to the widely accepted principle that submerged concrete is less vulnerable to corrosion as a result of insufficient oxygen. From this data, it can be sufficiently concluded that at an internal RH of 97% or more in concrete, the corrosion is stifled as a result of limited oxygen availability.

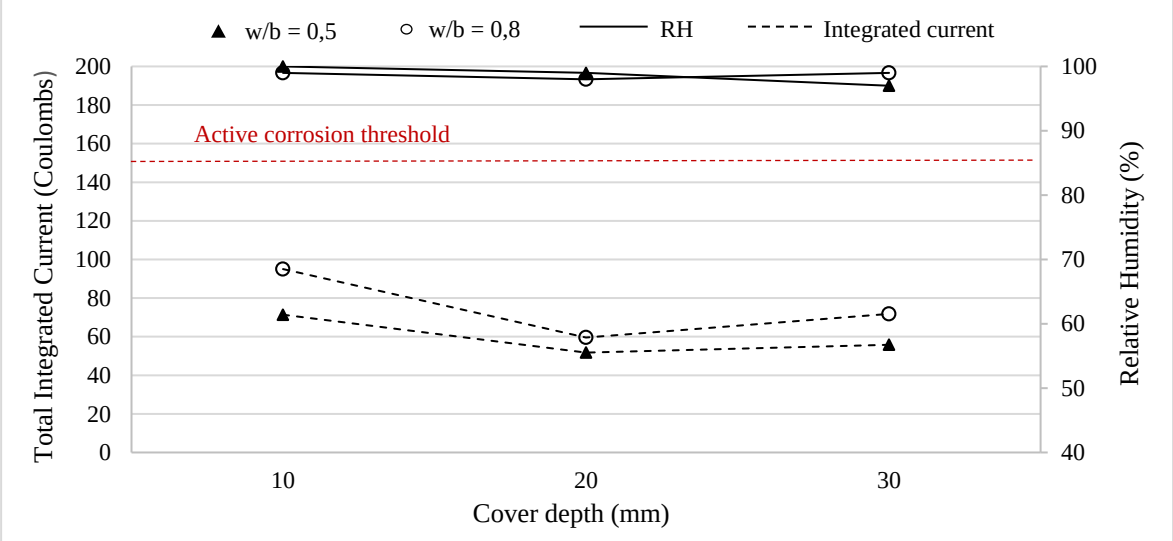

Figure 5 - 12: Total integrated current and RH profiles for specimens in the submerged zone

5.3.3 Tidal zone

Figure 5 - 13 shows the relationship between relative humidity and TIC_{corr} profiles for specimens subjected to 6 hour cycles of wetting and drying. The relative humidity close to the surface of the concrete (10 mm depth) is lower than the relative humidity deeper in the concrete (30 mm). Considering the relative humidity readings were recorded at the end of the 6 hour drying cycle, it makes sense that some of the surface concrete would have evaporated from the concretes surface resulting in a relative humidity of 86%.

The severity of the moisture loss in concrete is dependent on the environmental conditions. Concrete directly exposed to sunlight and wind will dry out faster than concrete sheltered from the elements. Seasonal changes that influence the temperature and climate also heavily influences the rate at which concrete dries. However, Hunkeler (2005) showed that short term environmental factors cannot influence the internal water content of concrete beyond a depth of 60 mm, while the water content can be influenced by as much as 30% within the first 10 mm of concrete cover. This is seen in which shows no change in the relative humidity value of the specimens when compared to the submerged zones, for a cover depth exceeding 20 mm.

Changing the w/b ratio from 0,8 to 0,5 does not have a significant influence on the relative humidity profile of the specimens. This is not expected, as research has shown that a lower w/b ratio dries out slower owing to a to (i) the less amount of free evaporable water in the concrete and (ii) a more refined pore structure which inhibits the escape of moisture (Nilsson, 2002). This point is not reflected in the results, possibly because both w/b ratio parameters selected (0,5 and 0,8) are quite high, and hence both have a sparser pore structure.

Figure 5 - 13 shows that for specimens with a cover depth of 10 mm, the TIC_{corr} is significantly higher than that of the specimens with a cover depth of 20 mm and 30 mm respectively. The same trend is found in specimens with a w/b of 0,5 and 0,8, although the specimens with the higher w/b ratio and less dense pore structure tends to have a higher TIC_{corr} at 10 mm ,than the lower w/b ratio. The difference in the TIC_{corr} values for specimens with a w/b ratio of 0,5 and 0,8 becomes less noticeable for higher cover depths. This difference in TIC_{corr} values cannot be attributed to a difference in moisture content (or relative humidity), as the relative humidity profile is very similar for specimens of both w/b ratios. The reason for the difference in the TIC_{corr} values is probably owing to low cover depths being controlled by the resistivity of the concrete itself.

Reducing the concrete cover thickness, lessens the path that oxygen is required to travel from a structure's surface to the embedded steel (Hawkins & McKenzie, 1996). The faster that oxygen can travel to reinforcing in concrete, the more oxygen is available for the cathodic reaction to proceed. These results show that the cover depth is more effective at reducing the corrosion rate via oxygen control than the quality of the cover. The same was found to be true only for concrete that was cathodically controlled, such as concrete made from OPC (Scott, 2004). Given the corrosion rate is cathodically controlled for these specimens, higher cover depths result in a

reduction in the availability of oxygen. The results achieved also indicates that if there is sufficient oxygen available to allow for high corrosion rates (at a cover of less than 10 mm), the resistivity of OPC can become the controlling factor in the corrosion rate.

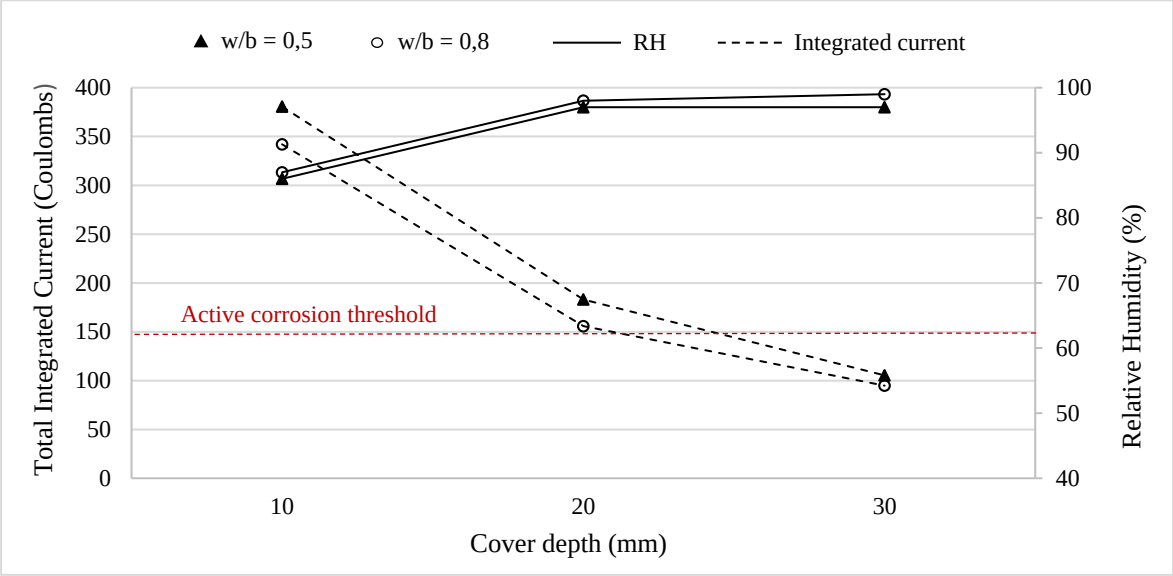

Figure 5 - 13: Total integrated current and RH profiles for specimens in the tidal zone

Relating the relative humidity profile and TIC_{corr} value to each other, it is evident that when the relative humidity value is high, the TIC_{corr} is low, and vice versa. For example, a low corrosion current of 155 C was associated with a relative humidity of 97%, while a reduction in the relative humidity by 11% results in an increase in the total integrated corrosion current by 300 C.

This shows how the moisture content of the specimens, and hence the oxygen availability, plays a large part in controlling the corrosion rate. For specimens with a high cover depth, 6 hours is not sufficient amount of time for the concrete to dry to the level of the steel. The pores surrounding the steel are therefore still partially or fully saturated with water. As a result, oxygen diffuses slower through the cover layer. Consequently, where the concrete in the tidal zone has drying time of 6 hours and large cover depths, the steel will be oxygen deprived, and corrosion will be stifled. This means that the concrete in the tidal zone would theoretically perform as if it were permanently submerged (provided sufficient cover depth).

Furthermore, it must be added that a layer of marine fouling can further slowdown the drying of the cover layer of concrete, and therefore inhibit the movement of oxygen into the concrete as a result of saturated or partially saturated pores. This was not investigated in this study but could the results of any investigation surrounding this could offer a natural buffer for chloride induced corrosion.

5.3.4 Splash zone

Figure 5 - 14 shows the relationship between TIC_{corr} and RH for specimens in the splash zone. The RH at 10 mm is approximately 65% while at 20 and 30 mm the RH is closer to 48%. The higher RH at the concretes surface could be as a result of the constant splashing on the concretes surface, while the concrete beyond a cover depth of 20 mm remains largely undisturbed by any surface splashing and is kept at equilibrium. It is clear to see that at a relatively low RH, oxygen would be able to diffuse through the pore system and facilitate corrosion in the specimen. This is owing to the pores around the steel not being saturated with moisture, and oxygen being readily available to participate in the cathodic reaction. This is reinforced by the high TIC_{corr} values that are plotted at 10, 20 and 30 mm depths.

As already discussed above, it is also evident that in the splash and spray zone the cover depth has a strong influence over the TIC. For example, as the cover depth increases from say 10 to 20 mm it can be seen that the TIC drops by 33%. This can be attributed to the longer distance deleterious substance (such as oxygen) would have to travel in order to reach the surface of the steel. For these specimens, the electrical resistivity of the concrete is the main limiting factor in controlling the corrosion rate (Raupach, 1996).

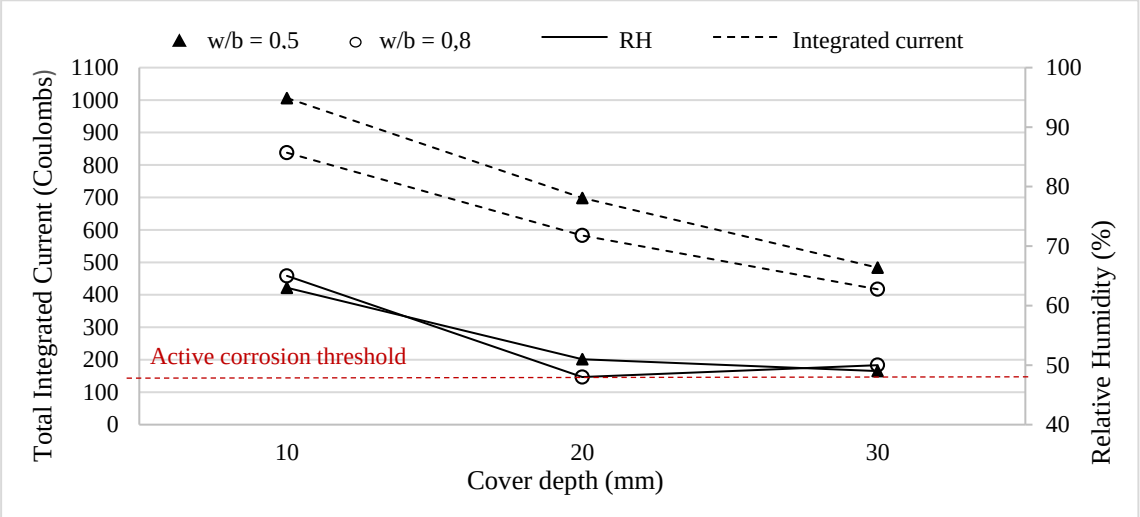

Figure 5 - 14: Total integrated current and RH profiles for specimens in the splash zone

From the results above, it is evident that specimens exposed to 6 hours of cyclic wetting and drying are cathodically controlled (given sufficient cover depth and quality of the concrete cover). This is owing to the high moisture content in these concretes not allowing sufficient oxygen to reach the surface of the steel. This lead to the conclusion that the tidal zone is far less vulnerable to chloride induced corrosion than previously thought.

6 Conclusions and recommendations

This chapter presents the conclusions to both the field structures and experimental work (Section 6.1 – 6.7). Recommendations and suggestions for improvements are given in Section 6.8.

6.1 Short summary of research aims and methodology

The aim of this research is to investigate the influence different environmental conditions have on the corrosion of reinforced concrete. The three exposure zones under investigation mimic certain marine environments and include (i) submerged conditions, (ii) cyclic wetting and drying conditions, and (iii) splashing conditions.

In order to do this, the corrosion assessments of field structures in marine environments were investigated. In addition, experimental corrosion cells were set-up in simulated marine environments and the corrosion rates and moisture distribution profiles recorded. The conclusions from the field structures and experimental work are given below.

6.2 Rebar corrosion damage in structures exposed to real marine conditions

Inspection of field structures in Southern Africa harbours showed the influence of the exposure zone on the durability conditions. For example, a sand filled caisson located at the end of an ore jetty, Saldanha Bay, was found to have corrosion induced damage only in the splash and spray zone with a cover depth of 50 mm, while the tidal zone with a cover of 46 mm once again remained in good condition. This could only be assumed to be a direct consequence of the different exposure environments, as the cover depths and quality of cover are relatively similar.

Another example is precast bearing piles from a jetty in Namibia which, despite high levels of chlorides (> 0,7 %), had no evidence of corrosion damage in both the tidal zone and the lower splash zone. There was evidence of marine biofilm on all piles in the tidal zone, which could in combination with large cover depths and high quality of precast concrete, have prevented the concrete from drying out. The same observations were made for numerous other structures along the coast.

Conversely, two structures were investigated that only existed within the submerged and tidal conditions (a tidal pool wall and launch ramp). These structures both had considerable level of reinforcement corrosion damage in the tidal zone. A possible explanation for this is that the steel within the tidal zone has a higher potential than that of steel within the submerged zone, leading the reinforced concrete in the tidal zone to be the preferential anode for corrosion. As opposed to structures that are continuous across all 3 exposure zones (i.e. piles or quay walls), where the steel in the splash zone prevents corrosion in the tidal zone by acting as a sacrificial anode.

The function of the structure is also crucial, as seen in the repair jetty, Namibia, which is used to offload fish and hold heavy repair equipment. The slab from this jetty experiences greater deterioration problems when compared to a slab that is used for small craft mooring and recreational activities. This is because heavily loaded structures develop more micro-cracks, which accelerate ingress of deleterious materials like moisture and chlorides. This in turn accelerates corrosion of the embedded steel.

6.3 The influence of cover depth on reinforcement corrosion for site and experimental data

The level of deterioration and cover depth were plotted for the site structures, and grouped into splash zone and tidal zone (Figure 3 - 8). It should be noted that the structures grouped together are all different in terms of location, function and quality, and so the conclusions drawn from this figure is just an indication of trends. Nonetheless, the results show that for cover depths of between 40 and 60 mm, the splash zone has significantly higher deterioration levels than concrete in the tidal zone. Presumably, at lower cover depths, oxygen is able to reach the rebar in the splash zone far faster by diffusing through the air-filled pores, while pores in concrete in the tidal zone are partially or fully saturated with seawater. Only at higher cover depths exceeding 80 mm, do the tidal and splash zones experience similar levels of deterioration. The low levels of deterioration at high cover depths in both exposure zones is as a result of chloride and moisture ions having a longer path to travel before reaching the rebar.

The results from the experimental work show similar trends to that of the site structures. In general, as is already well understood, a higher cover depth inhibits the movement of deleterious substances through the cover and slows corrosion. However, this impact that a larger cover depth has on reducing the corrosion rate was found to be depend on the environmental conditions. The corrosion durability of concrete in the splash zone is highly dependent on the cover, while in contrast the corrosion durability of concrete in the submerged is insignificant. Changing the cover depth had no conclusive effect on specimens in the submerged condition, as the fully saturated pores control the amount of oxygen available at the steel regardless of the cover depth. Interestingly, in the tidal zone, cover does tend to have an influence, indicating that oxygen does get supplied to the steel at different amounts (cover depending). From Figure 5 - 8 a cover of 30 mm effectively converts the tidal zone into the submerged zone, as these specimens have very similar corrosion rates.

6.4 The influence of quality on reinforcement corrosion for site and experimental data

No data was obtained on the quality of the concrete for the field structures investigated. For this reason, no inferences can be made on the effect of the quality of the reinforced concrete on corrosion for the field structures.

However, results for the experimental portion of the research shows how, generally, higher concrete quality leads to a reduction in the corrosion rate. As with the cover depth, the impact of changing quality on overall corrosion current had different effects on the specimens depending on the environmental conditions. For concrete in the splash zone, increase in the quality led to a reduction in permeability for oxygen, and hence an increase in the durability. In contrast, a change in the quality of concrete had no significant effect on the durability of concrete in the submerged zone, due to a lack of oxygen at the rebar as a result of slow diffusion rates through saturated pores. Concrete in the tidal zone show that increasing the quality of the cover has a minor effect on durability. This small change is owing to a more dense pore structure taking longer to dry out, resulting in suppression of the cathodic reaction through oxygen deprivation. However, this effect is so small for concrete in the tidal zone it can be considered negligible.

The results also show that the cover depth is more effective at reducing the corrosion rate via oxygen control than the quality of the cover.

6.5 The influence of exposure environment on rebar corrosion

It is very evident that the exposure environment strongly influences the amount of rebar corrosion. This can be linked to the moisture distribution or moisture content of the concrete under different environmental conditions.

The main finding from the field presented in this chapter is that concrete exposed to the splash and tidal zone deteriorate at different rates. In continuous structures, the tidal zone usually has no corrosion while the splash zone shows evidence of spalling and delamination. This occurs for two reasons, namely, (i) a lack of available oxygen at the steel from lack of drying of the cover concrete during low tide, and (ii) from steel in the splash zone protecting the steel in the tidal zone by acting as a sacrificial anode.

The experimental work yielded similar results. For concrete submerged and partially or completely saturated with water oxygen accessibility can become limited at the steel surface. High relative humidity (or moisture content) stifles the supply of oxygen to the steel, and hence prevents active corrosion. The results obtained conform to the widely accepted principle that submerged concrete is less vulnerable to corrosion as a result of insufficient oxygen.

Specimens exposed to a splash environment performed as expected. A relatively low moisture distribution profile showed how oxygen would be able to diffuse through the pore system and facilitate corrosion in the specimen. This is owing to the pores around the steel not being saturated with moisture, and oxygen being readily available to participate in the cathodic reaction. In the case of these specimens, the electrical resistivity of the specimen is the main limiting factor in controlling the corrosion rate (and not cathodic control as with tidal and submerged specimens).

For concrete exposed to 6 hour cycle of wetting and drying, the corrosion rate was significantly lower when the cover depth is high. This is because pores surrounding the steel are still partially or fully saturated with water, and haven't had time to dry out. As a result, oxygen diffuses slower through the cover layer. Consequently, where the concrete in the tidal zone has drying time of 6 hours and cover depths sufficiently high (in this case 30 mm), the steel will be oxygen deprived, and corrosion will be stifled. In the tidal zone at 10 mm cover, the moisture content is lower than in the submerged zone. This relates to slightly higher corrosion rates at 10 mm cover in the tidal zone. This is attributed to water in the pores being able to dry from the surface 10 mm of concrete in the 6 hours drying time. The pores are therefore air saturated, and allow the rapid ingress of oxygen to the rebar, resulting in higher corrosion values.

The severity of the moisture loss in concrete is dependent on the climate conditions. Concrete directly exposed to sunlight and wind will dry out faster than concrete sheltered from the elements. Seasonal changes that influence the temperature and climate also heavily influences the rate at which concrete dries.

6.6 Critique of design standards

From the case studies and experimental results, it is clear that the current classification of marine environmental conditions is highly over simplified. Marine structures tend to have a wide range of deterioration conditions depending on the location, exposure condition and function of the structure. A suggestion for improving the SANS guidelines is given in Table 6 - 1. Changes to the existing SANS table include adding a column that accounts for the function of the structure (that results in different corrosion risks), as well as adjusting the exposure zone classifications for the tidal zone. The SANS guidelines currently considers the splash and tidal zone as the same exposure class. However it is suggested that concrete with cover depths exceeding 30 mm be absorbed into the submerged zone category. The value of 30 mm cover depth based on the results of the experimental work, as it was found that at a cover of 30 mm, the tidal zone effectively behaves as a submerged specimen, producing similar corrosion rates. This value is a temporary place holder, and should be refined with further research on real structures.

Table 6 - 1: Recommended improvement to current SANS classification guidelines

Surface and exposure environment	Function	
	Increased corrosion potential*	**Normal corrosion potential****
1. Structures vulnerable to chloride induced corrosion		
(a) Near-coastal (1 km to 50 km from coastline) any climatic zone	C1	C1
(b) In direct contact with sea water	-	-
Permanently submerged (or tidal with cover exceeding 30 mm)	C2	C2
Exposed to splash and spray (or tidal with cover less than 30 mm)	C3	C4

* These functions need to be refined, but can include jetty's used for offloading fish, or structures susceptible to large cracks as a result of heavy loading on the slab.
** For any structure whose function does not enhance corrosion.

6.7 Practical implications

From this research, the influence of the environmental conditions on corrosion of reinforced concrete structures in the marine environment is now better understood. This is particularly important for the harsh marine environment, where consequences of inadequate design are high.

This outcome allows researchers, engineers and policy makers to improve design methodologies for marine structures, by refining current exposure classes given in local and international standards.

The application of these research findings is in infrastructure that is primarily exposed to only tidal and submerged marine conditions. A common example is concrete pipes where many pipelines have been in service for more 50 years despite sometimes having cover to reinforcement of as little as 20 mm. Concrete pipe manufacturers have claimed the unusually good durability was the result of denser microstructure of pipe concrete. It is more likely to be that corrosion is cathodically stifled due to low oxygen diffusion rates through concrete in these marine exposure environments as reported in this thesis.

Arguably the most significant implication of this research, is to assist engineers to have better informed condition assessments of existing structures in the marine environment. This leads to more sustainable and economical repair and maintenance decisions.

6.8 Recommendations

Based on the results and conclusions of this study, the following recommendations are given and should be implemented in future research. Any inadequacy in the design of the experiments is highlighted and in these cases suggestions for experimental work going forward are given.

6.8.1 Amendment of corrosion cell design

The distance between the anode and the cathode bar changed across all specimens depending on the cover depth (See diagrams in Appendix B: Details for experimental set-up). As this axial distance can affect the rate of movement of hydroxyl ions, it should be ensured in future that the axial distance between the anode and the cathode bar remains consistent. In this way it can be ensured that this distance is not limiting the corrosion current obtained, and any limitation is only as a result of cathodic control (or oxygen depletion).

6.8.2 Amendment of accelerated corrosion technique

A shortfall in the methodology programme implemented in this research includes the method of accelerated corrosion. Chlorides were admixed into the concrete and has been found to cause homogenous distribution of chlorides and hence does not allow for localised areas of corrosion, a common occurrence in natural conditions. Alternatively, it is recommended that the corrosion cells rather be exposed to more cycles of wetting and drying before being exposed to the specimens' respective exposure zone (i.e. submerged, tidal, or splash and spray). In this way the chloride distribution across the concrete will more accurately represent that of an in-situ structure.

6.8.3 Implications of modern binder types

Worldwide the use of CEM I in structures is declining, and blended and composite cements are becoming used instead. This is justified by the large CO_2 emissions produced in the manufacture of CEM I. Consequentially fly ash and slag is included into binders in an effort to reduce the environmental impact of the cement industry. While most of the structures containing these blended cements are still relatively new, research on the effect of using blended cements on the corrosion rates of reinforced concrete in the marine environment still needs to be investigated. For this reason, it is recommended that future research investigating the corrosion rate include a variety of binder types.

6.8.4 Correlation to structures in natural conditions

Although some site data was presented in this research, further testing on structures should be found to correlate the results to the laboratory-based experiments. This could better inform repair decisions when completing assessments of existing structures. Further research in this area should

also attempt to measure in situ corrosion rates in marine concrete structures in the tidal zone with a view to developing a corrosion propagation-based service life model.

References

Addis, B. & Goodman, J. 2009. Concrete Mix Design. In Fultons Concrete Technology. 9th ed., Owens, G., eds. Midrand: Cement & Concrete Institute.

Ahmad, S. 2003. Reinforcement corrosion in concrete structures, its monitoring and service life prediction—a review. *Cement and Concrete Composites*. 25(4–5), pp.459– 471.

Ahmad, S. 2009. Techniques for inducing accelerated corrosion of steel in concrete. *The Arabian Journal for Science and Engineering*. 34, pp. 95- 104.

Akita, H., Fujiwara, T. & Ozaka, Y., 1995. An analytical method of moisture transfer within concrete due to drying. Journal of Materials, (25).

Alexander, M. & Mackechnie, J. 2003. Concrete mixes for durable marine structures. *Journal of the South African Institution of Civil Engineers*. 45(2), pp. 20-25.

Alexander, M.G. 2016. Marine Concrete Structures Design: Durability and Performance. 1st ed. England: Woodhead Publishing.

Alexander, M.G., Beushausen, H. & Otieno, M.B. 2012. *Research Monograph No. 9 - Corrosion of steel in reinforced concrete: Influence of binder type, water/binder ratio, cover and cracking*. CoMIRU: UCT, Cape Town.

Alexander, M.G., Ballim, Y. & Stanish, K. 2008. A framework for use of durability indexes in performance based design and specifications for reinforced concrete structures. *Materials and Structures.* 41(5), pp. 921-936.

Allsopp, D., Seal, K. & Gaylarde, C. 2004. *Introduction to Biodeterioration*. 2nd ed. Cambridge University Press: Cambridge. pp. 119.

Alonso, C., Andrade, C., Rodriquez, J. & Diez, J.M. 1998. Factors controlling cracking of concrete affected by reinforcement corrosion. *Materials & Structures*. 31(1), pp. 435-441.

Andrade, C. & Alonso, C. 1996. Corrosion rate monitoring in the laboratory and on site. Construction and Building Materials. 10(5), pp. 315–328.

Andrade, C., Alonso, C. & García, A.M. 1990. Oxygen availability in the corrosion of reinforcements. *Advances in Cement Research*. 3(11), pp. 127–132.

Andrade, C., Sarría, J. & Alonso, C. 1999. Relative humidity in the interior of concrete exposed to natural and artificial weathering. *Cement and Concrete Research*. 29, pp. 1249–1259.

Angst, U. 2011. *Chloride induced reinforcement corrosion in concrete - Concept of critical chloride content – methods and mechanisms*. PhD Thesis. Norwegian University of Science and Technology.

Arito, P. 2012. *Discrete Sacrificial External Anodes and Their Use in Service Life Extension of Chloride Contaminated Reinforced Concrete Structures*. MSc Thesis. University of Cape Town.

ASTM C876 – 15. 2015. Standard Test Method for Corrosion Potentials of Uncoated Reinforcing Steel in Concrete. ASTM International: West Conshohocken, USA.

ASTM G109. 2013. Standard Test Method for Determining Effects of Chemical Admixtures on Corrosion of Embedded Steel Reinforcement in Concrete Exposed to Chloride Environments. ASTM International: West Conshohocken, USA.

Baboian, R. 2005. *Corrosion Tests and Standards: Application and Interpretation*. 2nd ed.. ASTM International. Printed: Baltimore, USA. pp. 407-411.

Ballim, Y., Alexander, M. & Beushausen, H. 2009. Durability of Concrete. In Fultons Concrete Technology. 9th ed., Owens, G., eds. Midrand: Cement & Concrete Institute.

Ballim, Y., Taylor, P. & Macdonald, H.K. 1993. A preliminary assessment of the effectiveness of a liquid membrane – forming curing compound. *Concrete Beton, Journal of the Concrete Society of Southern Africa*. 66, pp. 25-26.

Bamforth, P.B. 1994. Specification and design of concrete for the protection of reinforcement in chloride contaminated environments. UK Corrosion and Eurocorr. 3, pp. 249-258.

Beushausen, H. & Alexander, M.G. 2008. The South African Durability Index tests in an international comparison. *Journal of South African Institution of Civil Engineers*. 50(1)

Bentur, A., Diamond, S. & Berke, N. 1997. *Steel in Concrete: Fundamentals and Civil Engineering Practice*. London: E & FN Spon.

Berke, N., Shen, D.F. & Sundberg, K.M. 1990. Comparison of the polarization resistance technique to the macrocell corrosion technique. ASTM Special Technical Publication. pp. 38-51.

Bertolini, L., Elsener, B., Pedeferri, P., Redaelli, E. & Polder, R. 2013. *Corrosion of Steel in Concrete.* 2nd ed. Weinham, Germany: Wiley VCH.

Beunfeld, N. R. & Newman, J.B. 1986. The development and stability of surface layers on concrete exposed to sea-water. *Cement and Concrete Research.* 16. pp. 721 – 732.

Beushausen, H. & Alexander, M. 2009. Concrete Repair. In Fultons Concrete Technology. 9th ed., Owens, G., eds. Midrand: Cement & Concrete Institute.

Broomfield, J.P. 2006. *Corrosion of Steel in Concret: Understanding, Investigation and Repair*. 2nd ed. New York: CRC Press.

Broomfield, J.P., Rodriquez, J., Ortega, L.M. & Garcia, A.M. 1994. Corrosion rate measurements in reinforced concrete structures by a linear polarisation device. *Symposium on Corrosion of Steel in Concrete*.

EN 206, 2013. Concrete - Specification, performance, production and conformity. European Standards.

Budget, 2018. Spending cuts for infrastructure. *Industry insight*. Available online: http://industry insight.co.za/wp/2048-2. Retrieved [2018, Sep 11].

Burgh, J. & Foster, S. 2017. Influence of temperature on water vapour sorption isotherms and kinetics of hardened cement paste and concrete. *Cement and Concrete Research*. 92, pp. 37–55.

Burgh, J., Foster, S. & Valipour, H. 2016. Prediction of water vapour sorption isotherms and microstructure of hardened Portland cement pastes. Cement and Concrete Research. 81, pp. 134–150.

Cabrera, J. 1996. Deterioration of concrete due to reinforcement steel corrosion. *Cement and*

Concrete Composites. 18(1), pp. 47–59.

Cairns, J., Plizzari, G.A., Du, Y., Law. D.W. & Franzoni, C. 2005. Mechanical properties of corrosion-damaged reinforcement. ACI Materials Journal. 102(4). pp. 256

Castel, A., Vidal, T., François, R. & Arliguie, G. 2003. Influence of steel–concrete interface quality on reinforcement corrosion induced by chlorides. *Magazine of Concrete Research*. 55(2), pp. 151–159.

Chang, Y.T., Cherry, B. & Marosszeky, M. 2008. Polarisation behaviour of steel bar samples in concrete in seawater - Part I: Experimental measurement of polarisation curves of steel in concrete. *Corrosion Science*. 50(2), pp. 357-364.

Chen, F., Baji, H. & Li, C. 2018. A comparative study on factors affecting time to cover cracking as a service life indicator. *Construction and Building Materials*. 163, pp. 681 – 694.

Chin, R. & Lee, B. 2008. Principles and Practice of Clinical Trial Medicine. Analysis of Data. Academic press: USA

Claisse, P.A. 2005. Transport properties of concrete. *Concrete International*. *27*(1), pp. 43-48.

Clark, L.A., Shammas-Toma, M.G.K., Seymour, D.E., Pallett, P.E. & Marsh, B.K. 1997. How can we get the cover we need. *The Structural Engineer*. 75(17). pp. 289-296.

Comings, E.W. & Sherwood, T.K. 1934. The Drying of Solids – Moisture Movement by Capillarity in Drying Granular Materials. Industrial and Engineering Chemistry. 26(10), pp. 1096-1098.

Daian, J. 1988. Condensation and isothermal water transfer in cement mortar: Part I – pore size distribution, equilibrium water condensation and imbibition. *Transport of Porous Media*. 3(6), pp. 563-589.

DI Test Manual. 2018. Durability Index Testing Procedure Manual. UCT: South Africa.

Duracrete. 1998. Probabilistic performance based durability design: modelling of degradation, *Duracrete Project Document*. The Netherlands.

Duroudier, J.P. 2016. *Adsorption – Dryers for Divided Solids - Hysteresis and the Ink-Bottle Model*. Elsevier.

El Maaddawy, T. & Soudki, K. 2003. Effectiveness of Impressed Current Technique to Simulate Corrosion of Steel Reinforcement in Concrete. Journal of Materials in Civil Engineering. 15(1), pp.41–47.

Hellmich, C.P. & Bernhard, K. J. 2015. Concreep 10. Chapter: Approaches Based on the 2nd Law of Diffusion Considering the Convection Zone. Proceedings of the 10th International Conference. ASCE: Vienna, Austria.

Fagerlund, G. 1975. The significance of critical degrees of saturation at freezing of porous and brittle materials. *ACI SP47-02*. 7, pp. 13–66.

Feldman, R.H. 1968. Sorption and length change: scanning isotherms of methanol and water on hydrated portland cement. Proceedings of Fifth International Symposium Chem Cement, Tokyo. 3(3).

Foley, R. 1970. Role of the chloride ions in iron corrosion. *Corrosion*. 26(2), pp. 58-70.

Forde, M. 2009. ICE Manual of Construction Materials: Fundamentals and Theory. Chapter: Non-

destructive testing of concrete structures. ICE Publishing. pp. 193

Gallé, C. 2001. Effect of drying on cement-based materials pore structure as identified by mercury intrusion porosimetry. A comparative study between oven, vacuum and freeze drying. *Cement and Concrete Research*. 31(10), pp. 1467-1477.

Gaylarde, C.& Morton, L.H.G. 1999. Deteriogenic biofilms on buildings and their control; a review. *Biofouling*. 14, pp. 59-74.

Gehlen, C. 2000. *Probabilistic lifetime calculation of reinforced concrete structures – Reliability considerations for effective prevention of reinforcement corrosion.* PhD Thesis. RWTH Aachen University.

Gjorv, O.E. 1972. Protection of Reinforcing Steel against Corrosion. Nord Betong. 16(1), pp. 19-30.

Gjorv, O.E., Vennesland, O. & E1-Busaidy, A.H.S. 1977. Electrical resistivity of concrete in the oceans. *9th Annual Offshore Technology Conference.* Paper 2803. Houston, Texas.

Gjorv, O.E., Vennesland, O. & E1-Busaidy, A.H.S. 1975. Diffusion of dissolved oxygen through concrete. *Nace Corrosion.* 76, Paper 17. Houston, Texas.

Glass, G.K. & Buenfeld, N.R. 1997. Presentation of the chloride threshold for corrosion of steel in concrete. *Corrosion Science*. 39(5), pp. 1001-1013.

Glass, G.K., Hassanein, N.M. & Buenfeld, N.R. 1997. Neural network modelling of chloride binding. *Magazine of Concrete Research*. 49, pp. 323-335.

Golden, G. 2015. The effect of cyclic wetting and drying on the corrosion rate of steel in reinforced concrete. University of Cape Town.

Gower, K.R. & Millard, S.G. 1999. Electrochemical Techniques for Corrosion Assessment of Reinforced Concrete Structures. Proceedings of Institute Civil Engineering, Structures and Bridges. 134, pp. 129-137.

Grieve, G. 2009. Cementitious materials. In Fultons Concrete Technology. 9th ed., Owens, G., eds. Midrand: Cement & Concrete Institute.

Grudemo, A. 1976. Determination of desorption isotherms for cement paste.

Halabe, U., Kavi, J. & GangaRao, F. 2016. Innovative Sensors for Monitoring the Corrosion of Steel Embedded in Concrete Structural Components. *Geotechnical and Structural Engineering Congress*. ASCE. pp. 1019.

Hall, M., Najim, K.B. & Keikhaei, P. 2012. *Modern Earth Buildings - Materials, Engineering, Construction and Applications*. Woodhead Publishing: Cambridge.

Hansson, C.M., Poursaee, A. & Laurent, A. 2006. Macrocell and microcell corrosion of steel in ordinary Portland cement and high performance concretes. *Cement and Concrete Research*.

Hawkins, C. & McKenzie, M. 1996. Environmental effects on reinforcement corrosion rates. Proceedings of the fourth international symposium on corrosion of reinforcement in concrete construction. pp. 166-175.

Hearn, N., Hooten, D. & Nokken, M. 2006. *Pore structure, permeability, and penetration resistance characteristics of concrete. In Significance of tests and properties of concrete and concrete-making materials*. Lamond, J. & Pielert, J.H., eds. ASTM: Philadelphia.

Heckroodt, R.O. 2002. *Guide to the Deterioration and Failure of Building Materials*. London: Thomas Telford Publishing.

Hong, K. 1998. *Cyclic Wetting and Drying and its Effects on Chloride Ingress in Concrete.* Masters degree. University of Toronto.

Hope, B.B. & Manning, D.G. 1985. Corrosion and electrical-impedance in concrete. Cement and Concrete Research. 15(3), pp. 525–534.

Hornbostel, K., Larsen, C. & Geiker, M. 2013. Relationship between concrete resistivity and corrosion rate – A literature review. Cement and Concrete Composites. 39(5), pp. 60-72.

Hughes, P., Fairhurst, D., Sherrington, I., Renevier, N., Morton, L., Robery, P. & Cunningham, L. 2013. Microscopic study into biodeterioration of marine concrete. *International Biodeterioration & Biodegradation*. 79, pp. 14-19.

Hundt, J. & Kantelberg, H. 1978. Sorption of cement paste, cement mortar and concrete. *Deut. Ausschuss Stahlbeton.* 297, pp. 25-39.

Hunkeler, F. 1994. Fundamentals of corrosion and potential measurements of reinforced concrete structures. *Bericht*. pp. 510.

Hunkeler, F. 1995. The resistivity of pore water solution – a decisive parameter of rebar corrosion and repair methods. *Construction and Building Materials*. 10(5), pp. 381-389.

Hunkeler, F. 2005. Corrosion in reinforced concrete: processes and mechanisms. *In Corrosion in reinforced concrete structures.* Böhni, H., eds. Abington Cambridge, England: Woodhead Publishing Limited. pp. 1-45.

Hussain, R.R. 2011. Effect of moisture variation on oxygen consumption rate of corroding steel in chloride contaminated concrete. Cement and Concrete Composites. 33(1), pp.154–161.

Institution of Structural Engineers. 2010. *Appraisal of Existing Structures - Dynamic Testing of Structures*. 3rd ed. Institution of Structural Engineers.

Iverson, W.P. 1966. Direct evidence for the cathodic depolarization theory of bacterial corrosion. *Science.* 151, pp. 986-988.

Kanna, V., Olson, R.A. & Jennings, H.M. 1998. Effect of shrinkage and moisture content on the physical characteristics of blended cement mortars. *Cement and Concrete Research*. 28(10), pp. 1467–1477.

Kawabata, Y., Kato, E. & Iwanami, M. 2012. Enhanced Long-Term Resistance of Concrete with Marine Sessile Organisms to Chloride Ion Penetration. *Japan Concrete Institute*. 10. pp. 151-159.

Kim, J., McCarter, W.J., Suryanto, B., Nanukuttan, S., Basheer, P. & Chrisp, T.M. 2016. Chloride ingress into marine exposed concrete: A comparison of empirical and physically based models. Cement and Concrete Composites. 72, pp. 133-145.

King, R.A. & Miller, J.D.A. 1971. Corrosion by sulphate-reducing bacteria. *Nature*. 233, pp. 491-492.

Kuang, F., Wang, J., Yan, L. & Zhang, D. 2007. Effects of sulphate-reducing bacteria on the corrosion behaviour of carbon steel. *Electrochimica Acta*. 52(20), pp. 6084-6088.

Lambert, P., Page, G.L. & Vassie P.R. 1991. Investigations of reinforcement corrosion,

Electrochemical monitoring of steel in chloride-contaminated concrete. *Materials and Structures*. 24, pp. 351-358.

Mackechnie, J.R. 1996. *Predictions of reinforced concrete durability in the marine environment. PhD Thesis*. University of Cape Town.

Maekawa, K., Ishida, T. & Kishi, T. 2008. *Multi-Scale Modelling of Structural Concrete*. London and New York: Taylor & Francis.

Malumbela, G. 2010. *Measurable parameters for performance of corroded and repaired RC beams under load*. PhD Thesis. University of Cape Town.

Malumbela, G., Moyo, P. & Alexander, M. 2012. A step towards standardising accelerated corrosion tests on laboratory reinforced concrete specimens. *Journal of the South African Institution of Civil Engineering*. 54(2), pp. 78-85.

Mangat, P.S. & Molloy, B.T. 1992. Factors influencing chloride-induced corrosion of reinforcement in concrete. *Materials and Structures*. 25, pp. 404-411.

Mangat, P.S., Khatib, J. & Molloy, B.T. 1994. Microstructure, chloride diffusion and reinforcement corrosion in blended cement paste and concrete. *Cement and Concrete Composites*. 16, pp. 73-81.

Mangat, P.S. & Elgarf, M.S. 1999. Flexural strength of concrete beams with corroding reinforcement. *ACI Structural Journal*. 96(1), pp. 149–158.

Maruya, T., Iwanami, M., Sakai, E., Mashimo, M. & Hamada, H. 2003. Durability enhancement of RC covered with a dense layer formed by marine aquatic fouling organisms. *Journal of Materials, Concrete Structures and Pavements*. 739(60). pp. 61-74.

McLeish, A. 1994. *Underwater Concreting and Repair - Chemical Attack*. Taylor & Francis: United Kingdom.

Mehta, P.K. 1991. Concrete in the Marine Environment. 1st ed. Elsevier Applied Science.

Miyagawa, T. 1985. Early chloride corrosion of reinforcing steel in concrete. Thesis dissertation. University of Kyoto.

Miyazato, S. & Otsuki, N. 2010. Steel Corrosion Induced by Chloride or Carbonation in Mortar with Bending Cracks or Joints. Journal of Advanced Concrete Technology. 8(2), pp. 135-144.

Morris, W., Vico, A., Vazquez, M. & de Sanchez, S.R. 2002. Corrosion of reinforcing steel evaluated by means of concrete resistivity measurements. *Corrosion Science*. 44(1), pp. 81–99.

Moukwa, M. 1990. Deterioration of concrete in cold sea waters. *Cement and Concrete Research*. 20(3), pp. 439-446.

NACE International. 2011. Guide to Corrosion Management of Reinforced Concrete Structures: Inspection Management. NACE International. pp. 24

Newman, J. & Choo, B.S. 2003. Advanced Concrete Technology. Chapter: Specification and achievement of cover to reinforcement. Elsevier Ltd: Oxford.

Nilsson, L.O. 1980. Hygroscopic moisture in concrete – drying, measurements and material properties. University of California.

Nilsson, L.O. 2002. Long-term moisture transport in high performance concrete. *Material Structures.* (35), pp. 641–9.

Nilsson, L.O., Poulsen, E., Sandberg, P., Sorensen, H. E. & Klinghoffer, O. 1996. Chloride penetration into concrete – a state-of-the-art report. HETEK Report No. 53.

Nimmo, B. & Hinds, G. 2003. *Beginners guide to corrosion.* NPL: UK

Nganga, G., Alexander, M. & Beushausen. H. 2017. *Practical implementation of durability index performance-based specifications: current experience*. Concrete Beton. No. 150. pp 18-22

Nygaard, P.V., 2008. Non-destructive electrochemical monitoring of reinforcement corrosion. Denmark Technical University.

O'Donovan, R., O'Rourke, B., Ruane, K. & Murphy, J. 2013. Anaerobic Corrosion of Reinforcement. *Key Engineering Materials.* 569-570, pp. 1124-1131.

Ono, S. 2005. Physics-one point: surface tension. *Kyoritsu Shuppan CO*.

Otieno, M. 2008. *Corrosion propagation in cracked and uncracked concrete*. MSc Thesis. University of Cape Town.

Otieno, M., 2014. The Development of Emperical Chloride-induced Corrosion Rate Prediction Models for Cracked and Uncracked Steel Reinforced Concrete Structures in the Marine Tidal Zone. PhD Thesis. University of Cape Town.

Otieno, M. 2017. Sensitivity of chloride-induced corrosion rate of steel in concrete to cover depth, crack width and concrete quality. *Materials and Structures.* 50(9). pp. 1-10

Otieno, M., Beushausen, H. & Alexander, M.G. 2010. Corrosion propagation in RC structures – state of the art review and way forward. Conference proceedings. *6th Internation Conference on Concrete under Severe Conditions - Environment and Loading*.

Parrott, L.J. 1988. Moisture profiles in drying concrete. Advances in Cement Research. 1(3), pp. 164-170.

Persons, R. 2009. *ASHRAE Handbook - Fundamentals (SI Edition) - Moisture Storage Data.* American Society of Heating, Refrigerating and Air-Conditioning Engineers, Inc: USA.

Polder, R.B. & de Rooij, M.R. 2005. Durability of marine concrete structures – field investigations and modelling. HERON. 50(3), pp. 133-143.

Polder, R.B. 1996. The influence of blast furnace slag, fly ash and silica fume on corrosion of reinforced concrete structures in the marine environment. *Heron.* 41(4), pp. 287-300.

Port and Airport Research Institute. 2007. Manual on maintenance of Port and Harbour Facilities. *Coastal Development Institute of Technology*.

Poursaee, A. & Hansson, C.M. 2009. Potential pitfalls in assessing chloride-induced corrosion of steel in concrete. Cement & Concrete Research. 39(5), pp. 391–400.

Poursaee, A. 2016. *Corrosion of Steel in Concrete Structures*. Elsevier. pp. 28

Powers, T.C. 1965. Mechanism of shrinkage and reversible creep of hardened cement paste. *Proceedings International Symposium Concrete London and France*.

Poyet, S. & Charles, S. 2009. Temperature dependence of the sorption isotherms of cement-based materials: Heat of sorption and Clausius-Clapeyron formula. *Cement and Concrete Research.*

39, pp. 1060-1067.

Pullar-Strecker, P. 2002. *Concrete reinforcement corrosion: From assessment to repair decisions*. ICE Design and Practice Guide. Thomas Telford: London.

Rauf, S.B. 2017. *Electrical Engineering for Non-Electrical Engineers*. Chapter 2: DC Circuit Analysis and Basic Electronic Devices. 2nd ed. Fairmont Press: USA. pp. 50.

Raupach, M. & Buttner, T. 2014. *Concrete Repair to EN 1504 – Diagnosis, Design, Principles and Practice*. CRC Press: Florida.

Raupach, M. 1996. Investigations on the influence of oxygen on corrosion of steel in concrete. Materials and Structures - Part 1. 29(3), pp.174–184.

Revie, R. & Uhlig, H. 2008. *Corrosion and corrosion control*. 3rd ed. J Wiley & Sons: New Jersey.

Richardson, M.G. 2002. *Fundamentals of Durable Reinforced Concrete.* Bentur, A. & Mindess, S., eds. Spon Press.

Roy, S.K., Chye, L.K. & Northwood, D.O. 1993. Chloride ingress in concrete as measured by field exposure depths in the atmospheric, tidal and submerged zones of a tropical marine environment. *Cement and Concrete Research*. 23, pp. 1289 – 1306.

Ryu, D.W., Ko, J. & Noguchi, T. 2011. Effects of simulated environmental conditions on the internal relative humidity and relative moisture content distribution of exposed concrete. *Cement and Concrete Composites*. 33(1), pp. 142-153.

Ryu, D.W., Ko, J., Kanematsu, M. & Noguchi, T. 2007. Study on the moisture distribution in concrete associated with change of environmental conditions. *Journal of Structural and Construction Engineering*. 72(612), pp. 1-7.

Saleem, M., Shameem, M., Hussain, S.E. & Maslehuddin, M. 1996. Effect of moisture, chloride and sulphate contamination on the electrical resistivity of Portland cement concrete. *Construction and building materials*. 10(3), pp. 209–214.

SANS 10100-2. 2013. The Structural Use of Concrete Part 2: Materials and Execution of work. SABS: South Africa.

SANS 5863. 2006. Concrete tests - Compressive strength of hardened concrete. SABS: South Africa.

SANS 3001-CO3-1. 2015. Concrete durability index testing – Part 1: Preparation of test specimens. SABS: South Africa

SANS 3001-CO3-2. 2015. Concrete durability index testing – Part 2: Oxygen permeability test. SABS: South Africa

SANS 3001-CO3-3. 2015. Concrete durability index testing – Part 3: Chloride conductivity test. SABS: South Africa

Schiessl, P. & Lay, S. 2005. Influence of concrete composition. *In Corrosion in reinforced concrete structures.* Böhni, H., eds. Abington Cambridge, England: Woodhead Publishing Limited. pp. 91-134.

Scott, A.N. & Alexander, M.G. 2007. The influence of binder type, cracking and cover on corrosion rates of steel in chloride-contaminated concrete. Magazine of Concrete Research. 59(7), pp. 495–505.

Scott, A.N. 2004. *The influence of binder type and cracking on reinforcing steel corrosion in concrete*. PhD Thesis. University of Cape Town.

Šelih, J., Sousa, A.C.M. & Bremner, T.W. 1996. Moisture transport in initially fully saturated concrete during drying. Transport in porous media. 24(1), pp.81–106.

Sharp, J.V. 1979. Review: The use of steel and concrete in the construction of North Sea oil production platforms. *Journal of materials science*. 14, pp. 1773-1799.

Sivasubramanian, J. 2013. Covermeter for identifying cover depth and rebar diameter in high strength concrete. International Journal of Civil and Structural Engineering. 3(3), pp. 557-563.

Skaperdas, G. & Uhlig, H. 1942. Corrosion of Steel by Dissolved Carbon Dioxide and Oxygen. *Industrial and Engineering Chemistry*. 34 (6), pp. 748-754.

Smith, K.M., Schokker, A.J. & Tikalsky, P.J. 2004. Performance of supplementary cementitious materials in concrete resistivity and corrosion monitoring evaluations. *ACI Materials Journal.* 101(5), pp. 385–390.

Soroka, I. 2003. *Concrete in hot climate: modern concrete technology*. 2nd ed. London: E & FN Spon.

Stansbury, E.E. & Buchanan, R.A. 2000. *Fundamentals of electrochemical corrosion*. Materials Park, Ohio: ASM International.

Stern, M. & Geary, A.L. 1957. Electrochemical Polarization, A Theoretical Analysis of the Shape of Polarization Curves. *Journal of the Electrochemical Society*. 104(1), pp. 56-63.

Strohmeier, J.H. 1994. Deterioration of reinforced concrete in a marine environment; repair costs and maintenance strategies. MSc Thesis. University of Cape Town

Tang, L. 2008. Engineering expression of the ClinConc model for prediction of free and total ingress in submerged marine concrete. *Cement and Concrete Research*. 38(8-9), pp. 1092-1097.

Taywood Laboratories. 1980. *Marine Durability Survey of the Tongue Sands Tower*. Technical Report No. 5, Concrete in the Oceans. Taywood Laboratories.

Trejo, D. & Pillai, R.G. 2003. Accelerated chloride threshold testing: Part I - ASTM A-615 and A-706 reinforcement. *ACI Materials Journal*. 100(6), pp. 519-527.

Trejo, D., Halmen, C. & Reinschidt, K. 2009. *Corrosion Performance Tests for Reinforcing Steel in Concrete: Technical Report.* Texas Transportation Institute. Austin, Texas.

Tuutti, K. 1982. *Corrosion of Steel in Concrete.* Stockholm: Swedish Cement and Concrete Research Institute.

Uhlig, H., Triadis, D. & Stern, J. 1955. Effect of Oxygen, Chlorides and Calcium Ion on Corrosion Inhibition of Iron by Polyphosphates. *Electrochemical Society.* 102(2), pp. 59-66.

Valipour, M., Shekarchi, M. & Ghods, P. 2014. Comparitive studies of experimental and numerical techniques in measurement of corrosion rate and time to corrosion initiation of rebar in concrete in marine environments. *Cement & Concrete Composites*. 48. pp. 98-107.

Vidal, T., Castel, A. & François, R. 2007. Corrosion process and structural performance of a 17-year-old reinforced concrete beam stored in a chloride environment. *Cement & Concrete Research*. 37, pp. 1551-1561.

References

Wu, K., Shi, H., Xu, L., Ye, G. & Schutter, G.D. 2016. Microstructural characterization of ITZ in blended cement concretes and its relation to transport properties. 79(1), pp. 243-256.

Yang, L. 2008. Techniques for Corrosion Monitoring: Polarization Resistance Method. Woodhead Publishing: Cambridge.

Yaun, J., Jiang, J. & Peng, T. 2010. Corrosion process of steel bar in concrete in full lifetime. *Materials Journal*. 107(6), pp. 563-568.

Yuan, Y., Ji, Y. & Jiang, J. 2009. Effect of corrosion layer of steel bar in concrete on time-variant corrosion rate. *Materials and Structures.* 42. pp. 1443 – 1450.

Ye, T., Nanguo, J. & Xianyu, J. 2017. Coupling effect of temperature and relative humidity diffusion in concrete under ambient conditions. *Construction and Building Materials*. 159, pp. 673-689.

Yong Ann, K. & Song, H. 2007. Chloride threshold level for corrosion of steel in concrete. *Corrosion science*. 49, pp. 4113 – 4133.

Yuan, Y., Ji, Y. & Shah, S.P. 2007 Comparison of two accelerated corrosion techniques for concrete structures. *ACI Structural Journal*. pp. 344–347.

Zhang, R., Castel, A. & Francois, R. 2009. The corrosion pattern of reinforcement and its influence on serviceability of reinforced concrete members in chloride environment. *Cement and Concrete Research*. 39, pp. 1077-1086.

Zhang, Z. 2015. *Modelling of sorption hysteresis and its effects on moisture transport within cementitious materials*. PhD Thesis. Universite Paris.

Živica, V., Krajči, L., Bágel, L. & Vargová, M. 1997. Significance of the ambient temperature and the steel material in the process of concrete reinforcement corrosion. *Construction and Building Materials*. 11(2), pp. 99-103.

Appendix A: Laboratory mix design

A-1: Coarse aggregate properties

The coarse aggregate was characterised as shown in the table below.

Table A- 1: Coarse aggregate properties

Coarse aggregate properties	Greywacke (13.2 mm)
Dry compacted bulk density (CBD - kg/m^3)	1540
K factor (Pumped, slump 60-125 mm)	0,83
Particle relative density (RD_a)	2,72

A-2: Fine aggregate properties

The fine aggregate was characterised as shown in the table below.

Table A- 2: Fine aggregate properties

Fine aggregate properties	Crusher sand	Dune sand	50:50 Mixture
Fineness modulus (FM)	3,2	2,0	2,60
Particle relative density (RD_s)	2,70	2,67	2,68

A-3: Mix design

The C&CI method was used to determine the quantity of constituent materials required (Addis & Goodman, 2009) for the two different mixes. The quantities used for both Mix 1 and Mix 2 are given in Table 4 - 1**Error! Reference source not found.**. The detailed mix design procedure is then given for Mix 1 and 2 in Sections A-4: Mix 1 detailed calculations and A-5: Mix 2 detailed calculations respectively.

A-4: Mix 1 detailed calculations

Step 1: Water content

Water content of 190 ℓ/m^3 was selected by considering the quality of the sand as well as the stone size.

Step 2: Cement content

From the required w/b ratio and water content, the cement content was calculated.

$$cement = \frac{water}{w/b} = \frac{190}{0{,}5} = 380\ kg/m^3 \quad \text{(A- 3)}$$

Step 3: Stone content

The stone content was then calculated according to the coarse aggregate properties and the relevant equation as given in Addis & Goodman (2009).

$$Stone = CBD(K - 0{,}1\ FM) \quad \text{(A- 4)}$$

$$Stone = 1\ 540(0{,}83 - (0{,}1 \times 2{,}60)) = 878\ kg/m^3$$

Step 4: Sand content

The total sand content was then calculated. As the fine aggregate is to be made of both dune sand and crusher sand, the amount of each type of fine aggregate was calculated by dividing the total amount in half.

$$Sand = PRD_{sand} \times 1\ 000\left[1 - \frac{Mass_{cement}}{PRD_{cement} \times 1\ 000} - \frac{Mass_{stone}}{PRD_{stone} \times 1\ 000} - \frac{Mass_{water}}{1\ 000}\right] \quad \text{(A- 5)}$$

$$Sand = 2{,}68 \times 1\ 000\left[1 - \frac{380}{3\ 140} - \frac{878}{2\ 720} - \frac{190}{1\ 000}\right] = 983\ kg/m^3$$

$$Crusher\ sand = 492 kg/m^3$$

$$Dune\ sand = 492 kg/m^3$$

A-5: Mix 2 detailed calculations

Step 1: Water content

Water content of 190 ℓ/m^3 was selected by considering the quality of the sand as well as the stone size.

Step 2: Cement content

From the required w/b ratio and water content, the cement content was calculated.

$$cement = \frac{water}{w/b} = \frac{190}{0{,}8} = 238\ kg/m^3 \quad \text{(A- 6)}$$

Step 3: Stone content

The stone content was then calculated according to the coarse aggregate properties and the relevant equation given in Addis & Goodman (2009).

$$Stone = CBD(K - 0{,}1\ FM) \quad \text{(A- 7)}$$

$$Stone = 1\ 540(0{,}83 - (0{,}1 \times 2{,}60)) = 878\ kg/m^3$$

Step 4: Sand content

The total sand content was then calculated. As the fine aggregate is to be made of both dune sand and crusher sand, the amount of each type of fine aggregate was calculated by dividing the total amount in half.

$$Sand = PRD_{sand} \times 1\ 000\left[1 - \frac{Mass_{cement}}{PRD_{cement} \times 1\ 000} - \frac{Mass_{stone}}{PRD_{stone} \times 1\ 000} - \frac{Mass_{water}}{1\ 000}\right] \quad \text{(A- 8)}$$

$$Sand = 2{,}68 \times 1\ 000\left[1 - \frac{238}{3\ 140} - \frac{878}{2\ 720} - \frac{190}{1\ 000}\right] = 1\ 105\ kg/m^3$$

$$Crusher\ sand = 553\ kg/m^3$$

$$Dune\ sand = 553\ kg/m^3$$

Appendix B: Details for experimental set-up

B-1: Dimensions of mould fittings

Owing to the design of the moulds, the corrosion cells were cast upside down. This was done to allow for a ponding feature to be included. For this reason the dimensions of the mould and mould fittings are given upside down in Figure B - 1.

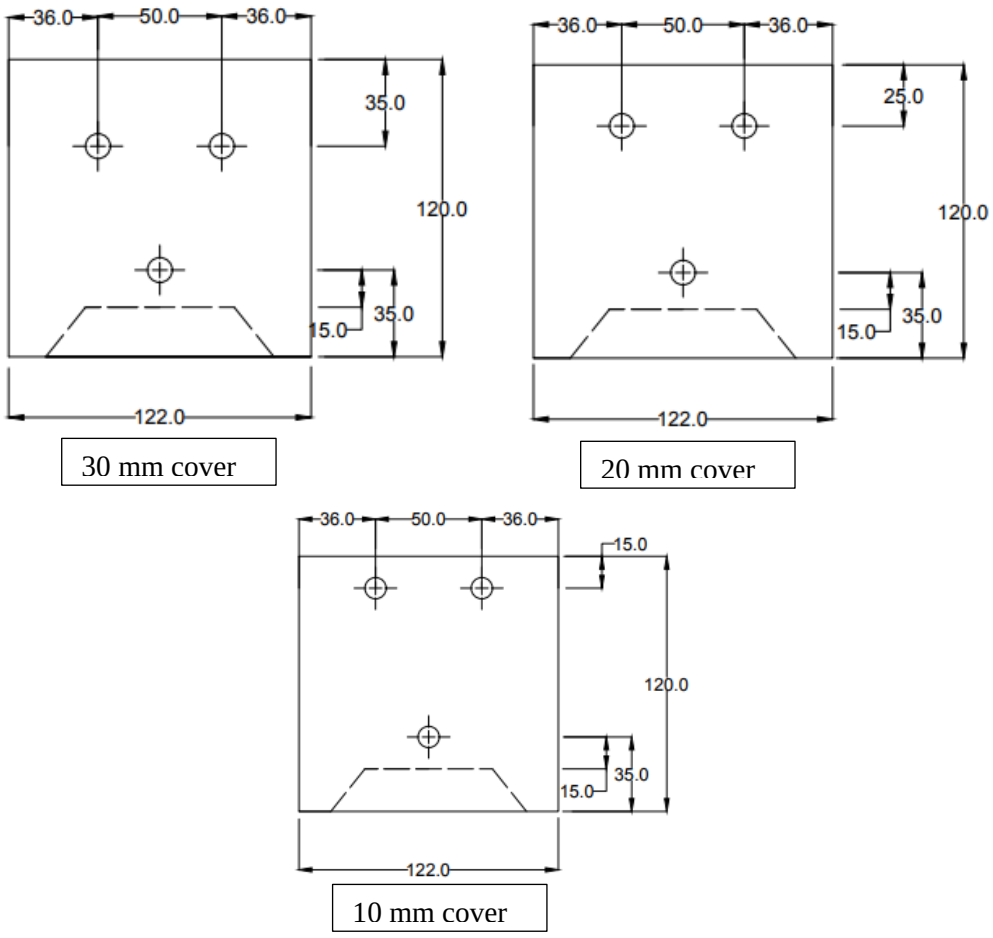

Figure B - 1: Mould dimensions (mm) for corrosion cells

B-2: Test for ensuring electrical connectivity

The circuit with LED, connecting wires, and 9V battery pack that was used to ensure electrical connectivity in soldered joints (Figure B - 2).

Figure B - 2: LED, wire connection and 9V battery pack

B-3: Test for adequate sealant

A moisture specimen was covered on all 6 faces with epoxy. The weight of the specimen was measured, after which the specimen was submerged in 5% NaCl solution for 72 hours. It was presumed that 72 hours is sufficient for any change in mass from moisture ingress to be observed. The mass before submersion and after submersion is given below, and the change in mass was found to be less than 0,1%. From this result it is clear that the epoxy used to seal the faces of the macrocells and moisture specimens is preventing any significant ingress of moisture.

$$mass_{t=0\ hours} = 5{,}845\ kg$$

$$mass_{t=72\ hours} = 5{,}849$$

$$\%\ change\ mass = \frac{mass_{t=72} - mass_{t=0}}{mass_{t=0}} = 0{,}068\ \%$$

Appendix C: Detailed compressive strength

The 28 day compressive strength value for each of the six cast dates was calculated and recorded to the nearest 0,5 MPa using equation C-1. The concrete was tested according to SANS 5863. The test results were considered valid as the difference between the highest and lowest results did not exceed an average of 15%.

$$f_{compressive} = \frac{F}{A_{cross-sectional}} \quad \text{(C-1)}$$

Where $f_{compressive}$ = compressive strength (MPa); F = failure load (N); and $A_{cross\text{-}sectional}$ = area on which the compressive force acts (mm^2)

Table C- 1: Detailed 28-day compressive strength results (C10-50)

Cube	Mass (kg)	Width (mm)	Breadth (mm)	Failure Load (N)	Strength (MPa)
A-1	2,440	99,8	102,1	543 000	53,5
A-2	2,380	101,5	98,45	523 000	52,5
A-3	2,420	100,1	99,7	535 000	53,5
Average	-	-	-	-	**53,0**

Casting date: 2/8/2017; w/b = 0,5; Mix 1

Table C- 2: Detailed 28-day compressive strength results (C10-80)

Cube	Mass (kg)	Width (mm)	Breadth (mm)	Failure Load (N)	Strength (MPa)
B-1	2,415	100,5	100,3	308 000	30,5
B-2	2,420	101,6	99,6	302 000	30,0
B-3	2,415	101,3	99,7	304 000	30,0
Average	-	-	-	-	**30,0**

Casting date: 7/8/2017; w/b = 0,8; Mix 2

Table C- 3: Detailed 28-day compressive strength results (C30-50)

Cube	Mass (kg)	Width (mm)	Breadth (mm)	Failure Load (N)	Strength (MPa)
C-1	2,440	100,0	102,9	566 000	55,0
C-2	2,455	99,9	101,3	552 000	54,5
C-3	2,370	99,8	100,0	535 000	53,5
Average	-	-	-	-	**54,0**

Casting date: 31/8/2017; w/b = 0,5; Mix 1

Table C- 4: Detailed 28-day compressive strength results (C30-80)

Cube	Mass (kg)	Width (mm)	Breadth (mm)	Failure Load (N)	Strength (MPa)
D-1	2,425	100,2	100,2	270 000	27,0
D-2	2,380	99,5	99,7	280 000	28,0
D-3	2,395	100,3	100,1	276 000	27,5
Average	-	-	-	-	**27,5**

Casting date: 2/9/2017; w/b = 0,8; Mix 2

Table C- 5: Detailed 28-day compressive strength results (C20-50)

Cube	Mass (kg)	Width (mm)	Breadth (mm)	Failure Load (N)	Strength (MPa)
E-1	2,410	100,2	100,6	542 000	54,0
E-2	2,395	99,8	99,5	535 000	54,0
E-3	2,405	100,1	100,3	530 000	53,0
Average	-	-	-	-	**53,5**

Casting date: 5/9/2017; w/b = 0,5; Mix 1

Table C- 6: Detailed 28-day compressive strength results (C20-80)

Cube	Mass (kg)	Width (mm)	Breadth (mm)	Failure Load (N)	Strength (MPa)
F-1	2,395	100,1	100,3	280 000	28,0
F-2	2,405	100,4	100,2	286 000	28,5
F-3	2,385	100,2	99,9	272 000	27,0
Average	-	-	-	-	**28,0**

Casting date: 8/9/2017; w/b = 0,8; Mix 2

Appendix D: Detailed durability indices

The potential durability of the concrete was established using the DI Test Manual (2018) and SANS 3001-C03. The durability index values were determined for each of the six cast dates.

D-1: Oxygen permeability

After curing the samples for 28 days, the concrete was cored into the required dimensions and placed in an oven at 50 ˚C for 7 days. After removal from the oven the samples were placed into oxygen permeability cells and a pressure of above 100 kPa applied. Pressure readings were recorded until pressure dropped to below 50 kPa or after 6 hours, whichever occurred first.

The line of best fit was determined using linear regression and by forcing the line through the point (0; 0).

$$z = \frac{\sum \left[\ln\left(\frac{P_0}{P_t}\right)\right]^2}{\sum \ln\left(\frac{P_0}{P_t}\right) t} \quad \text{(D- 1)}$$

Where z = slope of linear regression; P_0 = pressure at start of test (kPa); P_t = subsequent readings in pressure at time t (kPa); and t = time (seconds).

Darcy's law, which describes the flow of fluid through a porous medium, was used to determine the coefficient of permeability of the samples (Equation D-2).

$$k = \frac{\omega V g dz}{RA\theta} \quad \text{(D-2)}$$

Where k = coefficient of permeability (m/s); ω = molecular mass of oxygen (0,032 kg/mol); V = volume of oxygen under pressure in permeameter (m^3); g = acceleration due to gravity (9,81 m/s^2); d = average sample thickness (mm); z = slope of linear regression; R = universal gas constant (8,313 Nm/K mol); A = cross-sectional area (m^2); and θ = absolute temperature (K).

The oxygen permeability index (OPI) was given as the negative log of the average of the coefficients of the four samples (Equation D-3). The oxygen permeability results are given for each cast set.

$$OPI = -\log_{10}[\frac{1}{4}(k_1 + k_2 + k_3 + k_4)] \quad \text{(D-3)}$$

Where OPI = Oxygen permeability index; and k_x = coefficient of permeability for sample *x* (m/s).

Table D- 1: Set C10-80 Oxygen Permeability results

Measurement	Sample 1	Sample 2	Sample 3	Sample 4	Average
Diameter (mm)	68,50	68,52	68,51	68,67	**68,55**
Thickness (mm)	31,56	30,76	31,21	30,91	**31,11**
Slope of Regression	$2{,}241\times10^{-5}$	$2{,}207\times10^{-5}$	$2{,}197\times10^{-5}$	$2{,}224\times10^{-5}$	$\mathbf{2{,}217\times10^{-5}}$
k (m/s)	$1{,}132\times10^{-10}$	$1{,}079\times10^{-10}$	$1{,}091\times10^{-10}$	$1{,}088\times10^{-10}$	$\mathbf{1{,}098\times10^{-10}}$
Correlation Factor	0,9998	0,9997	0,9996	0,9996	**0,9997**
Oxygen Permeability	9,95	9,97	9,96	9,96	**9,96**

Table D- 2: Set C10-50 Oxygen Permeability results

Measurement	Sample 1	Sample 2	Sample 3	Sample 4	Average
Diameter (mm)	68,69	68,72	68,65	68,84	**68,73**
Thickness (mm)	28,35	29,77	30,60	31,25	**29,99**
Slope of Regression	$1{,}481\times10^{-5}$	$2{,}174\times10^{-5}$	$1{,}393\times10^{-5}$	$1{,}741\times10^{-5}$	$\mathbf{1{,}697\times10^{-5}}$
k (m/s)	$6{,}644\times10^{-11}$	$1{,}024\times10^{-10}$	$6{,}755\times10^{-11}$	$8{,}575\times10^{-11}$	$\mathbf{8{,}053\times10^{-11}}$
Correlation Factor	0,9993	0,9990	0,9994	0,9995	**0,9993**
Oxygen Permeability	10,18	9,99	10,17	10,07	**10,10**

Table D- 3: Set C30-80 Oxygen Permeability results

Measurement	Sample 1	Sample 2	Sample 3	Sample 4	Average
Diameter (mm)	68,77	68,64	68,81	68,56	**68,70**
Thickness (mm)	29,50	30,80	28,52	29,72	**29,64**
Slope of Regression	$2{,}394\times10^{-5}$	$2{,}170\times10^{-5}$	$2{,}270\times10^{-5}$	$2{,}691\times10^{-5}$	$\mathbf{2{,}381\times10^{-5}}$
k (m/s)	$1{,}115\times10^{-10}$	$1{,}060\times10^{-10}$	$1{,}021\times10^{-10}$	$1{,}271\times10^{-10}$	$\mathbf{1{,}117\times10^{-10}}$
Correlation Factor	0,9996	0,9995	0,9996	0,9994	**0,9995**
Oxygen Permeability	9,95	9,97	9,99	9,90	**9,95**

Table D- 4: Set C30-50 Oxygen Permeability results

Measurement	Sample 1	Sample 2	Sample 3	Sample 4	Average
Diameter (mm)	68,62	68,47	68,40	68,41	**68,48**
Thickness (mm)	30,67	29,94	30,36	29,21	**30,05**
Slope of Regression	$4{,}615\times10^{-6}$	$7{,}309\times10^{-6}$	$4{,}127\times10^{-6}$	$1{,}047\times10^{-5}$	$\mathbf{6{,}630\times10^{-6}}$
k (m/s)	$2{,}241\times10^{-11}$	$3{,}486\times10^{-11}$	$2{,}000\times10^{-11}$	$4{,}882\times10^{-11}$	$\mathbf{3{,}152\times10^{-11}}$
Correlation Factor	0,9980	0,9984	0,9984	0,9993	**0,9985**
Oxygen Permeability	10,65	10,46	10,70	10,31	**10,53**

Table D- 5: Set C20-80 Oxygen Permeability results

Measurement	Sample 1	Sample 2	Sample 3	Sample 4	Average
Diameter (mm)	68,51	68,52	68,51	68,67	**68,55**
Thickness (mm)	31,15	30,84	30,95	30,92	**30,97**
Slope of Regression	$3{,}525\times10^{-5}$	$3{,}258\times10^{-5}$	$2{,}633\times10^{-5}$	$3{,}076\times10^{-5}$	$\mathbf{3{,}123\times10^{-5}}$
k (m/s)	$1{,}731\times10^{-10}$	$1{,}598\times10^{-10}$	$1{,}296\times10^{-10}$	$1{,}507\times10^{-10}$	$\mathbf{1{,}533\times10^{-10}}$
Correlation Factor	0,9984	0,9988	0,9984	0,9984	**0,9985**
Oxygen Permeability	9,76	9,80	9,89	9,82	**9,82**

Table D- 6: Set C20-50 Oxygen Permeability results

Measurement	Sample 1	Sample 2	Sample 3	Sample 4	Average
Diameter (mm)	69,71	68,74	68,70	68,82	**68,99**
Thickness (mm)	28,47	28,79	28,97	29,06	**28,82**
Slope of Regression	$2{,}405\times10^{-5}$	$2{,}17\times10^{-5}$	$2{,}27\times10^{-5}$	$1{,}48\times10^{-5}$	$\mathbf{2{,}331\times10^{-5}}$
k (m/s)	$1{,}048\times10^{-10}$	$9{,}876\times10^{-11}$	$1{,}041\times10^{-10}$	$6{,}784\times10^{-11}$	$\mathbf{9{,}388\times10^{-11}}$
Correlation Factor	0,9996	0,9995	0,9996	0,9993	**0,9995**
Oxygen Permeability	9,98	10,01	9,98	10,17	**10,03**

D-2: Sorptivity and Porosity

The same samples that were used for the oxygen permeability test were used to determine the sorptivity and porosity values. Immediately after removal from the oxygen permeability chambers the samples were placed in calcium hydroxide (CaOH) solution and weighed at 3, 5, 7, 9, 12, 16, 20 and 25 minutes. Four samples were utilised per cast set to obtain an overage.

The mass gain and the square root of time were then plotted on a graph so that the slope of best fit (*F)*could be evaluated (Equation D-4).

$$M_{wt} = F\sqrt{t} \tag{D-4}$$

Where M_{wt} = mass gain after first exposure (g); F = slope of best fit (g/$\sqrt{\text{hr}}$); and $\sqrt{t}$ = square root of time after first exposure (hours).

From this, the moisture gradients were used in combination with the porosity values to determine the sorptivity (Equation D-5). The Water Sorptivity value is given as the average of four valid values.

$$S = \frac{Fd}{M_{sv} - M_{s0}} \tag{D- 5}$$

Where S = sorptivity (mm/$\sqrt{\text{hr}}$); F = slope of best fit (g/$\sqrt{\text{hr}}$); d = average sample thickness (mm); M_{sv} = vacuum saturated mass (g); and M_{s0} = mass at time is 0 (g).

After completion of the sorptivity test, the samples were placed in a vacuum saturation tank and left to soak for 18 hour. The saturated mass of each sample was obtained in this way. The porosity (another useful indicator of durability potential) was calculated using Equation D-6. The results for each cast set are shown in Table D-7 to D-12.

$$n = \frac{M_{sv} - M_{s0}}{Ad\rho_w} \times 100 \qquad \text{(D- 6)}$$

Where n = porosity (%); M_{sv} = vacuum-saturated mass (g); M_{s0} = mass at time is 0 (g); A = cross-sectional area (mm^2); d = average sample thickness (mm); and ρ_w = density of water (g/mm^3).

Table D- 7: Set C10-50 Sorptivity and Porosity results

Measurement	Sample 1	Sample 2	Sample 3	Sample 4	Average
Diameter (mm)	68,50	68,52	68,51	68,67	**68,55**
Thickness (mm)	31,56	30,76	31,21	30,91	**31,11**
Porosity (%)	9,34	9,64	9,51	9,71	**9,55**
Dry Mass (g)	273,4	268,3	272,6	267,7	**270,5**
Saturated Mass (g)	284,2	279,2	283,6	278,8	**281,45**
Gradient (g/$\sqrt{hr}$)	2,16	2,41	2,05	2,34	**2,24**
Correlation Factor	0,9953	0,9979	0,9988	0,9982	**0,9976**
Sorptivity (mm/$\sqrt{hr}$)	6,28	6,77	5,85	6,51	**6,35**

Table D- 8: Set C10-80 Sorptivity and Porosity results

Measurement	Sample 1	Sample 2	Sample 3	Sample 4	Average
Diameter (mm)	68,69	68,72	68,65	68,84	**68,73**
Thickness (mm)	28,35	29,77	30,60	31,25	**29,99**
Porosity (%)	12,82	12,68	12,25	12,06	**12,45**
Dry Mass (g)	240,9	250,1	257,3	262,2	**252,6**
Saturated Mass (g)	254,4	264,1	271,1	276,2	**266,5**
Gradient (g/$\sqrt{hr}$)	3,50	4,03	3,64	3,80	**3,74**
Correlation Factor	0,9996	0,9994	0,9981	0,9994	**0,9991**
Sorptivity (mm/$\sqrt{hr}$)	7,36	8,58	8,03	8,47	**8,11**

Table D- 9: Set C30-50 Sorptivity and Porosity results

Measurement	Sample 1	Sample 2	Sample 3	Sample 4	Average
Diameter (mm)	68,62	68,47	68,40	68,41	**68,48**
Thickness (mm)	30,67	29,94	30,36	29,21	**30,05**
Porosity (%)	9,03	7,99	8,14	8,35	**8,38**
Dry Mass (g)	264,0	263,0	265,3	256,9	**262,3**
Saturated Mass (g)	274,2	271,9	274,3	265,9	**271,6**
Gradient ($g/\sqrt{hr}$)	2,20	2,13	2,25	2,07	**2,16**
Correlation Factor	0,9987	0,9934	0,9915	0,9939	**0,9944**
Sorptivity ($mm/\sqrt{hr}$)	6,60	7,23	7,54	6,74	**7,03**

Table D- 10: Set C30-80 Sorptivity and Porosity results

Measurement	Sample 1	Sample 2	Sample 3	Sample 4	Average
Diameter (mm)	68,77	68,64	68,81	68,56	**68,70**
Thickness (mm)	29,50	30,80	28,52	29,72	**29,64**
Porosity (%)	13,10	12,38	12,86	13,72	**13,01**
Dry Mass (g)	249,5	263,4	241,6	251,4	**251,5**
Saturated Mass (g)	263,9	277,5	255,2	266,5	**265,8**
Gradient ($g/\sqrt{hr}$)	4,30	4,29	3,91	4,25	**4,19**
Correlation Factor	0,9994	0,9993	0,9984	0,9999	**0,9993**
Sorptivity ($mm/\sqrt{hr}$)	8,83	9,37	8,18	8,40	**8,70**

Table D- 11: Set C20-50 Sorptivity and Porosity results

Measurement	Sample 1	Sample 2	Sample 3	Sample 4	Average
Diameter (mm)	68,51	68,52	68,51	68,67	**68,55**
Thickness (mm)	31,15	30,84	30,95	30,92	**30,97**
Porosity (%)	7,34	8,07	8,58	8,37	**8,09**
Dry Mass (g)	271,34	272,34	269,22	274,78	**271,92**
Saturated Mass (g)	279,77	281,52	279,01	284,37	**281,17**
Gradient ($g/\sqrt{hr}$)	1,81	2,03	2,30	2,35	**2,12**
Correlation Factor	0,9921	0,9923	0,9965	0,9971	**0,9945**
Sorptivity ($mm/\sqrt{hr}$)	6,69	6,81	7,26	7,59	**7,09**

Table D- 12: Set C20-80 Sorptivity and Porosity results

Measurement	Sample 1	Sample 2	Sample 3	Sample 4	Average
Diameter (mm)	69,71	68,74	68,70	68,82	**68,99**
Thickness (mm)	28,47	28,79	28,97	29,06	**28,82**
Porosity (%)	11,96	11,73	11,74	11,68	**11,78**
Dry Mass (g)	272,51	271,97	273,07	272,94	**272,62**
Saturated Mass (g)	285,51	284,50	285,68	285,56	**285,31**
Gradient (g/$\sqrt{hr}$)	3,70	3,70	3,87	3,73	**3,75**
Correlation Factor	0,9947	0,9971	0,9971	0,9962	**0,9963**
Sorptivity (mm/$\sqrt{hr}$)	8,11	8,50	8,89	8,59	**8,52**

D-3: Chloride conductivity

As with the oxygen permeability test the samples were cured for 28 days, cored into the required dimensions and placed in an oven at 50 ˚C for 7 days. The samples were saturated with salt (NaCl) solution and weighed before being placed in a conduction cell. The voltage was maintained at approximately 10 V and the current recorded. Four samples were used per set in order to obtain an average.

For each specimen the chloride conductivity was calculated using Equation D-7.

$$\sigma = \frac{id}{VA} \tag{D-7}$$

Where σ = chloride conductivity (mS/cm); i = current (mA); d = average thickness of sample (cm); V = voltage difference (V); and A = cross-sectional area of the specimen (cm^2).

The porosity for each sample was obtained using Equation D-8. Both the chloride conductivity and the porosity results are given in Table D-13 to Table D-18. The porosity obtained from the sorptivity tests are used in the interpretation of the potential durability, as it is found to be more reliable than the porosity obtained from the chloride conductivity tests.

$$n = \frac{M_s - M_D}{Ad\rho_s} \times 100 \tag{D-8}$$

Where n = porosity (%); M_s = vacuum saturated mass (g); M_D = mass of dry specimen (g); A = cross-sectional area (mm^2); d = average sample thickness (mm); and ρ_s = density of salt solution ($1{,}19 \times 10^{-3}$ g/mm^3).

Table D- 13: Set C10-50 Chloride Conductivity results

Measurement	Sample 1	Sample 2	Sample 3	Sample 4	Average
Diameter (mm)	68,53	68,46	68,50	68,51	**68,5**
Thickness (mm)	31,57	30,99	30,16	31,79	**31,13**
Porosity (%)	3,69	3,78	3,44	3,93	**3,71**
Dry Mass (g)	271,80	268,70	265,70	275,60	**270,45**
Saturated Mass (g)	282,99	280,12	276,12	287,50	**281,68**
Voltage (V)	10,03	10,01	10,04	10,08	**10,04**
Current (mA)	100,1	98,2	91,1	98,9	**97,1**
Conductivity (mS/cm)	0,85	0,83	0,74	0,85	**0,82**

Table D- 14: Set C10-80 Chloride Conductivity results

Measurement	Sample 1	Sample 2	Sample 3	Sample 4	Average
Diameter (mm)	68,95	68,92	68,97	69,00	**68,96**
Thickness (mm)	29,58	29,06	29,98	29,62	**29,56**
Porosity (%)	4,80	4,66	5,04	4,75	**4,81**
Dry Mass (g)	253,38	249,73	252,97	257,09	**253,29**
Saturated Mass (g)	268,20	264,11	268,57	271,80	**268,17**
Voltage (V)	10,08	10,04	10,05	10,09	**10,07**
Current (mA)	232,1	250,5	235,0	256,2	**243,5**
Conductivity (mS/cm)	1,82	1,94	1,88	2,01	**1,91**

Table D- 15: Set C30-50 Chloride Conductivity results

Measurement	Sample 1	Sample 2	Sample 3	Sample 4	Average
Diameter (mm)	68,55	68,55	68,56	68,61	**68,57**
Thickness (mm)	31,09	30,26	31,70	29,58	**30,66**
Porosity (%)	3,33	3,35	3,67	3,19	**3,38**
Dry Mass (g)	271,19	261,00	273,86	258,43	**266,12**
Saturated Mass (g)	281,31	271,17	285,00	268,13	**276,40**
Voltage (V)	10,00	10,00	10,00	10,02	**10,01**
Current (mA)	91,0	100,4	93,4	90,0	**93,7**
Conductivity (mS/cm)	0,77	0,82	0,80	0,72	**0,78**

Table D- 16: Set C30-80 Chloride Conductivity results

Measurement	Sample 1	Sample 2	Sample 3	Sample 4	Average
Diameter (mm)	68,93	69,00	68,99	69,00	**68,98**
Thickness (mm)	30,39	29,17	28,10	29,79	**29,36**
Porosity (%)	5,12	5,17	4,72	5,50	**5,13**
Dry Mass (g)	259,14	247,50	240,53	251,55	**249,68**
Saturated Mass (g)	274,95	263,51	255,13	268,58	**265,54**
Voltage (V)	9,99	10,02	9,99	9,96	**9,99**
Current (mA)	225,1	250,0	258,1	262,0	**248,8**
Conductivity (mS/cm)	1,83	1,95	1,94	2,10	**1,95**

Table D- 17: Set C20-50 Chloride Conductivity results

Measurement	Sample 1	Sample 2	Sample 3	Sample 4	Average
Diameter (mm)	68,88	68,52	68,11	68,56	**68,52**
Thickness (mm)	30,98	30,81	30,17	31,13	**30,77**
Porosity (%)	4,32	4,27	5,01	4,72	**4,58**
Dry Mass (g)	271,90	268,54	272,45	269,12	**270,50**
Saturated Mass (g)	285,20	281,50	287,38	283,45	**284,38**
Voltage (V)	10,05	10,01	10,02	10,01	**10,02**
Current (mA)	96,1	100,6	96,5	103,6	**99,2**
Conductivity (mS/cm)	0,79	0,84	0,80	0,87	**0,83**

Table D- 18: Set C20-80 Chloride Conductivity results

Measurement	Sample 1	Sample 2	Sample 3	Sample 4	Average
Diameter (mm)	69,49	69,69	69,60	69,53	**69,58**
Thickness (mm)	29,52	29,37	29,05	29,59	**29,38**
Porosity (%)	4,76	4,96	4,99	4,24	**4,74**
Dry Mass (g)	263,38	259,40	265,08	251,67	**259,88**
Saturated Mass (g)	278,45	275,21	280,95	265,09	**274,93**
Voltage (V)	10,02	10,02	10,06	10,01	**10,03**
Current (mA)	234,5	248,2	254,1	258,8	**248,9**
Conductivity (mS/cm)	1,82	1,91	1,93	2,01	**1,92**

Appendix E: Cover readings

Table E 1: Cover depth readings for corrosion cells in the submerged zone

Exposure zone	Reference No.	Cover depth (mm)			
		1	2	3	Average
Submerged	C10-50 (1)	11	11	10	11
	C10-50 (2)	10	11	9	10
	C10-80 (1)	14	11	11	12
	C10-80 (2)	10	10	11	10
	C20-50 (1)	22	20	21	21
	C20-50 (2)	20	19	20	20
	C20-80 (1)	20	19	19	19
	C20-80 (2)	23	22	23	22
	C30-50 (1)	30	31	32	31
	C30-50 (2)	29	29	29	29
	C30-80 (1)	30	30	29	30
	C30-80 (2)	31	31	30	31

Table E 2: Cover depth readings for corrosion cells in the tidal zone

Exposure zone	Reference No.	Cover depth (mm)			
		1	2	3	Average
Tidal	C10-50 (1)	8	11	11	10
	C10-50 (2)	10	9	9	9
	C10-80 (1)	12	10	12	11
	C10-80 (2)	9	13	11	11
	C20-50 (1)	20	20	19	20
	C20-50 (2)	22	25	23	23
	C20-80 (1)	20	21	21	21
	C20-80 (2)	23	21	22	22
	C30-50 (1)	29	29	32	30
	C30-50 (2)	31	31	31	31
	C30-80 (1)	29	30	30	30
	C30-80 (2)	30	31	30	30

Table E 3: Cover depth readings for corrosion cells in the splash and spray zone

Exposure zone	Reference No.	Cover depth (mm)			
		1	2	3	Average
Splash and Spray	C10-50 (1)	10	8	8	9
	C10-50 (2)	9	10	9	9
	C10-80 (1)	8	8	9	8
	C10-80 (2)	12	10	11	10
	C20-50 (1)	19	18	20	19
	C20-50 (2)	22	19	19	20
	C20-80 (1)	22	20	21	21
	C20-80 (2)	24	21	21	22
	C30-50 (1)	30	27	27	28
	C30-50 (2)	31	30	31	31
	C30-80 (1)	29	30	30	30
	C30-80 (2)	29	29	29	29

Appendix F: Statistical Analysis

F-1: Hypothesis testing

When comparing if 2 sets of data are significantly different, hypothesis testing is used.

Step 1:

Indicate the level of significance and the degrees of freedom. In this case the level of significant was chosen to be 5% (α = 0,025) and the degree of freedom is 2 (n – 1). Using the t table a critical value is established. This critical value divides the rejection and non-rejection regions.

Step 2:

Determine the test statistic using the formula $t = \frac{X-\mu}{\sqrt{\frac{\sigma_1}{n_1}+\frac{\sigma_2}{n_2}}}$.

Where t = test statistic; X = average sample 1; μ = average sample 2; σ = standard deviation; and n = number of samples.

Step 3:

Make a statistical decision on whether it can be said with 95% confidence that the two samples are statistically different or the same. If the test statistic t is larger than the critical t value, the two sets of data are said to be significantly different.

F-2: ANOVA analysis

Step 1:

ANOVA analysis investigates the distribution of the variance of different datasets. The source values were determined using the equations below.

i is rows and j is columns; a is exposure condition; b is cover depth and c is w/b ratio

$$[A] = \frac{\sum\left(\sum a_j\right)^2}{(n)(b)(c)}$$

$$[B] = \frac{\sum\left(\sum b_j\right)^2}{(n)(a)(c)}$$

$$[C] = \frac{\sum\left(\sum c_i\right)^2}{(n)(a)(b)}$$

$$[T] = \frac{\sum\sum\left(\sum a_j + \sum c_i\right)^2}{(n)(a)(b)(c)}$$

Table F - 1: Results of Step 1

Source	Values
[A]	5914272,731
[B]	3889856,616
[C]	3496089,033
[AB]	6533281,281
[AC]	5956098,8
[BC]	3902957,8
[ABC]	6586000,906
[T]	3486827,515
[Y]	6602622,806

Step 2:

Enter all the values calculated in Step 1 into the table below to determine the critical factor F.

Table F - 2: Calculation of the critical F factor

Source	Sum of squares (SS)	DoF	MS	F
[A]	[A] – [T]	a-1	SS/df	MS/MS_E
[B]	[B] – [T]	b-1	SS/df	MS/MS_E
[C]	[C] – [T]	c-1	SS/df	MS/MS_E
[A×B]	[AB] – [A] – [B] + [T]	(a-1)(b-1)	SS/df	MS/MS_E
[A×C]	[AC] – [A] – [C] + [T]	(a-1)(c-1)	SS/df	MS/MS_E
[B×C]	[BC] – [B] – [C] + [T]	(b-1)(c-1)	SS/df	MS/MS_E
[A×B×C]	[ABC] – [AB] – [AC] – [BC] + [A] + [B] + [C] – [T]	(a-1)(b-1)(c-1)	SS/df	MS/MS_E
S/ABC	[Y] – [ABC]	abc(n-1)	SS/df	MS/MS_E
Total	[Y] – [T]	abcn-1	SS/df	MS/MS_E